CHEMICAL ENGINEERING SCIENCE
GENIE CHIMIQUE

VOL. 13 1961 No. 4

Studies in optimization—IV

The optimum conditions for a single reaction

R. ARIS

Department of Chemical Engineering, University of Minnesota, Minneapolis 14, Minn., U.S.A.

(*Received* 20 *June*, 1960)

Abstract—It is shown how an explicit solution to the problem of finding the minimum holding time and best temperature profile may be obtained for a tubular or batch reactor. The form which this takes allows a complete parametric study for given kinetics and full results are presented for a first-order reversible reaction. For the sequence of stirred tank reactors both the minimum holding time and optimum temperature of each stage can be found by a simple graphical construction.

Résumé—Le temps de séjour minimum et le meilleur profil de températures peuvent être obtenus par une solution mathématique explicite pour un réacteur tubulaire ou discontinu. Cette solution permet une étude paramétrique complète pour des cinétiques données, et des résultats complets sont donnés pour une réaction reversible du 1 er ordre. Pour la série de réacteurs à cuves agités une construction graphique simple permet de trouver le temps de séjour nimimum et la température optimum pour chaque stade.

Zusammenfassung—Es wird gezeigt, wie man eine explizite Lösung für die Ermittlung der kleinsten Verweilzeit und des günstigsten Temperaturprofils für einen Rohrreaktor oder einen diskontinuierlichen Reaktor erhält. Hieraus können bei gegebener Kinetik alle Parameter untersucht werden. Es werden die Ergebnisse für eine reversible Reaktion I Ordnung angegeben. Für eine Rührkesselkaskade kann die kürzeste Verweilzeit und die optimale Temperatur für jeden Kessel durch eine einfache graphische Methode ermittelt werden.

IT MIGHT be felt that little more could be added to the discussion of optimum temperature profiles in tubular or stirred tank reactors, when only a single reaction is taking place. It has long been known that the temperature should always be chosen to make the reaction rate as large as possible at each point or stage [1–3], and the consequent calculations are not difficult. Two observations, however, prompt a further remark on the subject. The first is that an explicit solution in terms of easily calculable integrals can be found and this allows a full parametric study of any particular reaction; the second, that DENBIGH's notion of the maximization of rectangles [4] can be adapted to give the optimum choice both of temperature and holding time at each stage. The example of a first-order reversible reaction has been used to illustrate the methods, but these are perfectly general and the explicit solution applies to the kinetic expression commonly given for a homogeneous reaction.

1. THE REACTION AND REACTOR SYSTEMS

We consider a single reaction between n chemical species $A_1, A_2, \ldots, A_n$, which we write in the form $0 = \sum_{i=1}^{n} \alpha_i A_i$ and observe the convention that the stoichiometric coefficients, α_i, of products should be positive whilst those of

reactants are negative. If c_i denotes the concentration (moles/unit volume) of A_i, and c_{i0} its concentration in the feed (or in some reference mixture from which the feed might be derived by reaction to a certain extent), then

$$c_i = c_{i0} + \alpha_i c, \tag{1}$$

where c is a measure of the extent of the reaction. The rate of the reaction, which we assume takes place without change of volume, is by definition dc/dt and is a function of all the concentrations and of the temperature. We therefore write

$$\frac{dc}{dt} = r(c_1, \ldots c_n, T) = r(c, T; c_{10}, \ldots c_{n0}) = \\ = r(c, T). \tag{2}$$

The expression commonly used to fit homogeneous reaction rate data is

$$r(c, T) = k_1(T) \prod_1^n c_i^{\beta_i} - k_2(T) \prod_1^n c_i^{\gamma_i} \tag{3}$$

where β_i and γ_i are experimentally determined indices with more or less theoretical backing, but in general restricted only by the equilibrium consistency condition, $\gamma_i - \beta_i = \alpha_i$. The explicit solution we give will be restricted to the kinetic expression (3), but the same method is applicable to any form of $r(c, T)$.

Equation (2) describes the course of the reaction for a batch or tubular reactor; for the batch reactor t is the actual time, for the tubular it is the length of reactor up to a given point divided by the linear velocity of flow. The optimum problem is to choose T as a function of t so that either the time (or reactor length) required for a given conversion is least, or the conversion is a given time is greatest. AMUNDSON and BILOUS have shown the equivalence of these problems [5] and we shall consider the first formulation. The admissible choice of temperature will usually be restricted by upper and lower bounds,

$$T_* \leqslant T \leqslant T^* \tag{4}$$

The sequence of stirred tank reactors is described by a set of difference equations analogous to (2). It is convenient to number the stages backwards, the first reactor of a battery of R reactors being labelled reactor R and the last, reactor 1. The state of the feed to reactor r is then specified by c_{r+1}, the extent of reaction in the previous reactor, whilst the composition within it, and so also its product composition, is denoted by c_r. (Fig. 1 illustrates this). The

FIG. 1. The stirred tank sequence.

design of the sequence involves the choice of the holding times $\theta_1, \ldots \theta_R$ and operating temperatures $T_1, \ldots T_R$ so that a given conversion may be attained with minimum total holding time $\Theta_R = \sum_1^R \theta_r$. A mass balance on the r^{th} reactor gives the difference equation

$$c_{r+1} - c_r = \theta_r r(c_r, T_r) \tag{5}$$

or

$$\frac{c_r - c_{r+1}}{\theta_r} = r(c_r, T_r)$$

In the latter form we see that, if θ_r is allowed to tend to zero, the differential equation (2) arises as the limit of the difference equation (5). Solving (5) for θ_r we have

$$\Theta_R = \sum_1^R \frac{c_r - c_{r+1}}{r(c_r, T_r)}, \tag{6}$$

and given the states of the feed and product, c_{R+1} and c_1, we have to choose the temperatures $T_1, \ldots T_R$ and the extents of reaction $c_R, \ldots c_2$ which will make Θ_R a minimum. This involves the choice of $2R - 1$ quantities, which concurs with the other formulation of the problem (namely the maximization $(c_1 - c_{R+1})$ for given Θ_R), for in this case the R temperatures have to be chosen and $R - 1$ of the holding times, the last being fixed by the value of Θ_R.

2. THE OPTIMUM TEMPERATURE POLICY

For completeness we shall give a brief demonstration of the fact that T should always be chosen to maximize $r(c, T)$. Earlier published proofs have not taken into account the restriction

(4) and, though true, it is not obvious that this does not change the result. For the batch reactor we observe that we have to minimize.

$$\int_{c_f}^{c_1} \frac{dc}{r(c, T)}$$

by choice of $T(c)$ in the range $c_f \leqslant c \leqslant c_1$. (Here we denote the product state by c_1 as in the case of the stirred tank sequence, but the feed state by c_f). T as a function of t will then be obtained by integrating equation (2) to get the relation between c and t. c_1 being fixed the minimum value of this integral will depend only on c_f, and we may write

$$f(c_f) = \text{Min} \int_{c_f}^{c_1} \frac{dc}{r(c, T)} \tag{7}$$

Now the range of integration may be broken up into a short interval (c_f, γ) and the remainder (γ, c_1). Moreover it is clear that whatever choice of $T(c)$ we make in the first interval we cannot do better than to make the best choice in the remainder of the interval to which the feed condition is $c = \gamma$. Indeed by trying different values of $T(c)$ in (c_f, γ) and always using the optimum choice in (γ, c_1) we shall eventually hit on the optimum choice for the first interval also. Thus

$$f(c_f) = \text{Min} \left[\int_{c}^{\gamma} \frac{dc}{r(c, T)} + f(\gamma) \right]$$

Now let $\gamma \to c_f$ and let T_f be the inlet temperature. Then

$$f(c_f) = \text{Min} \left[\frac{\gamma - c_f}{r(c_f, T_f)} + f(c_f) + \right.$$
$$\left. + (\gamma - c_f) f'(c_f) + 0(\gamma - c_f)^2 \right]$$

or

$$-f'(c_f) = \text{Min} \frac{1}{r(c_f, T_f)}$$

Since $f'(c_f) < 0$ this means that T_f must be chosen to make $r(c_f, T_f)$ as large as possible. This demonstration is valid under the restrictions (4), whereas proofs involving differentiation break down under this restriction.

For the stirred tank sequence we again argue that when the optimum choice has been made the minimum holding time will be a function of the feed state only. Let.

$$f_R(c_{R+1}) = \text{Min } \Theta_R \tag{8}$$

then whatever choice of c_R and T_R may be made in the first reactor we cannot do better than use the optimum policy for the remaining $(r-1)$ reactors, with respect to their feed c_R. Thus

$$f_R(c_{R+1}) = \text{Min} \left[\frac{c_R - c_{R+1}}{r(c_R, T_R)} + f_{R-1}(c_R) \right] \tag{9}$$

Now c_R and T_R are independent choices and the second term in the bracket depends only on c_R. It is thus clear that so far as the choice of T_R is concerned it should always be made to maximize $r(c, T)$. This may be determined by any means or be known experimentally; however, with the kinetic expression (3) we may find an explicit solution.

3. The Maximum Reaction Rate for Given Composition

In the general reaction-rate expression (3) k_1 and k_2 are assumed to have the Arrhenius form $k_i = k_i^* \exp(-E_i/RT)$, $i = 1, 2$. Then, since $dk_i/dT = E_i k_i/RT^2$, the maximum value of r is for T satisfying

$$E_1 k_1 \prod_1^n c_i^{\beta_i} - E_2 k_2 \prod_1^n c_i^{\gamma_i} = 0 \tag{10}$$

provided this falls in the interval T_*, T^* and makes the second derivative of r negative. But the second derivative of r at this extremum is proportional to

$$E_1^2 k_1 \prod_1^n c_i^{\beta_i} - E^2_2 k_2 \prod_1^n c_i^{\gamma_i}.$$

For an exothermic reaction when r, given by (3), is positive and the expression in (10) is zero this is certainly negative. For an endothermic reaction with r positive, r always increases with increase of T so that T should always have its maximum value T^*. The case of the endothermic reaction is thus rather trivial.

Equation (10) may be solved for T in the form

$$\exp(E_2 - E_1)/RT = \frac{k_2^* k_1}{k_1^* k_2} = \frac{k_2^* E_2}{k_1^* E_1} \prod_1^n c_i^{\alpha_i}$$

since $\gamma_i - \beta_i = \alpha_i$. Let us denote the dimensionless temperature by $\tau = RT/(-\Delta H)$, then since $\Delta H = E_1 - E_2$,

$$\tau = \frac{RT}{(-\Delta H)} = \left[\ln \frac{k_2^* E_2}{k_1^* E_1} \prod_1^n c_i^{\alpha_i}\right]^{-1} \tag{11}$$

The maximum reaction rate may now be written

$$R(c) = \frac{p^p}{(p+1)^{p+1}} \frac{k_1^{*p+1}}{k_2^{*p}} \prod_1^n c_i^{\beta_i - p\alpha_i} \tag{12}$$

where

$$p = \frac{E_1}{E_2 - E_1}. \tag{13}$$

The concentrations c_i are of course given by (1) and it is convenient to make c dimensionless by the following substitutions. Let

$$c_0 = \sum_1^n c_{i0}, \qquad \mu_i = c_{i0}/c_0, \qquad x = c/c_0,$$

$$\alpha = \Sigma \alpha_i, \qquad \beta = \Sigma \beta_i, \qquad \gamma = \Sigma \gamma_i$$

$$\delta_i = p\,\alpha_i - \beta_i = (E_1\,\gamma_i - E_2\,\beta_i)/(E_2 - E_1)$$

then

$$R(c) = c_0\, A \prod_1^n (\mu_i + \alpha_i x)^{-\delta_i} \tag{12}$$

where

$$A = \frac{p^p}{(p+1)^{p+1}} \cdot \frac{k_1^{*p+1}}{k_2^{*p}}\, c_0^{(p+1)\beta - p\gamma - 1} \tag{13}$$

has the dimensions of (time)$^{-1}$. The value of τ can now be written as

$$\tau = \left[\ln \kappa \prod_1^n (\mu_i + \alpha_i x)^{\alpha_i}\right]^{-1} \tag{14}$$

where

$$\kappa = \frac{p+1}{p} \frac{k_2^*}{k_1^*} c_0^{\alpha} \tag{15}$$

It thus appears that for reaction mixtures of given proportions (μ_i) and for given kinetics (β_i, γ_i) there are only two parameters p and κ that need to be varied to study the whole class of optimum problems, for A may be used to render time dimensionless.

If the value of T given by (11) does not lie in the interval (T_*, T^*) then T must take one of these values. In this case $R(c)$ the maximum value of r is either R^* or R_* given by (3) with $T = T^*$ or T_* respectively.

For the case of a first-order reversible reaction $0 = A_1 - A_2$, $\beta_2 = \gamma_1 = 1$, $\beta_1 = \gamma_2 = 0$, the stoichiometric relations imply $c_1 + c_2 = c_{10} + c_{20}$. In this case it is convenient to put $y = c_1/(c_{10} + c_{20}) = (c_{10} + c)/(c_{10} + c_{20})$ and we have

$$\left.\begin{aligned} &R(c) = A c_0\, y^{-p}(1-y)^{(p+1)} \\ &A = p^p\, k_1^{*p+1}/(p+1)^{p+1}\, k_2^{*p} \\ &\text{and} \\ &\tau = [\ln \kappa\, y/(1-y)]^{-1} \\ &\kappa = k^*_2\, E_2/k_1^*\, E_1 \end{aligned}\right\} \tag{16}$$

4. The Tubular Temperature Profile

From the relation (14) it follows that

$$\frac{d\tau}{dx} = -\tau^2 \sum_1^n \frac{\alpha_1^2}{(\mu_i + \alpha_i x)}$$

is always negative. Hence there will be two definite values x_* and x^* at which $\tau = \tau^*$ and τ^* ($T = T^*$, T_*) respectively, and only within the interval (x_*, x^*) will the expression (12) be used. Thus using the optimum policy and letting $At = z$, equation (2) becomes

$$\frac{dx}{dz} = P^*(x), \quad x \leqslant x_*, \tag{17}$$

$$\frac{dx}{dz} = P(x), \quad x_* \leqslant x \leqslant x^*, \tag{18}$$

$$\frac{dx}{dz} = P_*(x), \quad x^* \leqslant x, \tag{19}$$

where $P(x) = R(c)/c_0 A$.

From this the solution is immediately obtained by quadratures, and z, the dimensionless time or reactor length, is the area under the curve $1/P$ shown in Fig. 5 between the ordinates with values of x corresponding to c_f and c_1. The temperature profile may be immediately found by graduating this curve in values of τ calculated by (14). It is however interesting to see how a complete parametric study of a given reaction may be made and for this we may consider the first-order reversible reaction.

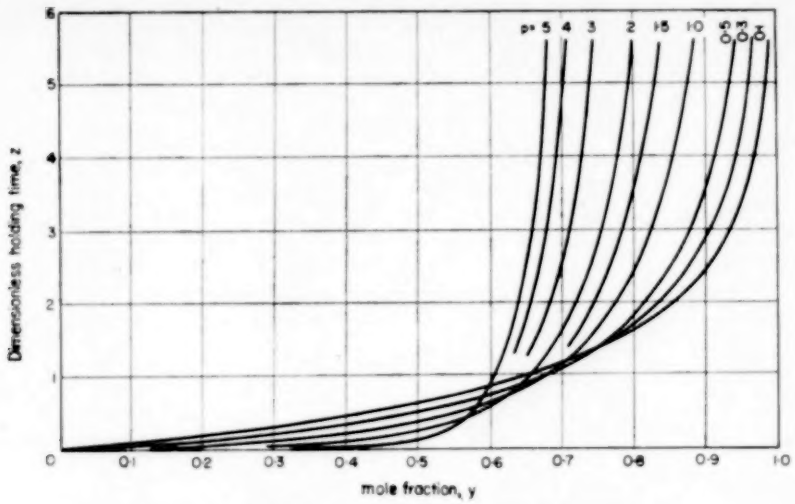

FIG. 2. Minimum length of reactor for first-order reactions.

Disregarding for the moment the restrictions on temperature we have from equations (16) and (18)

$$z = \int y^p (1 - y)^{-(p+1)}\, dy$$

the limits of the integration being the values of $y = c_1/(c_{10} + c_{20})$ in the feed and product. This integral depends only on p and hence a whole family of curves can be drawn as in Fig. 2 giving the relation between z and the upper limit of integration. Since $p = E_1/(E_2 - E_1)$ is positive for an exothermic reaction, the curves are as shown, sloping upward from the origin $y = 0$ to the asymptote $y = 1$.

In Fig. 3 the temperature policy τ is shown for the same range of y. Here the only parameter is κ and we have a family of curves all tending to

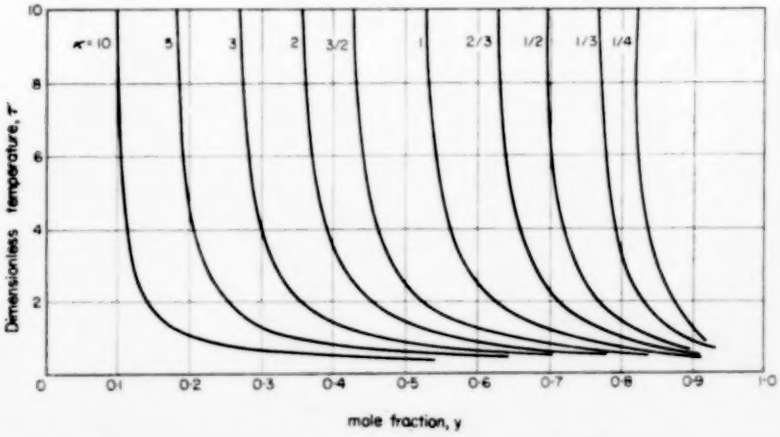

FIG. 3. Optimum temperature profiles for first-order reactions.

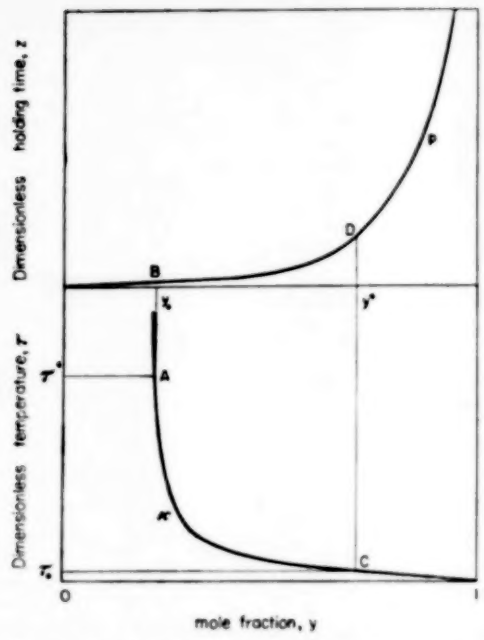

FIG. 4. Construction of the optimum temperature gradient.

$\tau = 0$ as $y = 1$ and having asymptotes at $y = (1 + \kappa)^{-1}$. Curves from the two figures are combined in Fig. 4. From this it is immediately clear what is the range of validity of (18). Given τ^* we find the point A on the appropriate κ curve and this gives y_*; likewise y^* is obtained from τ_* via the point C. Thus the relevant part of the z curve for the appropriate p is the arc BD. Outside this range we may immediately integrate either equation (17) or (19) to give

$$z - z_0 = \frac{A}{k_1 + k_2} \ln \frac{|k_1 - (k_1 + k_2)\, y_0|}{|k_1 - (k_1 + k_2)\, y|}$$

where k_1 and k_2 are evaluated either at temperature $T = T_*$ or at $T = T^*$.

The same treatment can be accorded the more general reaction, where the solution of (18) now is

$$z = \int \prod_1^n (\mu_i + \alpha_i x)^{\delta_i}\, dx,$$

an integral presenting little computational difficulty. We notice that for exothermic reactions $\delta_i = p\alpha_i - \beta_i$ will generally be negative for reactants and positive for products. The general form of the curve is as before with z tending to infinity as x approaches the least value of $-\mu_i/\alpha_i$. Of course this point is never reached for the optimum temperature here would be absolute zero, so that the lower bound T_* intervenes and beyond this the best that can be done is to allow the reactants to approach equilibrium.

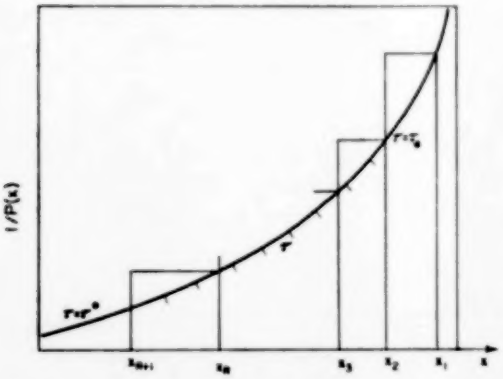

FIG. 5. Construction for the holding times of a sequence of stirred tanks.

5. THE STIRRED TANK SEQUENCE

The functional equation (9) by which the minimum holding time $f_R(c_{R+1})$ may be calculated has already been derived and since we now know that r should have its maximum value R we may write

$$f_R(c_{R+1}) = \text{Min}\left[\frac{c_R - c_{R+1}}{R(c_R)} + f_{R-1}(c_R)\right],$$

where the minimization is by choice of c_R in the range $c_{R+1} \leqslant c_R \leqslant c_1$. To make this dimensionless let $\zeta_r = A\,\theta_r$ and $\phi_R(x_{R+1}) = \text{Min} \sum_1^R \zeta_r$. Then

$$\phi_R(x_{R+1}) = \text{Min}\left[\frac{x_R - x_{R+1}}{P(x_R)} + \phi_{R-1}(x_R)\right] \qquad (20)$$

The holding time ζ_r of each stage is thus the area of the rectangle standing on the base (x_{r+1}, x_r) and of height $1/P(x_r)$. For any choice of $x_r, x_{r-1}, \ldots x_2$ these rectangles can be drawn as in Fig. 5 and serve to evaluate the holding

time of each stage. It is clear that the total holding time for the sequence of stirred tanks must exceed that of the tubular reactor, which is the area under the curve itself, and the problem is to minimize this area by the correct choice of $x_r, \ldots x_2$. This idea of minimization of rectangles derives from DENBIGH's recent presentation of a method of maximization of rectangles [4], which applies to the equivalent problem of maximizing the yield for given holding time. DENBIGH is concerned with more complicated reaction systems under isothermal conditions. For $R = 1$ there is no choice, for to attain a given conversion a holding time $\theta_1 = (x_1 - x_2)/P(x_1)$ is required. We therefore start the sequence with $R = 2$.

The value of

$$\phi_2(x_3) = \underset{x_3 \le x_2 \le x_1}{\text{Min}} \left[\frac{x_2 - x_3}{P(x_2)} + \frac{x_1 - x_2}{P(x_1)} \right]$$

may be obtained by direct calculation or trial and error and will yield both the minimum $\phi_2(x_3)$ and the value of $x_2(x_3)$ at which it occurs. We may then proceed to find $\phi_3(x_4)$ and $x_3(x_4)$ from (20) and so on. These could be tabulated as illustrated in an earlier paper [6]. However, it is interesting to observe that all this information can be included in a single graph such as Fig. 4. The curve marked Γ_∞ is the curve of $1/P(x)$ [continued at its extremities when the optimum temperature is outside (T_*, T^*) by the curves $1/P^*(x)$ and $1/P_*(x)$], the curve marked R has abcissa x_{R+1} and ordinate $1/P(x_R(x_{R+1}))$. To show how this suffices, consider four reactors with feed x_5 and product x_1. From x_5 and the curve Γ_3 we know $1/P(x_5)$ (point A) and hence by drawing a horizontal line we have x_4 (point B). Again from x_4 and the curve Γ_3 we have $1/P(x_3)$ (point C) and so x_3 (point D). Working up in this way from x_r to the curve Γ_{r-1} we have the complete optimum policy. The holding times of each stage can be quickly calculated from the area of the rectangles and the temperatures read off from the scale on the curve $1/P(x)$.

Furthermore the curves Γ_R may themselves be found graphically by a simple construction rather than by a trial and error calculation of (20). Since the minimizing values of $x_R, \ldots x_2$ are in the open interval (x_{R+1}, x_1) they satisfy

$$\frac{\partial}{\partial x_r}\left(\sum_1^R \zeta_r\right) = 0, \quad r = 2, \ldots R \qquad (21)$$

Thus

$$\frac{d\phi_R}{dx_{R+1}} = \frac{\partial}{\partial x_{R+1}}\left(\sum_1^R \zeta_r\right) + \sum_2^R \frac{\partial}{\partial x_r}\left(\sum_1^R \zeta_r\right)\frac{dx_r}{dx_{R+1}}$$

$$= \frac{\partial}{\partial x_{R+1}}\left(\sum_1^R \zeta_r\right) = \frac{-1}{P(x_R)}$$

by virtue of (21). To find the value of x_R which minimizes the right-hand side of (20) we have

$$\frac{d}{dx_R}\left[\frac{x_R - x_{R+1}}{P(x_R)} + \phi_{R-1}(x_R)\right] =$$

$$= \frac{1}{P(x_R)}\left\{1 - x_R\frac{P'(x_R)}{P(x_R)}\right\} +$$

$$+ x_{R+1}\frac{P'(x_R)}{P^2(x_R)} - \frac{1}{P(x_{R-1})} = 0 \qquad (22)$$

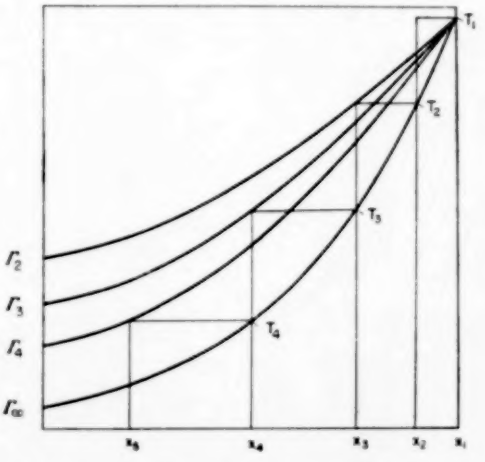

FIG. 6. Construction for the optimum holding times of a sequence of stirred tanks.

Consider the family of curves

$$h(x;\zeta) = \frac{1}{P(x)}\left\{1 - x\frac{P'(x)}{P(x)}\right\} + \zeta\frac{P'(x)}{P^2(x)} \qquad (23)$$

which may be drawn once and for all for given kinetics. Let this family be drawn for various ζ in the same plane as the curve Γ_∞, $1/P(x)$.

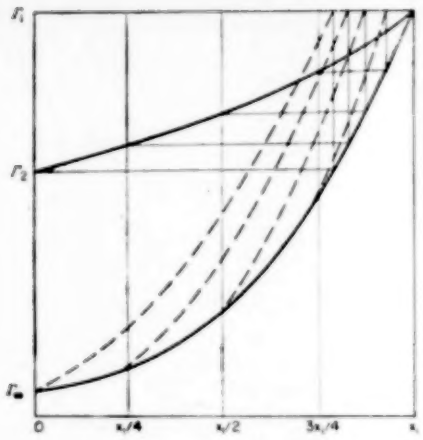

FIG. 7. Construction for the curves Γ_r.

(See Fig. 7, where four curves of the family are drawn). In case the temperature has to be held at τ_* or τ^* we interpret $P(x)$ to mean P_* or P^*. When x_1 is fixed the single-stage holding time ζ_1 is immediately determined for any x_2. The corresponding value $x_1(x_2)$ is always the given x_1 so that the curve Γ_1 is the horizontal line through A, the intersection of Γ_∞ and the ordinate $x = x_1$. Now for given x_3 the minimizing x_2 satisfies equation (22), i.e.

$$h(x_2; x_3) = \frac{1}{R[x_1(x_2)]} = \frac{1}{R(x_1)}$$

which means that the correct x_2 is the abcissa of the intersection of the curve $h(x; \zeta)$ for $\zeta = x_3$ with Γ_1, the point B. The point $x_3 = \zeta$ on the curve Γ_2 has ordinate $1/R[x_2(x_3)]$ and so is obtained by dropping vertically from B to the point C on Γ_∞ and going horizontally from C to D on the ordinate $x = \zeta$. Repeating this construction with the various members of the family $h(x, \zeta)$ for $0 \leqslant \zeta \leqslant x_1$ a sufficient number of points to draw the curve Γ_2 can rapidly be found. Γ_3 is then constructed from Γ_2 in precisely the same way as Γ_2 was obtained from Γ_1.

The value of this construction lies in the fact that Γ_∞ and the family $h(x, \zeta)$ depend only on

VOL. 13 1961

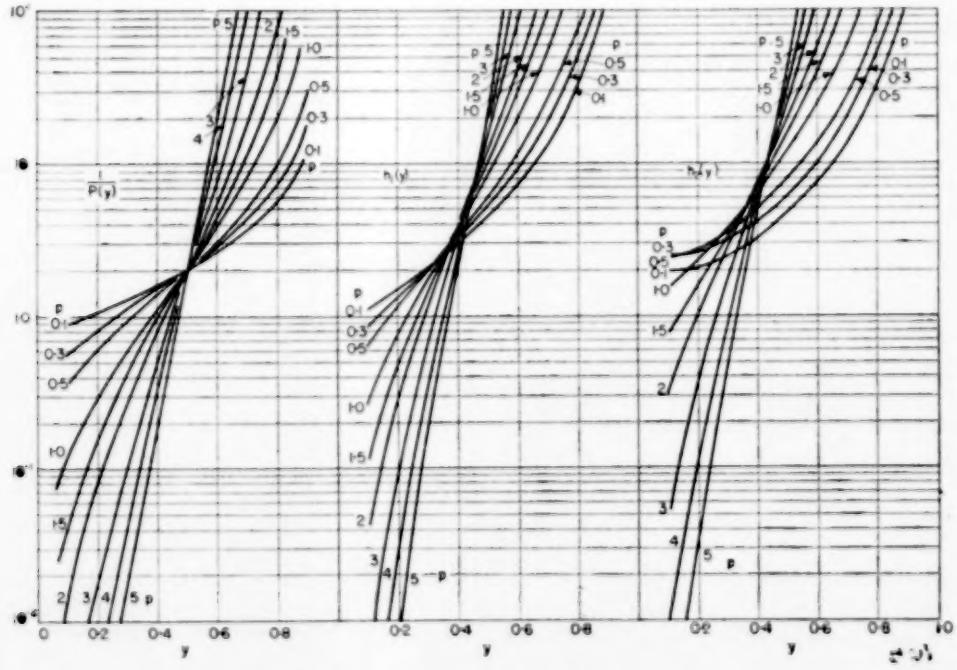

FIG. 8. The functions $1/P(y)$, $h_1(y)$ and $h_2(y)$.

the kinetics and the restriction on temperature; from them such a diagram as Fig. 6 can be obtained for any c_1. For the first-order reversible reaction we may use the variable y, as before, then

$$\frac{1}{P(y)} = y^p (1-y)^{-p-1} \text{ and } h(y, \zeta) = h_1(y) - \zeta h_2(y)$$

where $h_1 = (1+p)\, y^p (1-y)^{-p-2}$

and $h_2 = (p+y)\, y^{p-1} (1-y)^{-p-2}$.

$1/P(y)$, h_1 and h_2 are shown in Fig. 8 for the same values of p. Thus Figs. 2, 3 and 8 provide the material for a complete parametric study of the first-order reversible exothermic reaction.

It may be remarked in conclusion that a diagram such as Fig. 6 could be constructed if the objective were to minimize some more complicated function $F(\theta_1, \theta_2 \ldots \theta_R)$ than the sum $\Sigma\theta_r$. However it is unlikely that a simple graphical construction would exist and the functional equation corresponding to (20) would have to be solved by direct calculation.

Since this paper was completed the work of F. HORN has come to my attention. The closed form of the optimal temperature and the resulting integrals was given by him in [7], where also he has tabulated some particularly useful cases of the integral. He has also used the same technique in [8] and [9]; for a more complete review of his work see [10].

Acknowledgements—I am indebted to Professor K. G. DENBIGH for showing me his contribution to the Amsterdam conference before it was published. The presentation of the last section of this paper is closely related to the ideas of DENBIGH's paper.

The calculations on which Figs. 2, 3 and 8 are based were done by Messrs. K. Y. LEE and B. ANSHUS of this University.

NOTATIONS

A	constant defined by (13)
A_i	chemical species involved in reaction ($i = 1, \ldots n$)
c	extent of reaction
c_f	extent of reaction in feed
c_r	extent of reaction in reactor r
c_i	concentration of A_i
c_{i0}	concentration of A_i in reference state
c_0	$\sum_1^n c_{i0}$
E_i	activation energies $i = 1, 2$
$f(c_f)$	minimum time to achieve conversion c_1 with feed c_f in tubular or batch reactor
$f_R(c_{R+1})$	minimum total holding time to achieve conversion c_1 with feed c_{R+1} to R stirred tank reactors
ΔH	heat of reaction
k_i	$k_i^* \exp(-E_i/RT)$, reaction rate constants
P	$R/A\, c_0$, dimensionless maximum reaction rate
p	$E_1/(E_2 - E_1)$
$R(c)$	maximum reaction rate
R^*, R_*	$r(c, T^*)$, $r(c, T_*)$
$r(c, T)$	rate of reaction (dc/dt)
T	temperature
T^*, T_*	upper and lower bounds of permitted temperatures
t	time
x	c/c_0
y	$c_1/(c_{10} + c_{20})$
z	At
α_i	stoichiometric coefficient in reaction $0 = \Sigma \alpha_i A_i$
β_i, γ_i	exponents in rate expression
δ_i	$p\alpha_i - \beta_i$
ζ_r	$A\theta_r$
θ_r	holding time of stirred tank reactor r
Θ_R	$\sum_1^R \theta_r$
$\phi_R(x_{R+1})$	$\text{Min} \sum_1^R \zeta_r$
κ	constant defined by (15)
μ_i	c_{i0}/c_0
τ	$RT/(-\Delta H)$

REFERENCES

[1] ANNABLE D. *Chem. Engng. Sci.* 1952 **1** 145.

[2] DENBIGH K. G. *Trans. Faraday Soc.* 1944 **40** 352.

[3] TEMKIN M. and PYZHEV V. *Acta Phys-chim. URSS.* 1940 **12** 327.

[4] DENBIGH K. G. *2nd Conf. Reactor Design, Amsterdam* 1960. Pergamon Press, Oxford, 1960.

[5] AMUNDSON N. R. and BILOUS O. *Chem. Engng. Sci.* 1956 **5** 81.

[6] ARIS R. *Chem. Engng. Sci.* 1960 **13** 75.

[7] HORN F. Optimalprobleme bei kontinuerlichen chemischen Prozessen, Dissertation Techn. Hoeschule Wien 1958.

[8] HORN F. Optimale Temperatur-und Konzentrationsverläufe *Second European Symposium on Chemical Reaction Engineering. Chem. Engng. Sci.* 1961 **14** 77.

[9] HORN F. and TROLTENIER U. *Chem. Ing. Tech.* **32** 1960 382.

[10] ARIS R. The optimal design of chemical reactors. New York. Academic Press. 1961.

Chemical Engineering Science, 1961, Vol. 13, pp. 207 to 225. Pergamon Press Ltd., London. Printed in Great Britain

New methods for the liquid phase continuous operation of thermogravitational columns with reservoirs

J. R. Brock*

University of Wisconsin, Madison, Wisconsin, U.S.A.

(*Received* 18 *May* 1960; *in revised form* 27 *June* 1960)

Abstract—Experimental and theoretical results are presented for four new methods for the liquid phase continuous operation of thermogravitational columns with reservoirs. Two of the methods for continuous operation provide techniques for experimental study and refinement of thermogravitational column theory. The developed theory for the four new methods is in qualitative agreement with the experimental results obtained for the binary liquid system, *n*-heptane–benzene.

Résumé—Présentation des résultats théoriques et expérimentaux de quatre nouvelles méthodes pour la marche continue en phase liquide de colonnes à circulation thermique avec réservoirs. Deux de ces méthodes apportent des données techniques pour l'étude expérimentale et le perfectionnement de la théorie des colonnes à circulation thermique. La théorie des quatre nouvelles méthodes est en accord qualitatif avec les résultats expérimentaux obtenus pour le système liquide binaire *n*-heptane-benzène.

Zusammenfassung—Experimentelle und theoretische Ergebnisse werden für 4 neue Methoden des Betriebs von kontinuierlichen Flüssigphase–Thermogravitationssäulen mit Reservoirs mitgeteilt. Zwei dieser Verfahren für kontinuierlichen Betrieb liefern Hinweise über experimentiertechnische Studien und für eine Verfeinerung der Theorie der Thermogravitationssäulen. Die entwickelte Theorie für die vier Verfahren stimmt qualitativ mit den experimentellen Ergebnissen überein, die für das flüssige binäre System *n*-Heptan-Benzol erhalten wurden.

Considerable interest has been shown in the thermogravitational column with the result that quite an extensive body of literature has developed on the subject, as is evidenced by several reviews [1 – 3]. The majority of the experimental work on the thermogravitational column has involved operation of the column in what is termed a "batch" manner. Operation of the thermogravitational column in a "continuous" manner has been the subject of more recent investigations.

"Batch" operation of a thermogravitational column consists of charging the column initially with the mixture to be separated and permitting no additional material to cross the boundaries of the column during the course of the separation. The theory for batch operation has been treated by many investigators [4 – 9], resulting in at least a correct qualitative description of experimental results.

There have been a number of relatively recent experimental studies of the continuous operation of thermogravitational columns [2, 3, 10 – 12]. The increasing industrial importance of separation processes has resulted in a substantial patent literature relating to design modifications for continuous process separation equipment utilizing thermal diffusion e.g. [13 – 27]. Most of these patents represent some alteration of thermogravitational column construction or operation with the view of increasing separation efficiency. The theory for the operation of a "centre-fed" thermogravitational column has been considered by several investigators [2, 3, 7, 10]; the term "centre-fed" describes the continuous operation in which feed is introduced at some vertical point of the column (usually the vertical centre, thus "centre-fed") and product streams are withdrawn from the top and bottom of the column

*Present Address: Department of Chemical Engineering, University of Texas, Austin, Texas, U.S.A.

Description of the new methods for the liquid phase continuous operation of a thermogravitational column with reservoirs

Experimental studies, excluding patent work, have considered only one continuous method for operating a thermogravitational column, "centre-fed" operation. It is the purpose of this paper to describe four new methods proposed by the author for continuous operation of thermogravitational columns. While the new methods of operation in altered form might be applied to gases, only the operation with liquid mixtures is considered here.

The apparatus used in the present study is described as a parallel plane plate thermogravitational column with reservoirs at the extremities of the vertical dimension. The reservoirs have volumes which are effectively large with respect to the volume contained between the parallel plates; the liquid filling the reservoirs communicates freely with the liquid between the parallel plates (see Fig. 1).

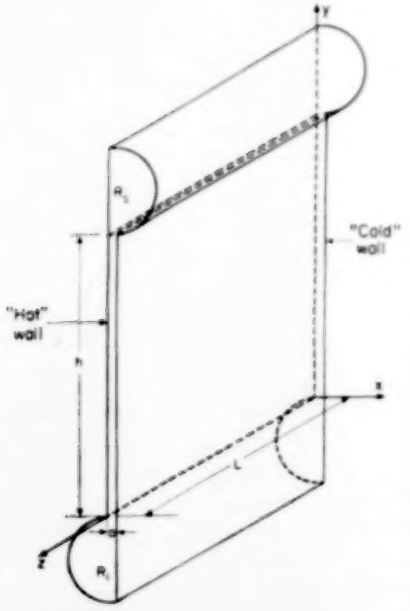

Fig. 1. A flat plate thermogravitational column with reservoirs: co-ordinate system and column dimensions

Legend:

R_s = Upper reservoir
R_i = Lower Reservoir
a = Plate spacing
h = Column heat transfer area height
L = Column length

Thermogravitational columns with reservoirs have been extensively employed in experimental studies of the unsteady-state batch operation of thermogravitational columns. The presence of reservoirs simplifies the mathematical description of the unsteady-state problem and has a practical effect in making possible greater accuracy in experimental work.

This study is concerned with the liquid phase continuous operation of a flat plate thermogravitational column with reservoirs. As an aid in understanding the description of the experimental and theoretical work which follows, each of the four new methods of continuous operation will be described briefly.

Two-feed cocurrent operation

The two-feed cocurrent operation of a flat plate thermogravitational column with reservoirs consists of the introduction at the same horizontal end of the column of liquid feed, not necessarily of the same concentration, at the upper and lower reservoirs. Liquid is withdrawn from the upper and lower reservoirs at the other horizontal end of the column. The flow pattern is indicated in Fig. 2 (a).

Introduction and withdrawal rates of liquid at the upper reservoir are adjusted so that there is a constant volumetric flow rate in the upper reservoir. Similarly a constant volumetric flow is maintained in the lower reservoir by proper adjustment of introduction and withdrawal rates.

In a thermogravitational column designed for operation with liquids the perpendicular distance between the hot and cold walls is usually in the range $10^{-2} - 10^{-1}$ cm. In this study the spacing between hot and cold walls was 0·0376 cm. The reservoirs were each semi-circular in section with a diameter of 0·952 cm. The significance of these dimensional values is that the pressure drop for flow between the parallel plates at isothermal conditions is of the order of a hundred times that for flow through the reservoirs.

Owing to this pressure-drop relation, the only

flow occurring during two feed cocurrent operation between the parallel plates is the natural convection arising from the temperature gradient; forced convection occurs only in the reservoirs. There are then two separate transverse flows in the column: natural convection in the $\pm y$ direction arising from the temperature gradient and forced convection in the $+z$ direction (cf. Fig. 2a) in each of the reservoirs arising from an externally imposed pressure gradient.

Calculations and experimental flow studies with the apparatus [28] showed that the flow conditions described above are substantially correct. Agreement between experimental and theoretical results lends further support for the described flow system.

There are several patents on cocurrent-type operation [15, 17, 29]. The various patented methods differ from that of the present study in that positive flow of material in the present method occurs only in the reservoirs. Some of the previous methods [15, 17] utilized plane plate construction without reservoirs; liquid was forced between the parallel plates with a resultant interference between forced convection in the $+z$ direction and natural convection in the $\pm y$ direction.

Two-feed countercurrent operation

This method of operation uses the same flow principles described above for two-feed cocurrent operation. The difference in two-feed countercurrent operation is that the feed streams to the two reservoirs enter at opposite ends of the apparatus as shown in Fig. 2(b). The product streams are also withdrawn from opposite ends of the column so that the flows in the two reservoirs move in a countercurrent manner to one another.

Just as for two-feed cocurrent operation natural convection occurs between the parallel plates and forced convection occurs in the reservoirs. Separate, transverse flows occur in the apparatus for two-feed countercurrent operation.

Single-feed cocurrent operation

Single-feed cocurrent operation denotes a method of operation in which liquid mixture is fed into only one of the two reservoirs. This procedure is illustrated in Fig. 2(c) where liquid is shown fed to the upper reservoir and product withdrawn from each reservoir at the other horizontal end of the column.

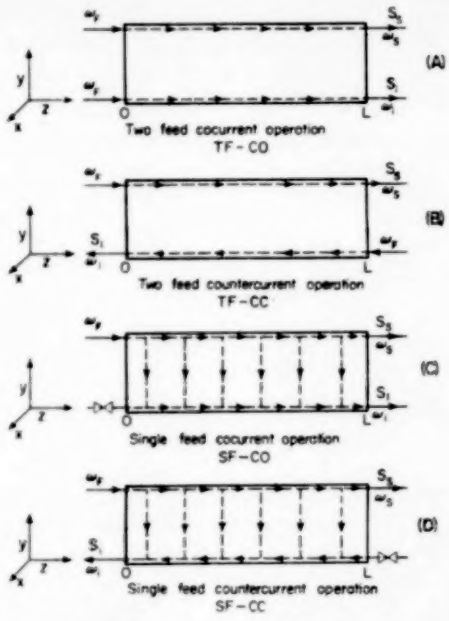

FIG. 2. Schematic flow diagram of the four methods for the liquid phase continouus operation of a thermogravitational column with reservoirs.

Legend:

ω = Mass fraction of that component of a binary mixture migrating to "hot" wall and concentrating toward the top of the column.

s = Product mass flow rate.

The pressure drop relation noted above in the discussion of two-feed cocurrent operation is of importance here. When liquid is withdrawn from the upper and lower reservoirs as shown in Fig. 2(c) the total product flow from the lower reservoir has come from the upper reservoir, and this flow was distributed uniformly over the horizontal length (z direction) of the column. Thus the volumetric flow rate determined from point to point between the parallel plates at isothermal conditions would have a constant value for fixed feed and withdrawal rates.

The difference between two-feed operation and single-feed operation now appears. With single-feed operation there is no longer a separation of

natural and forced convection. Between the parallel plates there occur both natural convection (in the $\pm y$ direction) and forced convection (in either, but not both, the $+$ or $-$ y direction). In addition with single feed operation the volumetric flow rate in the reservoirs is not a constant but is, to an approximation, a linear function of the horizontal dimension, z.

Single-feed countercurrent operation

Single feed countercurrent operation is similar to the single-feed cocurrent method described above, except that here liquid is withdrawn at opposite ends of the column. Fig. 2(d) illustrates the situation in which feed is introduced into the upper reservoir at one horizontal end ($z = 0$) and liquid is withdrawn from the upper reservoir at the other horizontal end of the column ($z = L$) and from the lower reservoir at the horizontal end where the feed was introduced ($z = 0$).

Experimental apparatus and procedure

Only a brief discussion will be given the experimental apparatus and procedure; full details can be found elsewhere [28].

Experimental apparatus

The flat plate thermogravitational column with reservoirs. The column was constructed of two rectangular pieces of Alcoa tool and jig plate, both plates having dimensions of approximately 34in. × 12in. × ¾in. The plates had been machine polished. The edges of the two plates were milled and one groove, semicircular in section and having a diameter of ¾in. was machined on the surface of each plate (see Figs. 3a and 4).

When placed in operating alignment the groove in the "hot" plate was at the bottom of the column and the groove in the "cold" plate was at the top of the column. The parallel surfaces between the two grooves had a height of 19·33 cm.

Sealing and formation of the space between the two plates was accomplished with a gasket cut from a sheet of Teflon, 34in. × 12in. × 0·0150in. ± 0·0005in. as shown in Fig. 3(b). Thin vertical strips at the positions indicated in the Fig. were found necessary for the achievement of a suitable plate spacing. For the column dimensions and the methods of operation studied these strips had a negligible influence on the experimental results.

In assembling the column the gasket was sandwiched between the surfaces of the two flat plates, the cooling conduit was placed on the back of the "cold" plate and the whole assembly was held together with sixty-five

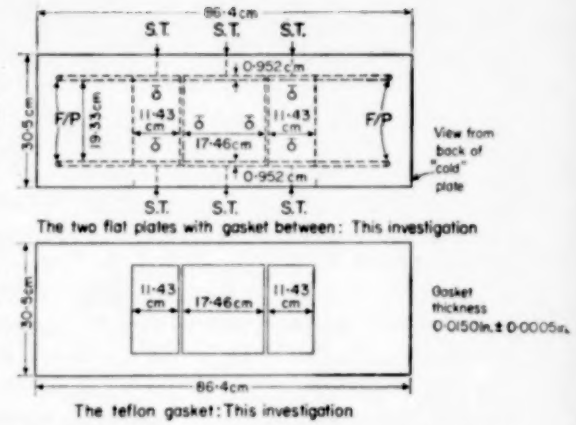

FIG. 3. Details of construction of thermogravitational column with reservoirs: column assembly and gasket.

Legend:
S.T. = Sample tap
δ = Thermocouple
F/P = Feed or product access
Scale: 1in. = 6in.

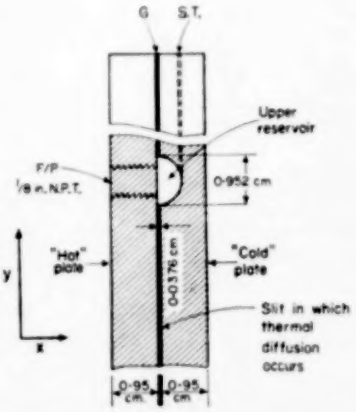

FIG. 4. Details of construction of thermogravitational column with reservoirs.
Detail section of upper reservoir

Legend:
S.T. = Sample tap
F/P = Feed or product access
G = Gasket
Scale: 1in. = 2in.

2½in. C-clamps placed at determined positions. Tests under pressure revealed no leaks in the assembly.

A satisfactory plate spacing was achieved by a system of pressure bolts which could be tightened against the back of the cold plate, thus pushing the cold plate toward the hot plate and eliminating a bowing tendency found when

VOL. 13 1961

the plates were clamped together. Three small ($\frac{1}{16}$in. × $\frac{3}{32}$in. × *a*) aluminium spacers were used together with the Teflon strips of the gasket to maintain a given plate spacing; "*a*" is the plate spacing.

Plate spacing was determined by injecting a modified liquid plaster of Paris mixture into the assembled column and allowing the mixture to harden. Through a trial-and-error procedure the correct torque wrench setting for the pressure bolts was determined to give a desired plate spacing. In a typical plate spacing determination, out of 26 measurements spaced over the heat transfer surface, 20 were within ± 0·0002in. of 0·0152in.; the remainder deviated at most by ± 0·0005in.

In order that all experimental runs would be self-consistent the column was assembled in the manner described above and sufficient time was allowed for cold flow of materials to take place (judged as 2 months). All experimental runs were then conducted with the assembly with checks on plate spacing furnished periodically by batch steady-state separation determinations. After all runs were completed a plaster of Paris plate spacing determination was made. For the experimental runs reported here the periodic steady state separation determinations gave the same value over the time of the runs and the final plate spacing determination based on 26 measurements gave a vlaue of 0·0148in. ± 0·0005in. This is the plate spacing value used in all subsequent calculations.

Cooling system. The "cold" wall temperature was maintained by flowing water through a conduit which fitted over the back of the "cold" plate. The area perpendicular to the flow direction was 9·5in. × $\frac{3}{32}$in.

Provision was made for mixing water available at 80 °C with water available at a minimum of 13 °C so that the "cold" wall temperature could be adjusted to a desired value.

The cooling water was passed through a series of two surge tanks to eliminate small pressure fluctuations produced by the control valves. Connection was made to the cooling conduit by two $\frac{1}{8}$in. inlets; cooling water exited from the conduit through two $\frac{1}{4}$in. outlets. Vibration was minimized by the use of rubber hose connections.

During operation the "cold" wall temperature over the plate surface deviated from an average value by ± 0·5 °C.

Temperature of the "cold" wall was determined by six iron–constantan thermocouples distributed over the "cold" plate. The junctions were fitted into holes extending to within $\frac{1}{32}$in. or less of the "cold" wall. The thermocouple leads were connected to a Leeds and Northrup Speedomax recorder. Recorder and thermocouples were calibrated against a Leeds and Northrup Precision potentiometer.

Heating system. The "hot" wall temperature was maintained by a specially constructed electrical radiant heater. By varying the radiant properties of the back of the "hot" plate, end losses and convection effects could be corrected.

A General Radio Corp. Type 50B, 230 V, 7 kVA, 50–60 cycle variable reactance provided a variable voltage to the heating unit.

Using the heating system just described it was found that the "hot" wall temperature could be maintained to within ± 0·7 °C of a given value over the surface in the range 49–59 °C. The "hot" wall temperatures were measured by six iron–constantan thermocouples placed with junctions $\frac{1}{32}$in. or less from the "hot" wall. The thermocouple leads were connected to the temperature recorder described above.

Feed and product system. The flow system used in this investigation is shown schematically in Fig. 5. Feed mixture was pumped by a Milton-Roi "miniPump" from a stirred collecting vessel to a constant-head feed vessel; overflow from the feed vessel returned to the collecting vessel.

Liquid feed was conducted from the feed vessel through two feed rotameters (for two-feed operation) with regulation supplied by two feed needle valves. Product from the thermogravitational column was passed through two product rotameters with regulation supplied by two product needle valves and 3in. lengths of copper tubing packed with 200 mesh glass spheres.

Feed and product rotameters were obtained from the

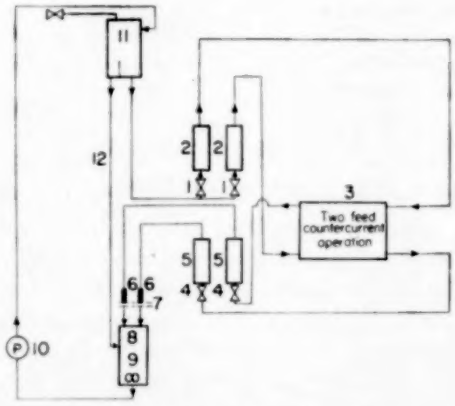

FIG. 5. Flow system for flat plate thermogravitational column with reservoirs.

Legend:

1. Feed valves
2. Feed rotameters
3. Thermogravitational column with reservoirs
4. Product valves
5. Product rotameters
6. Packed resistance tubes
7. Product mass flow rate measurement
8. Collecting tank
9. Magnetic stirrer
10. Feed pump
11. Constant head feed tank
12. Overflow return line

Manostat Corp., Cat. # 9143b. Modification of the tubes to eliminate parallax made it possible to reproduce a given flow rate in the rotameters to ± 0·1 per cent or better.

The liquid mixture studied in this investigation contacted only the following materials: glass, stainless steel, brass, copper, tin, aluminium, Teflon and sapphire.

Experimental procedure

Feed mixture. The binary mixture, *n*-heptane–benzene was chosen for this study.

Benzene (Reagent grade) was obtained from the Fisher Scientific Co. and had a measured refractive index at 25 °C of 1·4979 which agrees with the quoted literature value [30]. *n*-Heptane was obtained from the same vendor and had a refractive index at 25 °C of 1·3852 which agrees with the quoted literature value [30]. No further purification of the chemicals was made.

Flow rate measurement. A timed sample of each product flow was taken in a glass weighing bottle fitted so as to prevent evaporation. The timing of the collected sample was performed with an electric timer from the Standard Electric Time Co. The collected, timed samples were weighed on a Christian Becker Chainomatic analytical balance.

Composition measurement. Composition of the liquid feed and product streams was determined by measurement of the refractive index at 25 °C with a Bausch and Lomb Abbe Refractometer.

THEORETICAL DESCRIPTION

Description of the four methods of operation in terms of experimental quantities depends on solution of the equations of conservation of mass, momentum and energy for the physical system. This solution is accomplished here by development of the " transport " equation through a procedure originated by FURRY *et al.* [7] for gases and extended to liquids by DE GROOT [8]. The " transport " equation is a statement in differential form of the net rate at which a particular component of a binary mixture is being " transported" in the vertical direction in a thermogravitational column.

Other methods have been developed for the solution of the conservation equations in describing the operation of the thermogravitational column. The various methods of solution have been discussed in a comprehensive review by LONGMIRE [2].

Derivation of the transport equation for the liquid phase continuous operation of a flat-plate thermogravitational column with reservoirs

The equations of conservation of mass, momentum and energy have been discussed by BIRD [31] whose nomenclature will be used in this discussion.

Fig. 1 presents the description of the geometry of the flat plate thermogravitational column with reservoirs. The right-handed Cartesian co-ordinate system has its origin at the lower edge of the " hot " wall. The $+z$ axis runs along the lower edge of the " hot " wall. " L " denotes the length of the heat transfer area along the z axis. " a " is the distance along the $+x$ axis to the " cold " wall. " h " is the height of the heat transfer area along the $+y$ axis.

The following assumptions are made in the development which follows:

1. Steady state
2. Binary mixture
3. No chemical reaction
4. Laminar, Newtonian, flow

   $v = v_y(x)$; $0 < y < h, x, z$. $p = p(y)$; $0 < y < h, x, z$.

   $v = v_s$; $h < y, x, z$. $v = v_i$; $0 > y, x, z$. $p \doteq$ const; $0 > y$, $h < y, x, z$.
5. Only thermal and ordinary diffusion contribute to the mass flux.
6. Thermal conduction is the only important mode of heat transport

   $T = T(x)$; $0 < y < h, x, z$.

   $T = (T_R)_{av.}$; $0 > y, h < y, x, z$.

where v denotes the velocity, v_s is the average velocity in the upper reservoir, v_i the average velocity in the lower reservoir, p is the pressure, T the temperature, and $(T_R)_{av.}$ the average temperature in the reservoirs.

The transport equation will now be developed for two-feed operation; assumptions described later permit a simple modification of this development so that single-feed operation is described.

With the assumptions noted above the solution

VOL. 13 1961

of the energy balance equation for the region $0 < y, < h, x, z$ is

$$\frac{dT}{dx} = \frac{T_H - T_C}{a} = \frac{\Delta T}{a} \tag{1}$$

The solution of the equation of motion becomes for the same region with the usual assumptions and boundary conditions:

$$v_y(x) = -\frac{(\cos\theta)\,\beta\rho\,g}{6\mu}\frac{\Delta T}{a}\,x\,(x - \tfrac{1}{2}a)\,(x - a); \qquad 0 < y < h, x, z \tag{2}$$

a third-degree equation for the velocity.

For the assumptions above the mass flux expression for component "1" of the binary mixture is

$$\vec{j}_1 = -\rho\,D_{12}\,\vec{\nabla}\,\omega_1 - \rho\,D_{12}\,\sigma_1\,\omega_1\,\omega_2\,\vec{\nabla}\,T \tag{3}$$

where $\vec{j}_1$ is the mass flux vector referred to a coordinate system moving with the mass average velocity, [g/(cm² sec⁻¹)], ρ is the mass density of the solution, (g/cm³), D_{12} is the mutual diffusion coefficient for a binary mixture, (cm²/sec), ω_1 the mass fraction of that component of the binary mixture travelling to the "hot" wall and enriched at the top of the column (component "1") σ_1 is the Soret coefficient of "1", (degree⁻¹).

Inserting equation (6) in the equation of continuity gives with appropriate assumptions for the region $0 < y < h, x, z$.

$$0 = -v_y\frac{\partial\omega_1}{\partial y} + D_{12}\left(\frac{\partial^2\omega_1}{\partial x^2} + \frac{\partial^2\omega_1}{\partial y^2} + \frac{\partial^2\omega_1}{\partial z^2}\right) + \sigma_1\,D_{12}\,\frac{\Delta T}{a}\,\frac{\partial\,(\omega_1\omega_2)}{\partial x} \tag{4}$$

where it has been assumed that the dependence of ρ, D_{12}, and σ_1 on x, y and z can be accounted by assuming average values. A solution of equation (7) is sought for the boundary conditions on x

$$\frac{\partial\omega_1}{\partial x} + \sigma_1\frac{\Delta T}{a}\,\omega_1\omega_2 = 0\,; \quad x = 0, a \tag{5}$$

Conditions for the y and z dimensions will be introduced below.

In developing the "transport" equations FURRY *et al.* [7] and DE GROOT [8] neglect for the moment the diffusion in the y direction and later in the development account for this term. It will be found that only for very small values of the plate spacing, a, does this neglected term contribute to the "transport."

Strictly the term accounting for diffusion in the z direction cannot be neglected at this point unless it is negligible. Here diffusion in the z direction will be assumed negligible on the same basis that diffusion in the y direction can be neglected; this basis is that the transfer of "1" by the convective flows is much greater than the transfer of "1" by ordinary diffusion.

These diffusion terms may be introduced by writing for the net rate of transport of component "1" up the column, $m\,(x, y, z)$, at any point, z

$$\frac{\partial\,m\,(x, y, z)}{\partial y} = \int_0^a \tau\,(x, y, z)\,dx$$

where $\tau\,(x, y, z)$ is the concentration diffusion flux in the z direction at a point in the column in the region $0 < y < h, x, z$. Since the change in concentration in the x direction is small, an average value, $\bar{\tau}\,(y, z)$, for this diffusion flux can be assumed

$$\frac{\partial\,m\,(x, y, z)}{\partial y} = \bar{\tau}\,(y, z) = -\rho\,D_{12}\frac{\partial\bar{\omega}_1}{\partial z}$$

where $\bar{\omega}_1$ denotes the mass fraction of "1" averaged over x. It follows that

$$m\,(x, y, z) = m\,(x, 0, z) + \int_0^y \bar{\tau}\,(\xi, z)\,d\xi$$

This equation indicates that if concentration diffusion in the z direction is negligible the net rate of transport of component "1" is a function only of x and z. By a similar procedure diffusion in the y direction can be accounted by including in the net rate of transport of "1" up the column the transfer by diffusion in the y direction.

Assume that concentration diffusion in the z direction is negligible compared with the rate at which "1" is transported by free convection. With this assumption one then obtains the result of FURRY *et al.* [7] and DE GROOT [8] which states that in the x–y plane at any point z the net rate

at which component "1" is moving up the column, $m(z)$ is:

$$m(z) = -\left[\frac{1}{9!}\left(\frac{\beta\rho g}{\mu}\right)^2 \frac{\rho a^7}{D_{12}}(\Delta T)^2 \cdot \cos^2\theta + \rho D_{12} a\right] \times \times \frac{\partial \bar{\omega}_1}{\partial y} - \left[\frac{1}{6!}\left(\frac{\beta\rho g}{\mu}\right)\rho\sigma_1 a^3 (\Delta T)^2 \cdot \cos\theta\right] \bar{\omega}_1\bar{\omega}_2 \quad (6)$$

for the region $0 < y < h, x, z$. The usual assumptions have been made in obtaining this equation.

The difference between equation (6) and the "transport" equations of Furry *et al.* and de Groot is that equation (6) defines the "transport" in a plane perpendicular to the z axis in a system in which z is an independent variable; [7] and [8] did not consider z as a variable in their developments.

Introducing the notation of the "transport constants" H^* and K^* into equation (6)

$$m(z) = -H^* \omega_1\bar{\omega}_2 - K^* \frac{\partial \omega_1}{\partial y} \quad (7)$$

where H^* and K^* are defined by equation (6). Equation (7) is the form of the "transport" equation to be used in the developments for two-feed cocurrent and countercurrent operation.

Separation equations for two-feed cocurrent and countercurrent operation

Two-feed cocurrent operation. This method of operation has been described previously and is illustrated schematically in Fig. 2(a).

In what follows it is assumed that the same degree of mixing prevails along the entire length of the reservoirs. This assumption applies to the other methods of operation to be discussed. The assumption holds since temperature conditions are the same over the length of the reservoir and there is a relatively large natural convective velocity in the reservoir which describes, in column operation, a helical path about the z axis.

In the development of equation (7) it has been assumed that there are separate, transverse flows in the column corresponding to the forced convection in the reservoirs and natural convection between the parallel plates. With this assumption a material balance can be written about any element Δz of the reservoir length, L. For two-feed cocurrent operation, the reservoir material balances are

$$s_s \frac{d\omega_{1s}}{dz} = m(z) \quad (8)$$

$$s_i \frac{d\omega_{1i}}{dz} = -m(z) \quad (9)$$

where average values for the mass densities of the solutions in the reservoirs have been assumed to account for the variation of ρ with z. s_s and s_i are the average mass flow rates in the upper and lower reservoirs respectively (g/sec) and ω_{1s} and ω_{1i} are the mass fractions of component "1" in the upper and lower reservoirs.

Since the "transport" $m(z)$, at any z is independent of y (if concentration diffusion in the z direction is negligible) the integrations of equation (7) over y and z may be performed separately.

Equation (7) can be integrated over the y direction as it is written. However, the non-linearity does not permit the following integration in the z direction in closed form. The problem of the integration of the "transport" equation has received attention from Jones and Furry [32] who recognize two approximations, which for the present purpose will give expressions for the separation over the column in a convenient form.

The following approximations are made:

$$\bar{\omega}_1\bar{\omega}_2 \doteq \tfrac{1}{4}; \quad 0{\cdot}3 < \bar{\omega}_1 < 0{\cdot}7$$
$$\bar{x}_1\bar{x}_2 \doteq \tfrac{1}{4}; \quad 0{\cdot}3 < \bar{x}_1 < 0{\cdot}7 \quad (10)$$

for concentrated solutions where $\bar{x}_1$ and $\bar{x}_2$ are average mole fractions of "1" and "2." For dilute solutions the linear approximation

$$\bar{\omega}_1\bar{\omega}_2 \doteq a'\bar{\omega}_1 + b \quad (11)$$

will be used. For all dilute solution experimental runs of this investigation the constants are taken to be $a' = 0{\cdot}7$, $b = 0{\cdot}02$.

Equation (7) is integrated over y with the boundary conditions

$$\bar{x}_1 = x_{1s}, \quad y = h$$
$$\bar{x}_1 = x_{1i}, \quad y = 0 \quad (12)$$

Equations (8) and (9) and the integrated form

VOL. 13 1961

of equation (7) are solved for the boundary condition:

$$\Delta = x_{1s} - x_{1i} = 0, \quad z = 0 \tag{13}$$

The solution is for the approximation of equation (10)

$$x_{1s} - x_{1i} = \\ = \frac{H^* h}{4K^*}\left[\exp\left\{-\frac{K^* z}{h}\left(\frac{1}{s_s}+\frac{1}{s_i}\right)\right\} - 1\right] \tag{14}$$

For the dilute linear approximation equation (11), the solution is

$$\omega_{1s} - \omega_{1i} = -\left(\omega_F + \frac{b}{a'}\right) \times \\ \times \left[\frac{1-\exp(-\phi_1)}{1+(s_s/s_i)\exp(-\phi_1)}\right] \times \\ \times \left[1 - \exp\left\{-\frac{[1+(s_s/s_i)\exp(-\phi_1)]z}{(s_s/a'H^*)[1-\exp(-\phi_1)]}\right\}\right] \times \\ \times \left(1+\frac{s_s}{s_i}\right) \tag{15}$$

where: $\phi_1 = a'H^*h/K^*$ (16) and ω_F denotes the mass fraction of "1" in the feed mixture.

Two-feed countercurrent operation. The development of separation equations for two-feed countercurrent operation parallels the development for two-feed cocurrent operation.

The reservoir material balances are

$$s_s \frac{d\omega_{1s}}{dz} = m \tag{17}$$

$$s_i \frac{d\omega_{1i}}{dz} = m \tag{18}$$

Equations (17), (18) and (7) are to be solved for the boundary conditions

$$\begin{aligned} \bar{\omega}_1 &= \omega_{1s}, \quad y = h \\ \bar{\omega}_1 &= \omega_{1i}, \quad y = 0 \\ \omega_{1s} &= \omega_F, \quad z = 0 \\ \omega_{1i} &= \omega_F, \quad z = L \end{aligned} \tag{19}$$

The separation equation for the dilute approximation, equation (11), is

$$\omega_{1s} - \omega_F = -\frac{[\omega_F + (b/a')][1-\exp(\phi_1)]}{(s_s/s_i)\exp(-BL) - \exp(\phi_1)} \times \\ \times [1 - \exp(-Bz)] \tag{20}$$

where ϕ_1 is defined in equation (16). Also

$$B = \frac{a'H^*}{s_s}\left[\frac{\exp(\phi_1) - (s_s/s_i)}{\exp(\phi_1) - 1}\right] \tag{21}$$

Separation equations for single-feed operation

In single-feed operation there is a positive flow of fluid in the y direction produced by a pressure difference between the two reservoirs. Thus, in the space between the parallel plates forced convection is superimposed on the free convection arising from the temperature gradient.

For a unidirectional velocity field produced by a very small additional pressure difference JONES and FURRY [32] point out that this field may be superimposed on the free convection field.

If the further assumption is made of a small variation of the concentration of "1" in the y direction (this assumption was implied in the derivation of the "transport" equation) the only change in the "transport" of "1" up the column for single feed operation takes the form of an additional term to account for the positive transport of "1" in the $+$ or $-y$ direction caused by forced convection.

It was pointed out that to an approximation the total flow out of the feed reservoir to the other reservoir is distributed uniformly over the total column length, L. With the assumptions discussed above the "transport" equation for single-feed operation becomes

$$m'(z) = H^* \bar{\omega}_1 \bar{\omega}_2 + K^* \frac{\partial \bar{\omega}_1}{\partial y} + r\bar{\omega}_1 \tag{22}$$

where m' is now the g cm^{-1} sec^{-1} of species "1" transported down the column; r is the positive total flow down the column (g cm^{-1} sec^{-1}).

Separation equations for single-feed cocurrent operation. The development of separation equations for single-feed operation is analogous to the procedure followed for two-feed operation.

The reservoir material balances have the form

$$(s_0 - rz)\frac{d\omega_{1s}}{dz} - r\omega_{1s} = -m' \tag{23}$$

$$rz\frac{d\omega_{1i}}{dz} + r\omega_{1i} = m' \tag{24}$$

where s_1 is the total feed rate to the column

(g/sec). The solution to equations (22), (23) and (24) is subject to the boundary conditions on y.

$$\bar{\omega}_1 = \omega_{1s}, \quad y = h \tag{25}$$

$$\bar{\omega}_1 = \omega_{1i}, \quad y = 0 \tag{26}$$

In order to obtain equations in closed form the following assumptions are made in solving equations (22), (23) and (24) :

$$\exp\left(-\frac{rh}{K^*}\right) \ll 1 \tag{27}$$

for the case of concentrated solutions and

$$\exp\left[-\frac{(a' H^* + r)\, h}{K^*}\right] \ll 1 \tag{28}$$

for dilute solutions.

The separation equation for the concentrated solution approximation, equations (10) and (27), is

$$\omega_{1s} - \omega_{1i} = \left(\frac{s_0}{rz}\right)\frac{H^*}{4r} \ln\left(1 - \frac{rz}{s_0}\right) \tag{29}$$

For the dilute linear approximation, equations (11) and (28),

$$\omega_{1s} - \omega_{1i} = \left(\frac{s_0}{rz}\right)\left(\omega_F + \frac{b}{a'}\right)\left[\left(1 - \frac{rz}{s_0}\right)^{\frac{a'H^*}{r}} - 1\right] \tag{30}$$

the separation equation for dilute solutions is obtained.

Separation equations for single-feed countercurrent operation. The development of separation equations for this method of operation follows the procedure given for single-feed cocurrent operation.

The reservoir material balances are

$$(s_0 - rz)\frac{d\omega_{1s}}{dz} - r\omega_{1s} = -m'$$

$$r(L - z)\frac{d\omega_{1i}}{dz} - r\omega_{1i} = -m'$$

When the assumptions of equations (27) and (28) are made the developed separation equations for this method of operation are identical to equations (29) and (30).

Experimental results

Experimental runs were made for the four methods of operation using the binary system, *n*-heptane–benzene. Additional experimental data were taken for the unsteady state batch operation of the column of this investigation ; these data are reported elsewhere [28] and are not given here.

Two-feed cocurrent operation results

The most direct test of the various assumptions given above in the discussion of the theory of two-feed cocurrent operation is provided by a comparison of the experimental data for two-feed cocurrent operation with the corresponding separation equations, equations (14) and (15).

For the concentrated solutions the separation equation, equation (14), may be arranged to give the following indicated relationship :

$$-\left(\frac{1}{s_s} + \frac{1}{s_i}\right) = C_1 \ln\left(1 - \frac{\Delta}{\Delta_0}\right) \tag{31}$$

where C_1 is a constant :

$$C_1 = (h/K^*L) \tag{32}$$

and s_s and s_i are the mass flow rates in the upper and lower reservoirs, g sec^{-1}, Δ is the difference in concentration of species " 1 " in the upper and lower reservoirs for given mass flow rates and Δ_0 is that steady state separation determined by extrapolation of experimental data for two-feed cocurrent operation to zero mass flow rate, and as also determined from experimental batch separation data.

For the case of dilute solutions the separation equation, equation (15), may be arranged :

$$-\left(\frac{1}{\bar{s}}\right) = C_2 \ln\left(1 - \frac{\Delta}{\Delta_0}\right) \tag{33}$$

where C_2 is a constant :

$$C_2 = \frac{[1 - \exp(-\phi_1)]}{a'H^* L\,[1 + \exp(-\phi_1)]} \tag{34}$$

and $\bar{s}$ is the average of the flow rates for " symmetric " runs in the upper and lower reservoirs. The term " symmetric " indicates that the experimental run was performed with approximately equal mass flow rates in the upper and

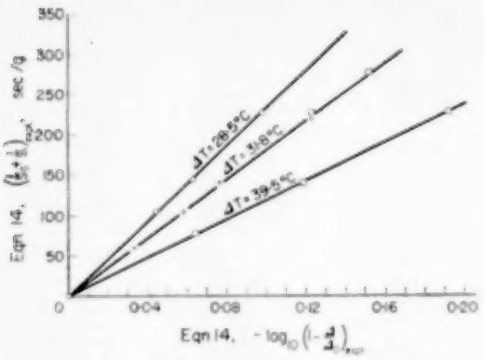

FIG. 6. Agreement of experimental data with linear relation predicted by equation (14) for two-feed co-current operation.

Legend:

	○	+	■	□
ΔT	28·5C	31·8C	39·5C	31·8C
x_F	0·500	0·500	0·500	0·500

Runs	TF–SCO–K 1, 3, 4	TF–SCO–K 1–5
	TF–SCO–K 3–5	TF–USCO–K 6, 7

$\Delta = x_s - x_i$, separation
Δ_0 = Separation, zero flow rate
x = Mole fraction n-heptane in reservoir product
s = Product mass flow rate

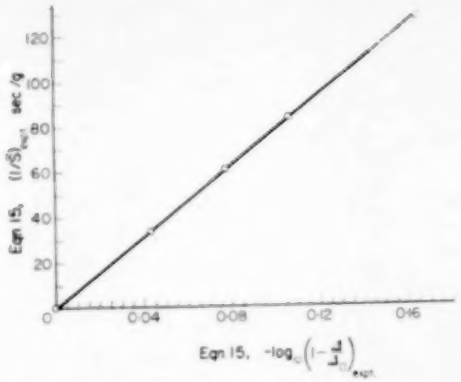

FIG. 7. Agreement of experimental data with linear relation predicted by equation (15) for two-feed cocurrent operation.

Legend:

○ = Two-feed cocurrent experimental point: Runs TF–SCO–D, 1–4
ΔT: 31·6 °C
ω_F: 0·150
Δ_0 = Steady state separation, zero flow rate
$\Delta = \omega_s - \omega_i$, separation
ω = Mass fraction n-heptane in reservoir product
$\bar{s}$ = Arithmetic average of upper and lower product flow rates $= \frac{1}{2}(s_s + s_i)$

lower reservoirs, – a situation realized to $\pm 0{\cdot}1$ per cent of the average for the larger flow rates.

Figures 6 and 7 present the experimental substantiation of the indicated relationships of equations (31) and (33). Fig. 6 presents experimental data for a feed concentration of 0·500 mole fraction n-heptane (termed the " K " series) and the indicated three different temperature differences. Fig. 7 shows experimental data for a feed concentration of 0·150 weight fraction n-heptane (termed the " D " series) at a temperature difference of 31·6 °C. It can be seen that the agreement with the indicated relationship is good. At lower reservoir mass flow rates the experimental data do not follow these straight lines, since for these low flow rates the separation becomes large and therefore the linear approximations, equations (10) and (11), and the assumption of constant mass flow rate in the reservoirs fail to describe the physical situation; also restrictions applied in the derivation of the " transport " equation, equation (7), are violated.

The constant in equation (31), the slopes of the straight lines of Fig. 6, contains the column height, h, length, L and the " transport constant," K^*. Therefore K^* can be measured by direct experimentation. This is analogous to the procedure which has been used [3, 33] for determination of " transport constants " from unsteady-state batch operation data. H^* can be calculated in turn from

$$\Delta_0 = \frac{-H^* h}{4K^*} \tag{35}$$

using the experimentally determined zero flow rate steady state separation Δ_0. Another method for determination of H^*, which in general will not agree with the value determined from equation (35), since the linear approximation is introduced in deriving equation (35), is to calculate H^* from

Table 1. *Comparison of experimental and calculated values of "Transport Constants*[1]*."*

Experimental series[2]	$K^*_{expt.}$ *equation* (14, 15)	$K^*_{calc.}$ *equation* (6)	$H^*_{expt.}$ *equation* (36)	$H^{*3}_{expt.}$	$H^*_{calc.}$ *equation* (6)
TF–SCO–K $\Delta T = 31{\cdot}8$ °C $\bar{T} = 307{\cdot}3$ °K	$6{\cdot}17 \times 10^{-4}$ $\pm 0{\cdot}60 \times 10^{-4}$	$4{\cdot}4 \times 10^{-4}$ $\pm 0{\cdot}2 \times 10^{-4}$	$-6{\cdot}77 \times 10^{-5}$ $\pm 0{\cdot}06 \times 10^{-5}$	$-6{\cdot}20 \times 10^{-5}$ $\pm 0{\cdot}06 \times 10^{-5}$	$-1{\cdot}83 \times 10^{-5}$ $\pm 0{\cdot}03 \times 10^{-5}$
TF–SCO–K $\Delta T = 28{\cdot}5$ °C $\bar{T} = 304{\cdot}9$ °K	$4{\cdot}78 \times 10^{-4}$ $\pm 0{\cdot}05 \times 10^{-4}$	$3{\cdot}5 \times 10^{-4}$ $\pm 0{\cdot}1 \times 10^{-4}$	$-5{\cdot}24 \times 10^{-5}$ $\pm 0{\cdot}05 \times 10^{-5}$	$-4{\cdot}78 \times 10^{-5}$ $\pm 0{\cdot}05 \times 10^{-5}$	$-1{\cdot}42 \times 10^{-5}$ $\pm 0{\cdot}03 \times 10^{-5}$
TF–SCO–K $\Delta T = 39{\cdot}5$ °C $\bar{T} = 312{\cdot}4$ °K	$9{\cdot}38 \times 10^{-4}$ $\pm 0{\cdot}09 \times 10^{-4}$	$7{\cdot}0 \times 10^{-4}$ $\pm 0{\cdot}3 \times 10^{-4}$	$-10{\cdot}3 \times 10^{-5}$ $\pm 0{\cdot}1 \times 10^{-5}$	$-9{\cdot}39 \times 10^{-5}$ $\pm 0{\cdot}09 \times 10^{-5}$	$-2{\cdot}66 \times 10^{-5}$ $\pm 0{\cdot}03 \times 10^{-5}$
TF–SCO–D $\Delta T = 31{\cdot}6$ °C $\bar{T} = 306{\cdot}1$ °K	$4{\cdot}44 \times 10^{-4}$ $\pm 0{\cdot}04 \times 10^{-4}$	$4{\cdot}7 \times 10^{-4}$ $\pm 0{\cdot}2 \times 10^{-4}$	— —	$-9{\cdot}26 \times 10^{-5}$ $\pm 0{\cdot}09 \times 10^{-5}$	$-3{\cdot}91 \times 10^{-5}$ $\pm 0{\cdot}03 \times 10^{-5}$

[1]. K series transport constants calculated from mole fractions; D series transport constants calculated from mass fractions.

[2]. Code explanation: K, Feed concentration 0·500 mole fraction *n*-heptane in benzene; D, Feed concentration 0·150 mass fraction *n*-heptane in benzene; TF, Two feed operation; CO, Cocurrent operation; S, Symmetrical operation, approximately equal product mass flow rates.

[3]. H^* values for K series calculated using equation (35); H^* values for D series calcualted using equation (15).

the solution of the "transport" equation, at zero flow rate and steady state. The solution is:

$$\frac{\omega_{1s}}{1-\omega_{1s}} \cdot \frac{1-\omega_{1i}}{\omega_{1i}} = \exp\left[-\left(\frac{H^* h}{K^*}\right)\right] \qquad (36)$$

For consistency the calculation of H^* by equation (35) is to be preferred.

By a similar procedure for the dilute solutions H^* and K^* can be calculated from the slope of the line of Fig. 7 and equation (33).

It is well known that experimentally determined "transport constants" do not agree in general with values calculated from the defining equation, equation (6) for example. The disagreement is particularly serious for liquids and has not yet been satisfactorily explained.

Table 1 is a summary of the comparison of calculated (equation 6) and experimental values of the "transport constants." Physical property data for the system *n*-heptane–benzene used in calculating H^* and K^* from equation (6) are from Refs. [10] and [34]. In agreement with comparisons for other liquid systems the Soret coefficient determined in the thermogravitational column is much larger than the coefficient determined by the methods in which all convection effects are eliminated. For the present system the comparison of the Soret coefficient determined by the thermogravitational column with values determined by the unsteady-state cell method [34] is made at two difierent concentrations in Table 2.

In further consideration of the other operating methods of this investigation the experimentally determined "transport constants" of Table 1 will be used in the various equations which have been developed.

Table 2. Comparison of Soret coefficients determined from thermogravitational column measurement in this investigation with Soret coefficients determined by measurement of pure Soret effect. System: n-heptane–benzene

Average temperature: 307·2 °K
Pressure: 1 atm

Mass fraction n-*heptane*	TG. *col. this investigation*[1,2]	USS *Cell measured by* BIERLEIN *et al.* [34]
0·562	$-4{\cdot}9 \pm 0{\cdot}2\ (10^{-3})$	$-1{\cdot}37 \pm 0{\cdot}04\ (10^{-3})$
0·150	$-7{\cdot}1 \pm 0{\cdot}3\ (10^{-3})$	$-3{\cdot}02 \pm 0{\cdot}04\ (10^{-3})$

[1] Sign is negative if *n*-heptane goes to "hot" wall.
[2] Calculated from mass fractions.

Figures 8 and 9 represent all the data for two-feed cocurrent "symmetrical" operation. For both the concentrated solution (0·500 mole fraction *n*-heptane) and the dilute solution (0·150 mass fraction *n*-heptane) it can be seen that equations (14) and (15) predict larger separations at the lower flow rates than found experimentally. The assumptions made in deriving the separation equations are valid only for small separations; the disagreement at the lower flow rates therefore is to be expected.

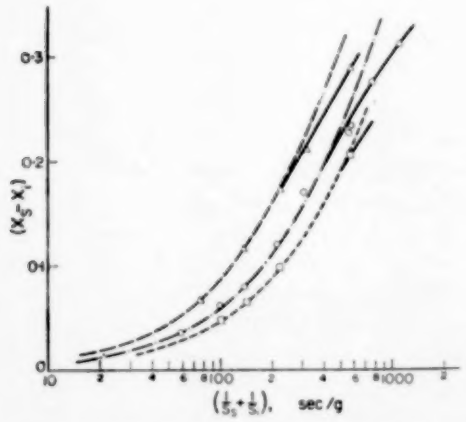

FIG. 8. Upper and lower reservoir product concentration difference vs. sum reciprocal product rates: two-feed cocurrent operation.

Legend:

	△	○	□
ΔT (°C)	39·5	31·8	28·5
Runs	TF–SCO–K 1–5	TF–SCO–K 1–9	TF–SCO–K 1–4
Eqn. (14)	— — —	— — — —	— · —

x = Mole fraction *n*-heptane in product
s = Reservoir product mass flow rate

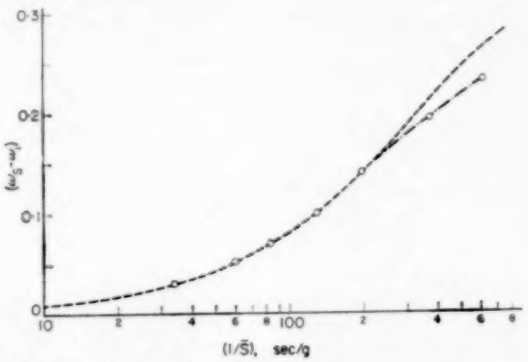

FIG. 9 Upper and lower reservoir product concentration difference vs. reciprocal average product rate: two-feed cocurrent operation.

Legend:
○ = Runs TF–SCO–D, 1–7
– – – – equation (15): $a' = 0{\cdot}7$, $b = 0{\cdot}02$
$\Delta T = 31{\cdot}6$ °C
$\omega_F = 0{\cdot}150$
ω = Mass fraction *n*-heptane in product
$\bar{s}$ = Arithmetic average of reservoir product mass flow rates $= \frac{1}{2}(s_s + s_f)$

Figures 10 and 11 present the experimental results of "asymmetric" (unequal flow rates in the two reservoirs) two-feed cocurrent operation. The experimental results are indicated by the solid curves which represent separations obtained at a fixed lower reservoir product mass flow rate while varying the upper reservoir product mass flow rate. Comparison is made between the experimental curves and those predicted by equations (14) and (15). As expected, the agreement becomes poorer with increasing separation.

It is of interest to compare the experimental separations found with two-feed cocurrent operation with those found in "centre-fed" operation of a thermogravitational column. Fig. 12 presents such a comparison. The two upper curves represent the experimental curves obtained in the

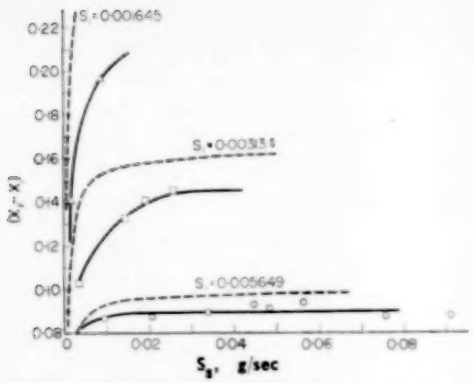

FIG. 10. Feed and lower reservoir product concentration difference vs. upper reservoir flow rate: two-feed cocurrent operation.

Legend:
ΔT = 31·7 °C
Runs TF–USCO–K, 1–13
s_i = 0·001645 g/sec
s_i = 0·003134 g/sec
s_i = 0·005649 g/sec
– – – – – equation (14)
x = Mole fraction *n*-heptane
s = Product mass flow rate

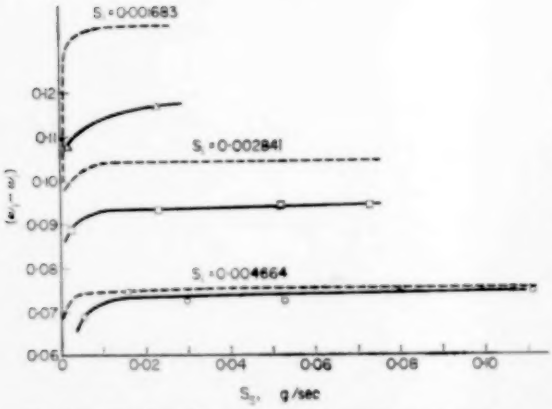

FIG. 11. Feed and lower reservoir product concentration difference vs. upper reservoir flow rate: two-feed cocurrent operation.

Legends:
ΔT = 31·6 °C
Runs TF–USCO–D 1–10
△ s_i = 0·001683 g/sec
□ s_i = 0·002841 g/sec
○ s_i = 0·004664 g/sec
– – – – equation (15) a' = 0·7; b = 0·02
ω = Mass fraction *n*-heptane
s = Product mass flow rate

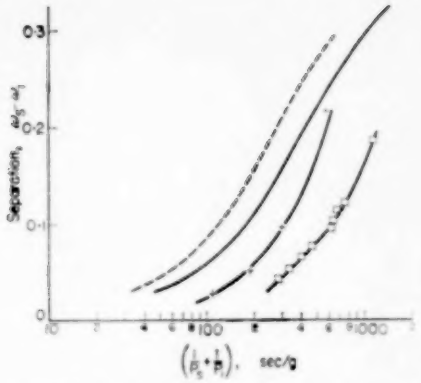

FIG 12. Comparison of "centre-feed" operation with two-feed cocurrent operation.

Legend:
This investigation:
——— TF–SCO–K, ΔT = 31·8 °C
– – – – – TF–SCO–K, ΔT = 39·5 °C
a = 0·0376 cm
Data of LONGMIRE [2];
"Centre-feed operation"
+ ΔT = 37·2 °C; a = 0·079 cm
□ ΔT = 36·0 °C; a = 0·043 cm
ω = Mass fraction *n*-heptane in product
P = Product mass flow rate.

present study for two-feed cocurrent operation; the separations were performed with a feed mixture of 0·500 mole fraction *n*-heptane in benzene at a ΔT for the upper curve of 39·5 °C and for the lower of 31·8 °C. The experimental points indicated for "centre-fed" operation are from LONGMIRE [2]; the separations were performed with an average feed concentration of 0·500 mole fraction *n*-heptane in benzene. The upper of the two curves was obtained at a ΔT of 37·2 °C and a plate spacing, a, of 0·079 cm; the lower of the two curves was obtained at a ΔT of 36·0 °C and a plate spacing of 0·043 cm. The remaining column specifications for the two curves are the same; the thermogravitational column used by LONGMIRE was a concentric tube device with a height, h, of 183 cm and a heat transfer surface area of 961·8 cm². By way of comparison the experimental data for two-feed cocurrent operation (this investigation) were obtained with a flat plate thermogravitational column with rservoirs; the column had a heat

transfer area of 779·4 cm² with a height, h, of 19·33 cm and a plate spacing of 0·0376 cm.

For the particular conditions described above it can be seen that two-feed cocurrent operation as carried out in this investigation produces much larger separations at the higher flow rates than obtainable from "centre-fed" operation. The column with a plate spacing of 0·079 cm used in obtaining the upper of the two "centre-fed" curves gave a batch steady-state separation of 0·376; the other "centre-fed" column with a plate spacing of 0·043 cm gave a batch steady-state separation of 0·961. The column of this investigation gave a batch steady-state separation of 0·477. These separations are all mass fraction differences.

Two-feed countercurrent operation

Figure 13 shows the experimental results for "symmetrical" two-feed countercurrent operation with a feed mixture composition of 0·150 mass fraction n-heptane; the column was operated at a ΔT of 32·1 °C. The experimental points agree quite well with the predicted curve calculated from equation (20) at the higher flow rates; the two curves are not in agreement for the larger separations as a result of assumptions involved in the derivation of the separation equation.

Also shown in Fig. 13 are the experimental and theoretical curves for "symmetric" two-feed cocurrent operation taken at approximately the same operating conditions as the data for two-feed countercurrent operation. The cocurrent and countercurrent curves coincide at the higher product mass flow rates; at lower product flow rates two-feed countercurrent operation gives larger separations than found for cocurrent operation. The theoretical curves for the two methods are also shown and substantiate the experimental results.

Figure 14 presents experimental results for two-feed countercurrent operation with feed mixture composition of 0·500 mole fraction n-heptane in benzene and at a ΔT of 32·5 °C.

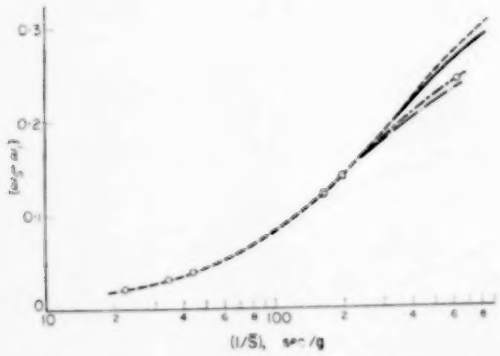

FIG. 13. Upper and lower reservoir product concentration difference vs. reciprocal average product rate: two-feed countercurrent operation.

Legend:

○ Two-feed countercurrent experimental point: TF–SCC–D, 1–6; $\Delta T = 32{\cdot}1$ °C
$\omega_F = 0{\cdot}150$

— · — Two-feed cocurrent experimental curve

– – – – Two-feed countercurrent equation (20), $a' = 0{\cdot}7$, $b = 0{\cdot}02$

——— Two-feed cocurrent, equation (15)

ω = Mass fraction n-heptane in product

$\bar{s}$ = Arithmetic average product mass flow rate $= \frac{1}{2}(s_a + s_i)$

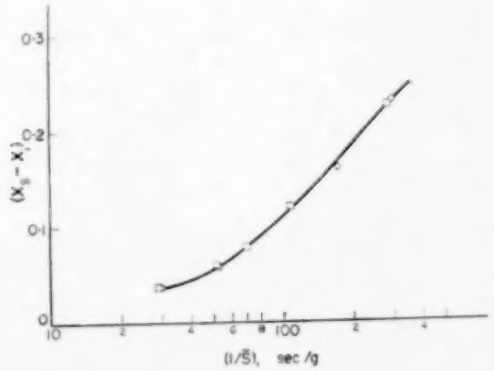

FIG. 14. Upper and lower reservoir concentration difference vs. reciprocal average product rate: two-feed countercurrent operation.

Legend:

○ Two-feed countercurrent experimental point: runs TF–SCC–K, 1–4

□ Two-feed cocurrent experimental point: runs TF–SCO–K, 1–4, 6

x = Mole fraction n-heptane in product

$\bar{s}$ = Arithmetic average product mass flow rate $= \frac{1}{2}(s_a + s_i)$

Single-feed cocurrent operation

A difficulty with the theoretical discussion of single-feed cocurrent and countercurrent operation is that the modification of the "transport" equation (22), introduced the restriction that the flow parameter, r, be small so that the free and forced convection flows may be superimposed. This restriction is in conflict with the approximations of equations (27) and (28); therefore, the area of agreement between experimental and predicted results for single-feed operation should be smaller than found with two-feed operation.

Figure 15 presents experimental separation data for single-feed cocurrent operation at a feed concentration of 0·500 mole fraction n-heptane in benzene; the operating ΔT was 32·4 °C. Other operating conditions for the data were the same as described in previous experimental work.

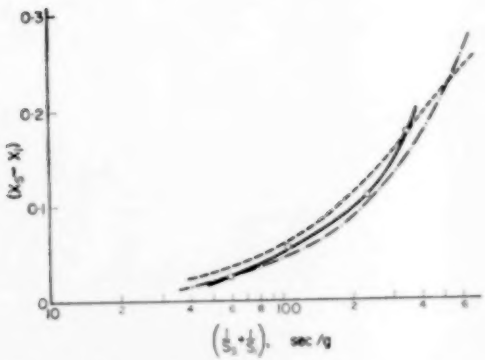

Fig. 15. Upper and lower reservoir product concentration difference vs. sum reciprocal product rates: single-feed cocurrent operation.

Legend:

○ Single-feed cocurrent operation: Runs SF–SCO–K, 1–4

– – – – – – Two-feed cocurrent experimental curve, K

– – – – – Single-feed cocurrent, equation (39)

x = Mole fraction n-heptane in product

s = Product mass flow rate

The theoretical curve calculated from equation (29) predicts the shape of the experimental curve but does not provide a quantitative prediction. A comparison between two-feed and single-feed cocurrent operation is shown in the Fig.; the two-feed cocurrent experimental curve taken at approximately the same condition is plotted.

Experimental data for single-feed cocurrent operation and theoretical separations, calculated from equation (30), are given in Fig. 16 for a feed concentration of 0·150 mass fraction n-heptane in benzene and a column ΔT of 32·1 °C. Also shown in this Fig. is the experimental two-feed cocurrent curve taken at the same conditions.

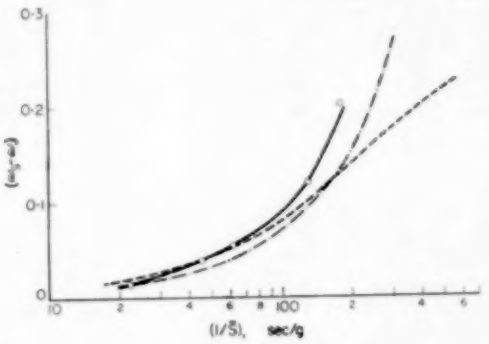

Fig. 16. Upper and lower reservoir product concentration difference vs. reciprocal average product rate; single-feed cocurrent operation.

Legend:

○ Single-feed cocurrent experimental point: Runs SF–SCO–D, 1–5; ΔT = 32·1 °C

– – – – – – Two-feed cocurrent experimental curve, TF–SCO–K

– – – – – Single-feed cocurrent equation (30)

ω = Mass fraction n-heptane in product

$\bar{s}$ = Arithmetic average product mass flow rate $= \frac{1}{2}(s_s + s_i)$

Single-feed countercurrent operation

Figure 17 shows the experimental separations for "symmetric" single-feed countercurrent operation; the experimental data were taken at a feed concentration of 0·150 mass fraction n-heptane in benzene and a column ΔT of 32·4 °C. Other conditions are the same as described for previous experimental work. Single-feed countercurrent separations are compared with two-feed cocurrent separations taken at the same conditions; two-feed cocurrent operation gives greater separations at the higher flow rates, but at the lower flow rates single-feed countercurrent separations

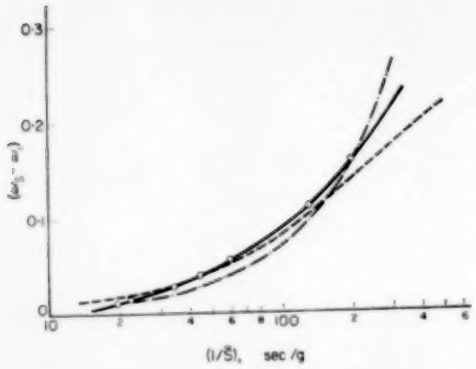

FIG. 17. Upper and lower reservoir product concentration difference vs. reciprocal average product rate: single-feed countercurrent operation.

Legend:

○ Single-feed countercurrent experimental point: Runs SF–SCC–D, 1–6, 8; ΔT = 32·4 °C

– – – – – – Two-feed cocurrent experimental curve, TF–SCO–D

—·—·— Single-feed countercurrent, equation (30)

ω = Mass fraction *n*-heptane in product

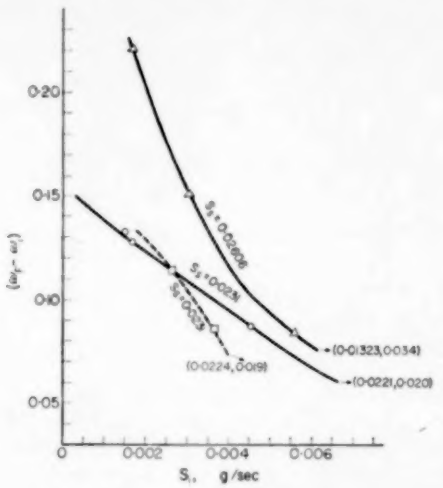

FIG. 18. Feed and lower reservoir product concentration difference vs. lower reservoir product flow rate: single-feed countercurrent operation.

Legend:

○ s_g = 0·0231 g/sec
△ T = 32·0 °C
Runs SF–USCC–D, 6–8, 3
△ s_g = 0·02606 g/sec
△ T = 32·1 °C
Runs SF–USCC–K, 1–3
□ s_g = 0·0231 g/sec
△ T = 32 · 1°C
Runs SF–USCO–D, 1, 2
ω = Mass fraction *n*-heptane in product
s = Product mass flow rate

are greater. Just as for two-feed operation, the single-feed cocurrent and countercurrent experimental curves coincide (this coincidence is not shown) at the higher product flow rates. At lower product flow rates the experimental separations for single-feed cocurrent operation become greater than those for single-feed countercurrent operation; the opposite result was found for two-feed operation.

Also given in Fig. 17 is a comparison between the experimental separations found for single-feed countercurrent operation and the separations predicted by equation (30). The agreement is far from quantitative for reasons mentioned earlier. However, the theory correctly predicts the experimentally observed coincidence of the separation curves for single-feed cocurrent and countercurrent operation at the higher flow rates.

Experimental data for "asymmetric" single-feed countercurrent operation are given in Fig. 18 for feed mixtures of 0·150 mass fraction and 0·500 mole fraction *n*-heptane in benzene. For these runs the upper reservoir product flow rate is fixed and the lower reservoir product flow rate is varied. The data for the dilute case indicate that the lower reservoir product becomes pure benzene at a finite flow rate; this result suggests that this method of operation could be quite useful for the purification of substances.

Conclusions

1. Theory and experiment for two-feed and single-feed operation are in qualitative agreement; quantitative agreement is obtained for the two-feed operation methods at the higher product flow rates through the use of experimentally determined "transport constants."

2. Two-feed cocurrent and countercurrent operation of a flat plate thermogravitational column with reservoirs should provide additional methods for the experimental measurement of the

liquid phase "transport constants" and refinement of thermogravitational column theory.

3. All four of the operation methods discussed may be of use in liquid mixture separation problems.

4. It is suggested that the two-feed operation methods coupled with a method for controlling the natural convection (applied electric fields or moving walls would be two possible methods) would provide a relatively efficient method for effecting separations in the liquid phase with thermal diffusion.

Acknowledgments—The author would like to express his thanks to Professor R. BYRON BIRD for his guidance and encouragement which made this study possible, to Professor W. K. NEILL and Dr. D. R. LONGMIRE for their advice, and to the Shell Fellowship Committee, the Wisconsin Alumni Research Foundation and the Engineering Experiment Station of the University of Wisconsin for financial support during this investigation.

NOTATION

a	Perpendicular distance between "hot" and "cold" walls in a flat plate thermogravitational column
a'	Slope of linear approximation to $\bar{\omega}_1\bar{\omega}_2$ for dilute binary mixtures
b	Intercept of linear approximation to $\bar{\omega}_1\bar{\omega}_2$ for dilute binary mixtures
D_{12}	Mutual diffusion coefficient in binary mixtures
H^*	"Transport" constant from solution of continuity equations for the physical system of this investigation
h	Vertical height of thermogravitational column
$\vec{j}$	Mass flux vector with respect to mass average velocity
K^*	"Transport constant" from solution of continuity equations for the physical system of this investigation
L	Horizontal length of flat plate thermogravitational column
m	Net rate at which component "1" is moving up the column
m'	Net rate at which component "1" is moving down the column
s	Product mass flow rate
s_0	Feed mass flow rate in single-feed operation
$\bar{T}$	Arithmetic mean temperature of "hot" and "cold" walls
v	Mass average velocity
x	Cartesian co-ordinate perpendicular to heat transfer surface
x_i	Mole fraction of i-th component
y	Cartesian co-ordinate parallel to heat transfer surface
z	Cartesian co-ordinate parallel to heat transfer surface, horizontal direction
β	Volumetric coefficient of thermal expansion
θ	Angle of flat plates from the vertical
μ	Coefficient of shear viscosity
ρ	Mass density
σ_1	Soret coefficient of component "1"
τ	Flux of "1" in z direction produced by concentration diffusion
ω_1	In a binary system the mass fraction of that component which in the presence of a temperature gradient migrates to the "hot" wall and concentrates at the top of a thermal diffusion column
$\bar{\omega}_1$	Mass fraction averaged over x, dz horizontal plane at a vertical position, y
F (subscript)	Quantity pertaining to feed
i (subscript)	Quantity pertaining to lower reservoir in thermogravitational column
s (subscript)	Quantity pertaining to upper reservoir in thermogravitational column
$\rightarrow$ (above symbol)	Vector

Explanation of code in Figs.

K	Feed composition 0·500 mole fraction n-heptane in benzene
D	Feed composition 0·150 mass fraction n-heptane in benzene
S	"Symmetrical" operation; equal product mass flow rates
US	"Asymmetrical" operation; unequal product mass flow rates
TF	Two-feed operation
SF	Single-feed operation
CO	Cocurrent operation
CC	Countercurrent operation

Column data for all runs

a = 0·0376 cm
h = 19·33 cm
L = 40·32 cm
θ = 6·1 deg.

REFERENCES

[1] GREW K. E. and IBBS T. L. *Thermal Diffusion in Gases.* Cambridge University Press, New York 1952.

[2] LONGMIRE D. R. Ph.D. Thesis. University of Wisconsin, Madison, Wisconsin 1937.

[3] POWERS J. E. Ph.D. Thesis. University of California, Berkeley, California 1954.

[4] BARDEEN J. *Phys Rev.* 1940 **57** 35.

[5] Debye P. J. W. *Ann. Phys. Lpz.*, 1939 **356** 284.

[6] Debye P. J. W. and Beuche A. M. *Collected Papers of P. J. W. Debye* Interscience, New York 1954.

[7] Furry W. H., Jones R. C and Onsager L. *Phys. Rev.* 1939 **55** 1083.

[8] de Groot S. R. *L'Effet Soret* N. V. Noord Hollandsche Uitgevers Maatschappij, Amsterdam 1945.

[9] Majumdar S. D. *Phys. Rev.* 1951 **81** 844.

[10] Heines T. S. Jr. Ph.D. Thesis. University of Michigan, Ann Arbor, Michigan 1954

[11] Kingrea C. L. Ph.D. Thesis. Virginia Polytechnic Institute, Blacksburg, Virginia 1953.

[12] Thomas W. J. and Watkins S. B. *Chem. Engng. Sci.* 1956 **5** 34; **6** 26.

[13] Barton H. M. *U.S. Pat.* 2699836. 18 January 1955

[14] Gary J. H. *U.S. Pat.* 2751082. 19 June 1953.

[15] Jones A. L. and Hughes E. C. *U.S. Pat.* 2541071. 13 February 1951.

[16] Jones A. L. and Milberger E. C. *U.S. Pat.* 2712386. 5 July 1955.

[17] Jones A. L. and Frazier D. *U.S. Pat.* 2720975. 18 October 1955.

[18] Jones A. L. and Frazier D. *U.S. Pat.* 2720976. 18 October 1955

[19] Jones A. L. and Frazier D. *U.S.Pet.* 2720977. 18 October 1955.

[20] Jones A. L. and Frazier D. *U.S. Pat.* 2720978. 18 October 1955.

[21] Jones A. L. and Frazier D. *U.S.Pat.* 2720979. 18 October 1955.

[22] Jones A. L. and Fay P. S. *U.S.Pat.* 2723033. 18 November 1955.

[23] Jones A. L. and Fay P. S. *U.S. Pat.* 2723034. 8 November 1955.

[24] Jones A. L. and Hughes E. C. *U.S. Pat.* 2734633. 14 February 1956.

[25] Scovill W. E. *U.S. Pat.* 2752042. 26 June 1956.

[26] Thomas J. W. *U.S. Pat.* 2720980. 18 October 1955.

[27] Wahl W. *U.S. Pat.* 2688404. 7 September 1954.

[28] Brock J. R. Ph.D. Thesis. University of Wisconsin, Madison, Wisconsin 1959.

[29] Lupfer G. L. and Atkinson R. G. *U.S. Pat.* 2723758. 15 November 1955.

[30] Timmermans J. *Physico-Chemical Constants of Pure Organic Compounds.* Elsevier, Amsterdam 1950.

[31] Bird R. B. Theory of Diffusion, Chapter in *Advances in Chemical Engineering* Vol. 1, Academic Press, New York 1956.

[32] Jones R. C. and Furry W. H. *Rev. Mod. Phys.* 1946 **18** 151.

[33] Trevoy D. J. and Drickamer H. G. *J. Chem. Phys.* 1949 **17** 1120.

[34] Bierlein J. A., Finch C. R. and Bowers H. E. *J. Chim. Phys.* 1957 **54** 872.

Chemical Engineering Science, 1961, Vol. 13, pp. 226 to 236. Pergamon Press Ltd., London. Printed in Great Britain

Intraparticle diffusion and conduction in porous catalysts—I

Single reactions

R. E. Schilson* and Neal R. Amundson

University of Minnesota, Minneapolis 14, Minnesota, U.S.A.

Abstract—Calculations are made for a single porous catalytic sphere in which a single chemical reaction is carried out. Transport within the sphere is by Knudsen diffusion. Heat is carried by molecular flow and by conduction through the solid structure. Approximate and rigorous calculations are made for partial pressure and temperature profiles and an approximate solution based on a linearization of the heat generation function is shown to be adequate for a number of cases. Effectiveness factors are computed based on the external surface conditions.

Résumé—Cet article traite des calculs relatifs à une réaction chimique simple se produisant au contact d'un catalyseur poreux de forme sphérique. Le transfert dans la sphère se fait par diffusion de Knudsen. L'écoulement moléculaire et la conduction à travers la structure solide assurent le transfert de chaleur. Des calculs approximatifs et rigoureux de la pression partielle et des profils de température et une solution approximative supposant la linéarité du dégagement, conviennent dans la plupart des cas. Les facteurs d'activité sont calculés d'aprés les conditions de surface extérieure.

Zusammenfassung—Berechnungen für eine einzige katalytische Kugel, in welcher sich eine einzige chemische Reaktion stattfindet, sind durchgeführt. Beförderung innerhalb der Kugel ist durch Knudsen Diffusion. Die Wärme ist durch molekularen Fluss und Leitung durch die solide Struktur übertragen. Annähernde und genaue Berechnungen für partielle Druck- und Temperatur-profile sind gemacht, und es ist gezeigt, dass eine annähernde Lösung, auf der Grundlage der Linearisierung der Wärmeerzeugung-funktion in zahlreichen Fällen hinreichend ist. Wirksamkeits-faktoren sind den äusseren Oberflächen-verhältnissen ertsprechend berechnet.

The purpose of this paper is to discuss and develop methods for the prediction of the rate of reaction from a single porous catalyst particle under the assumption that the kinetics of the reaction are known, that Knudsen diffusion obtains in the void volume of the catalyst and that the only mode of heat release is by intraparticle conduction in the porous structure. Simpler problems have been considered and the main deterrent to progress has been the fact that the equations which need solving are highly non-linear. In fact, the only system which yields analytic solutions is the simple reversible reaction first order in each direction for a reaction carried out in particles of spherical, cylindrical, plate-like, or rectangular catalyst shapes at constant temperature. Problems of this kind were considered by Thiele [1] and Zeldowitsch [2] almost simultaneously. Wheeler [3] and Prater and Weisz [4] have discussed the problem of intraparticle diffusion in some detail generally for isothermal operation. The former, along with Aris [5] has considered the effect of geometry of the catalyst while Prater and Weisz have made use of Thiele's and Wheeler's results to interpret data and design experiments. Finally, Wicke [6–9] in a number of papers has discussed the effect of intraparticle diffusion in carbon burning. Sehr [10] has investigated thermal conductivities of catalyst pellets. Many of the pertinent literature references in the field are given by Weisz in Ref. [11] and others [3, 12–18].

Equations for a single reaction

Consider a single reaction $\sum_{i=1}^{n} a_i M_i = 0$, $a_i > 0$ for a product and $a_i < 0$ for a reactant, taking place in a porous catalyst pellet of spherical shape.

*Present address: The Ohio Oil Company, Littleton, Colorado, U.S.A.

Suppose the particle has randomly interconnected pores and a fractional void volume γ. It is assumed that reactant and product molecules diffuse through the fractional void volume. The reaction rate within the sphere is given by f_i where f_i is the rate of formation of component i in moles per unit time per unit area of catalyst surface. If a mass balance on a spherical shell of inside radius ρ and thickness $\Delta\rho$ is made, then the rate of diffusion through the inner surface outward is

$$-\left(4\pi\rho^2 D_i \frac{dp_i}{d\rho}\right)_\rho$$

in moles per unit time where the subscript ρ indicates that the quantity in parentheses must be evaluated at ρ. D_i is the diffusion coefficient computed from

$$D_i = \frac{\gamma}{2} \cdot \frac{8}{3} \frac{\bar{r}}{\sqrt{2\pi R m_i T}} = \frac{E_i}{\sqrt{T}}$$

in which the factor $\gamma/2$ has been suggested by WHEELER. The rate at which component i leaves the spherical surface at $\rho + \Delta\rho$ is

$$-\left(4\pi \rho^2 D_i \frac{dp_i}{d\rho}\right)_{\rho+\Delta\rho}$$

and the rate at which M_i is formed in the reaction in the volume $4\pi \rho^2 \Delta\rho$ is

$$\Delta\rho\,(4\pi \rho^2 \rho_p S_g f_i)_{\bar{\rho}}$$

where $\rho < \bar{\rho} < \rho + \Delta\rho$. S_g is the surface area per gram of pellet and ρ_p is the pellet density. Summing these three quantities, dividing by $\Delta\rho$ and passing to the limit, there results

$$\frac{d}{d\rho}\left(\rho^2 D \frac{dp_i}{d\rho}\right) + \rho^2 \rho_p S_g f_i = 0, \quad i = 1, 2 \ldots n \quad (1)$$

From the stoichiometry of the reaction it is clear that

$$\frac{f_i}{a_i} = \frac{f_j}{a_j}$$

so that for any other specie M_j

$$\frac{d}{d\rho}\left(\rho^2 D_j \frac{dp_j}{d\rho}\right) + \rho^2 \rho_p S_g f_i \frac{a_j}{a_i} = 0$$

Appropriate manipulation of these two equations gives

$$\frac{1}{a_i}\frac{d}{d\rho}\left(\rho^2 D_i \frac{dp_i}{d\rho}\right) = \frac{1}{a_j}\frac{d}{d\rho}\left(\rho^2 D_j \frac{dp_j}{d\rho}\right) \quad (2)$$

Two successive integrations give

$$\frac{E_i}{a_i}(p_i - p_{is}) = \frac{E_j}{a_j}(p_j - p_{js})$$

or

$$p_j = p_{js} + \frac{a_j}{a_i}\frac{E_i}{E_j}(p_i - p_{is})$$

$$= p_{js} + \frac{a_j}{a_i}\sqrt{\left(\frac{m_j}{m_i}\right)}(p_i - p_{is}) \quad (3)$$

Thus instead of there being a differential equation for each component as in equation (1), there is a single differential equation for the conservation of mass, since in f_i, which may be a function of the partial pressures of each component, one may use equation (3) to eliminate all partial pressures save that of the i-th. f_i is then a function of one partial pressure p_i and all partial pressures at the surface of the particle, i.e.

$$f_i = f_i(p_i, p_{1s}, p_{2s}, \ldots, p_{ns}, T)$$

Let us consider now the equation of conservation of energy within the particle. It will be assumed that the diffusing molecules carry their partial molar enthalpy, and, since only Knudsen flow is being considered, this is the only mode of transfer in the gas phase. In the solid phase heat will be transported by conduction. It should be noted that the partial molar enthalpy should be corrected for the heat of transport. Once again, analysing a spherical shell, the rate at which heat enters the inner surface is

$$-4\pi\left((1-\gamma)k_s \rho^2 \frac{dT}{d\rho}\right)_\rho$$

by intraparticle conduction and

$$-4\pi\left(\rho^2 \sum_{i=1}^{n} D_i \frac{dp_i}{d\rho}\bar{H}_i\right)_\rho$$

by molecular flow.

It may then be shown that the conservation equation is

$$(1-\gamma)\frac{d}{d\rho}\left(k_s \rho^2 \frac{dT}{d\rho}\right) + \frac{d}{d\rho}\left(\rho^2 \sum_{i=1}^{n} D_i \frac{dp_i}{d\rho}\bar{H}_i\right) = 0$$

One integration may be easily made

$$(1-\gamma)k_s\frac{dT}{d\rho}+\sum_{i=1}^{n}D_i\mathcal{H}_i\frac{dp_i}{d\rho}=0 \qquad (4)$$

and from a single integration of equation (2)

$$\frac{D_i}{a_i}\frac{dp_i}{d\rho}=\frac{D_j}{a_j}\frac{dp_j}{d\rho}$$

This when substituted into equation (4) gives

$$(1-\gamma)k_s\frac{dT}{d\rho}+\frac{D_j}{a_j}\frac{dp_j}{d\rho}\sum_{i=1}^{n}\mathcal{H}_i a_i=0$$

Now it may be shown easily that in molecular flow through a capillary $\mathcal{H}_i$ is not the partial molar enthalpy but rather $\widetilde{H}_i$, the partial molar enthalpy diminished by $\frac{1}{2}RT$, so

$$\mathcal{H}_i=\widetilde{H}_i-\tfrac{1}{2}RT$$

Thus

$$\sum_{i=1}^{n}a_i\mathcal{H}=\sum_{i=1}^{n}a_i\widetilde{H}_i-\tfrac{1}{2}RT\sum_{i=1}^{n}a_i$$

$$=\Delta H_T-\tfrac{1}{2}RT\sum_{i=1}^{n}a_i$$

where ΔH_T is the heat of reaction of the reaction $\sum_{i=1}^{n}a_i M_i=0$.

Therefore

$$(1-\gamma)k_s\frac{dT}{d\rho}+\frac{D_j}{a_j}\frac{dp_j}{d\rho}\left(\Delta H_T-\tfrac{1}{2}RT\sum_{i=1}^{n}a_i\right)=0$$

It will be assumed that the term involving $\frac{1}{2}RT$ is small compared to ΔH_T so that

$$(1-\gamma)k_s\frac{dT}{d\rho}+\frac{D_j}{a_j}\frac{dp_j}{d\rho}\Delta H_T=0 \qquad (5)$$

This equation may be used to estimate the maximum temperature difference within the particle if it is assumed that p_j falls to zero somewhere.

Then

$$(\Delta T)_{\max}=\frac{p_{j_s}D_j\Delta H_T}{(1-\gamma)k_s a_j}$$

Equation (5) may be rearranged and integrated to give

$$p_j=p_{j_s}-\frac{a_j(1-\gamma)}{E_j}\int_{T_s}^{T}\frac{k_s\sqrt{T}\,dT}{\Delta H_T} \qquad (6)$$

and since k_s and ΔH_T may be expressed as functions of the temperature the integral may be evaluated. Equation (5) may also be written

$$p_j=p_{j_s}-\frac{(1-\gamma)k_s a_j}{D_j\Delta H_T}(T-T_s) \qquad (7)$$

where the parameters must take on average values over the temperature range $T-T_s$. If k_s and ΔH_T are assumed to be constant equation (7) may be written

$$p_j=p_{j_s}-\frac{2(1-\gamma)k_s a_j}{3E_i\Delta H_T}(T^{3/2}-T_s^{3/2})$$

and this along with equation (7) will be used in the examples.

From equations (1) and (3) one may now write

$$\frac{d}{d\rho}\left[\frac{\rho^2(1-\gamma)k_s a_i}{\Delta H_T}\frac{dT}{d\rho}\right]-\rho^2\rho_p S_g f_i=0 \qquad (8)$$

where f_i, as written in this formula, is a function of the temperature alone, the ith partial pressure having been eliminated through equation (6) or its modification. Equation (8) then is a fairly rigorous equation and its solution along with the boundary conditions

$$T=T_s \quad \text{at} \quad \rho=R$$

$$\frac{dT}{d\rho}=0 \quad \text{at} \quad \rho=0$$

should give the temperature profile within a single catalyst particle.

The assumption will now be made that k_s and ΔH_T are constant so that equation (8) may be written in the form

$$\frac{d^2T}{d\rho^2}+\frac{2}{\rho}\frac{dT}{d\rho}-\frac{\rho_p S_g\Delta H_T}{(1-\gamma)k_s a_i}f_i=0 \qquad (9)$$

and with $rR=\rho$

$$\frac{d^2T}{dr^2}+\frac{2}{r}\frac{dT}{dr}-\frac{R^2\rho_p S_g\Delta H_T}{(1-\gamma)k_s a_i}f_i=0 \qquad (10)$$

$$T=T_s \quad \text{at} \quad r=1 \qquad (11)$$

$$\frac{dT}{dr}=0 \quad \text{at} \quad r=0 \qquad (12)$$

In addition to the temperature profile one is interested in the effectiveness factor for the catalyst. The effectiveness factor is defined as

VOL. 13 1961

the rate of production of a given chemical specie by a single particle divided by the fictitious rate assuming all the catalytic surface is available to reactants at the temperature and partial pressures at the surface. The rate of production per particle is

$$-4\pi R^2 \left(D_i \frac{dp_i}{dr}\right)_{\text{surface}}$$

The fictitious rate is

$$\frac{4}{3}\pi R^3 \rho_p S_g (f_i)_{\text{surface}}$$

and the effectiveness factor is

$$\text{E.F.} = -\frac{3}{\rho_p R S_g}\left(D_i \frac{dp_i}{dr} f_i^{-1}\right)_{\text{surface}}$$

In terms of the temperature profile

$$\text{E.F} = \frac{3 a_i (1-\gamma)}{\rho_p R S_g}\left(\frac{k_s}{\Delta H_T}\frac{dT}{dr} f_i^{-1}\right)_{\text{surface}}$$

Solution for a single reaction

The purpose of the remainder of the paper is to show how solutions of equations (10)–(12) may be obtained approximately and rigorously, the approximate method by an analytical formula and the rigorous method by a technique which will give answers to any preassigned accuracy. Before proceeding, however, the function

$$q(T) = \frac{R^2 \rho_p S_g (-\Delta H_T)}{(1-\gamma) k_s a_i} f_i$$

will be examined. Note first that $q(T)$ has the sign of $(-\Delta H_T)$ since $f_i a_i^{-1}$ is always positive. In general it has been found that for a large number of cases the function $q(T)$ takes on the general forms shown in Figs. 1(a), 1(b) and 1(c). Figs. 1(a) and 1(b) are typical of exothermic reactions while (Fig. 1(c) is typical of endothermic reactions. The temperature T_L is defined by

$$q(T_L) = 0$$

and gives the temperature at which either the limiting reactant has been exhausted or is, alternatively, the point at which chemical equilibrium has been established in the particle. In any event $T_s - T_L$ is a measure of the maximum temperature difference in the particle and so is a generalization of $(\Delta T)_{\max}$ previously mentioned.

First an approximate solution of equation (10) will be developed. Since it is apparent that the heat generation function $q(T)$ may be approximated in two of the cases, Figs. 1(a) and Fig.1(c), by a straight line with good accuracy, the temperature profile with $a - bT$ replacing $q(T)$ should give a good approximation to the real temperature profile. Thus

$$\frac{d^2T}{dr^2} + \frac{2}{b}\frac{dT}{dr} + a - bT = 0$$

$$T = T_s \quad \text{at} \quad r = 1$$

$$\frac{dT}{dr} = 0 \quad \text{at} \quad r = 0$$

needs solving. This is a straightforward problem and the solution may be written

$$T(r) = \frac{a}{b} + \frac{T_s - (a/b)}{r}\frac{\sinh r\sqrt{b}}{\sinh \sqrt{b}} \qquad (13)$$

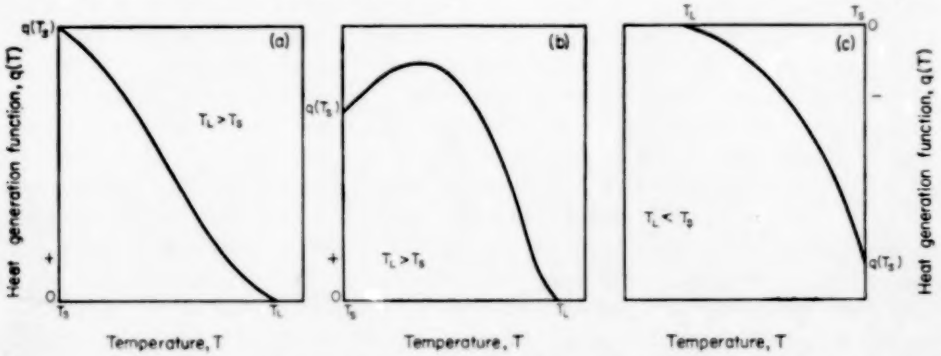

Fig. 1. Typical heat generation function.
(a) Exothermic reaction type 1 (b) Exothermic reaction type 2 (c) Endothermic reaction

To solve equation (10) the following procedure will be adopted. Write it in the form

$$\frac{d^2T}{dr^2} + \frac{2}{r}\frac{dT}{dr} + q(T) + a - bT = a - bT$$

then

$$\frac{d^2T}{dr^2} + \frac{2}{r}\frac{dT}{dr} - bT = Q(r) - a \qquad (14)$$

where

$$Q(r) = a - bT - q(T)$$

If one supposes for the moment that $Q(r) - a$ is a known function of r then the solution of equation (15) may be generated by methods readily available to give

$$T(r) = \frac{a}{b} + \frac{T_s - (a/b)}{b}\frac{\sinh r\sqrt{b}}{\sinh \sqrt{b}} + \int_0^1 G(r,t)\, t\, Q(t)\, dt \qquad (15)$$

with

$$G(r,t) = \begin{cases} -\dfrac{\sinh \sqrt{b}\,(1-r)\sinh \sqrt{b}\,t}{r\sqrt{b}\sinh\sqrt{b}}, & 0 \leqslant t \leqslant r \\ +\dfrac{\sinh \sqrt{b}\,(1-t)\sinh \sqrt{b}\,r}{r\sqrt{b}\sinh\sqrt{b}}, & r \leqslant t \leqslant 1 \end{cases}$$

The solution, equation (15) consists of three terms. The first two terms on the right-hand side make up the approximate solution. The third or integral term may be considered to be a correction term to this first approximation. In order to evaluate the correction term a method of successive substitutions will be applied. $Q(t)$ depends upon $T(r)$, the temperature profile, which is at this point unknown and therefore equation (15) is an integral equation with the unknown function $T(r)$ appearing on the left as well as under the integral sign. If the function $q(T)$ is almost linear $q(T) - a + bT$ is small provided that a and b are chosen properly. If the process of successive substitutions converges, then using the temperature profile, $T(r)$, the profile obtained by assuming $q(T) = a - bT$ as a first approximation and

$$Q_1(t) = a - bT_1 - q(T_1)$$

then

$$T_2(r) = T_1(r) + \int_0^1 G(r,t)\, t\, Q_1(t)\, dt$$

should be a better approximation. The process may be repeated using $Q_2(r) = a - bT_2 - q(T_2)$ to define a new profile

$$T_3(r) = T_1(r) + \int_0^1 G(r,t)\, t\, Q_2(t)\, dt$$

and in general

$$T_n(r) = T_1(r) + \int_0^1 G(r,t)\, t\, Q_{n-1}(t)\, dt \qquad (16)$$

with $Q_{n-1}(t) = a - bT_{n-1} - q(T_{n-1})$, and so a sequence of profiles T_1, T_2, T_3, . . . etc. may be computed to give ultimately a profile $T_n(r)$ which differs from the previous profile $T_{n-1}(r)$ or the succeeding profile $T_{n+1}(r)$ to any preassigned accuracy. For Type 1(a) and Type 1(c) heat generation functions this process appears to converge and produces profiles which satisfy the differential equation and boundary conditions numerically.

A word is needed concerning the method of evaluation of the integrals. Many methods for the numerical evaluation of integrals may be suitable but in this paper the integral was replaced by a sum, using the trapezoidal rule for each sub-interval. The interval from zero to one was broken into twenty equal subintervals. Greater accuracy may be obtained with a finer subdivision but in the cases investigated here, the number twenty appeared adequate. The choice of which linear function $a - bT$ to be used is not difficult. One may use the Taylor series approximation about the surface conditions or one might fair a straight line to $q(T)$ by eye as shown in Fig. 2.

If the heat generation function $q(T)$ is of Type 1(b) the method described above may be unsatisfactory, but as shown in Fig. (5) the curve may be approximated by two straight lines. Let the point of intersection of these lines be r_x and the temperature at r_x be T_x. The general problem to be solved then reduces to the set of equations

VOL. 13 1961

$$\frac{d^2T_c}{dr^2} + \frac{2}{r}\frac{dT_c}{dr} - b_c T_c = Q_c(r) - a_c \qquad (17)$$

$$T_c = T_x \quad \text{at} \quad r = r_x \qquad (18)$$

$$\frac{dT}{dr} = 0 \quad \text{at} \quad r = 0 \qquad (19)$$

$$\frac{d^2T_0}{dr^2} + \frac{2}{r}\frac{dT_0}{dr} + b_0 T_0 = Q_0(r) - a_0 \qquad (20)$$

$$T_0 = T_x \quad \text{at} \quad r = r_x \qquad (21)$$

$$T_0 = T_s \quad \text{at} \quad r = 1 \qquad (22)$$

$$\frac{dT_c}{dr} = \frac{dT_0}{dr} \quad \text{at} \quad r = r_x \qquad (23)$$

with

$$Q_c(r) = a_c - b_c T - q(T), \qquad 0 < r < r_x$$

$$Q_0(r) = a_0 + b_0 T - q(T), \qquad r_x < r < 1$$

The solution of this problem is obtained by solving for T_c from equations (17), (18) and (19) and for T_0 from equations (20), (21) and (22). These two solutions are obtained by a straightforward method of variation of parameters and will involve r_x and T_x as

$$T_c = \frac{a_c}{b_c} + \frac{[T_x - (a_c/b_c)]}{r}\frac{\sinh r\sqrt{b_c}t}{\sinh\sqrt{(b_c)}\,r_x} + \int_0^{r_x} G_1(r,t)\,t\,Q_c(t)\,dt \qquad (24)$$

$$G_1(r,t) = \begin{cases} -\dfrac{\sinh\sqrt{(b_c)}\,(r_x - r)\sinh\sqrt{(b_c)}\,t}{r\sqrt{(b_c)}\sinh\sqrt{(b_c)}\,r_x}, & 0 \leqslant t \leqslant r \\ +\dfrac{\sinh\sqrt{(b_c)}\,r\sinh\sqrt{(b_c)}\,(r_x - t)}{r\sqrt{(b_c)}\sinh\sqrt{(b_c)}\,r_x}, & r \leqslant t \leqslant r_x \end{cases}$$

and

$$T_0 = -\frac{a_0}{b_0} + \frac{r_x}{r}\left(T_x + \frac{a_0}{b_0}\right)\frac{\sin\sqrt{(b_0)}\,(1-r)}{\sin\sqrt{(b_0)}\,(1-r)_x} + \int_{r_x}^{1} G_2(r,t)\,t\,Q_0(t)\,dt \qquad (25)$$

$$G_2(r,t) = \begin{cases} -\dfrac{\sin\sqrt{(b_0)}\,(1-r)\sin\sqrt{(b_0)}\,(t-r_x)}{r\sqrt{(b_0)}\sin\sqrt{(b_0)}\,(1-r_x)}, & r_x < t < r \\ +\dfrac{\sin\sqrt{(b_0)}\,(r-r_x)\sin\sqrt{(b_0)}\,(1-t)}{r\sqrt{(b_0)}\sin\sqrt{(b_0)}\,(1-r_x)}, & r < t < 1 \end{cases}$$

The temperature T_x may be determined from the solution of

$$a_c - b_c T_x = a_0 + b_0 T_x$$

as a first approximation.

In order to determine the value of r_x the two equations above must be differentiated and evaluated at $r = r_x$,

$$\frac{dT_c}{dr} = \frac{dT_0}{dr} \quad \text{at} \quad r = r_x$$

A first approximation to the temperature profile may be obtained from the equations

$$T_{c1}(r) = \frac{a_c}{b_c} + \frac{T_x - (a_c/b_c)}{r}\frac{\sinh r\sqrt{b_c}}{\sinh r_x\sqrt{b_c}} \quad 0 < r < r_x \qquad (26)$$

$$T_{01}(r) = -\frac{a_0}{b_0} + \frac{r_x[T_x + (a_0/b_0)]}{r}\frac{\sin\sqrt{(b_0)}\,(1-r)}{\sin\sqrt{(b_0)}\,(1-r_x)} \quad r_x < r < 1 \qquad (27)$$

where r_x is determined by equating the derivatives at $r = r_x$, or

$$\left(T_x - \frac{a_c}{b_c}\right)\left[\sqrt{(b_c)}\coth\sqrt{b_c}\,r_x - \frac{1}{b_x}\right] = \left(T_0 + \frac{a_0}{b_0}\right)\frac{\sqrt{b_0}}{r_x\sin\sqrt{b_0}\,(1-r_x)} - \left(T_x + \frac{a_0}{b_0}\right)\left[\frac{1}{r_x} + \sqrt{b_0}\cot\sqrt{b_0}\,(1-r_x)\right]$$

Further approximations may be obtained by the successive substitutions

$$T_{c2} = T_{c1} + \int_0^{r_x} G_1(r,t)\,t\,Q_{c1}(t)\,dt \qquad (28)$$

$$T_{02} = T_{01} + \int_{r_x}^{1} G_2(r,t)\,t\,Q_{01}(t)\,dt \qquad (29)$$

with T_{cn} and T_{0n} having obvious representations.

It is apparent that a correction must be made to r_x at some point. This need not be done at each iteration since it is found that r_x does not change appreciably. It should be calculated, however, and it may be obtained by equating the derivatives of equations (24) and (25) and solving for r_x.

NUMERICAL EXAMPLES

Four numerical examples will be given which should serve to illustrate the principles developed above. The diffusion coefficients will be calculated from

$$D_i = \frac{59{\cdot}109\ \bar{r}\ \gamma}{\sqrt{m_i\ T}}$$

Example I. $2\ A \rightarrow B$

$\Delta H_T = -140{,}000$ cal/g mole B $R = 0{\cdot}4762$ cm
$m_A = 45$, $m_B = 90$ $\bar{r} = 35$ Å
$T_s = 600$ °K $k_s = 3 \times 10^{-4}$ cal/sec cm °K
$p_{As} = 3{\cdot}20$ atm $\gamma = 0{\cdot}35$

$f_A = -2{\cdot}888\ (10^{-6})\ \exp\ (-9058/T)\ p_A^2$, g mole A/cm² sec

$D_A = 4{\cdot}407\ (10^{-6})$, g mole/atm sec cm

$q(T) = 4{\cdot}703\ (10^{-8})\ p_A^2 \exp(-9058/T)$, °K

$p_A = 41{\cdot}13 - 0{\cdot}06321\ T$, atm

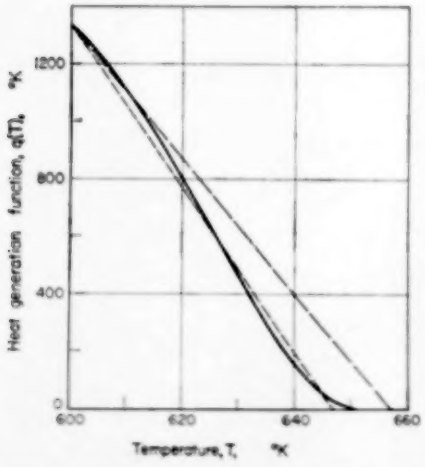

FIG. 2. Heat generation function for Example I and two linear approximations.
1 —— —— $a - bT = 15487 - 23{\cdot}58T$
2 - - - - - $a - bT = 18480 - 28{\cdot}57T$

Fig. 2 gives the graph of $q(T)$ vs. T and shows two linear approximations,

line 1 $\sim a - bT = 15{,}480 - 23{\cdot}58T$ °K
line 2 $\sim a - bT = 18{,}480 - 28{\cdot}57T$ °K

Fig. 3 shows the temperature profile within the particle using line 1 as a first approximation. The second and third approximations are also shown using equation (16) as well as the higher order approximation assumed to be the rigorous solution. Fig. 4 shows the first approximations using lines 1 and 2. The effectiveness factors are

rigorous solution	0·461
line 1 approximation	0·490
line 2 approximation	0·456

Example II. $A \rightarrow B$

$\Delta H_T = -30{,}000$ cal/g mole B $R = 0{\cdot}5$ cm
$m_A = 36$ $\bar{r} = 40$ Å
$T_s = 625$ °K $\gamma = 0{\cdot}40$
$p_{As} = 10$ atm $k_s = 8{\cdot}0 \times 10^{-4}$ cal/sec cm °K

$f_A = 0{\cdot}06254 \exp(-15{,}000/T)\ p_A$, g mole A/cm² sec

$p_A = 115{\cdot}74 - 6{\cdot}767\ (10^{-3})\ T^{3/2}$, atm

$q(T) = 1{\cdot}9542\ (10^{12}) \exp(-15{,}000/T)\ p_A$, °K

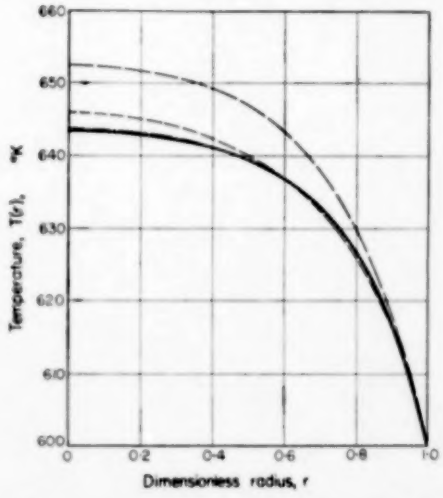

FIG. 3. Temperature profile for Example I.
—— —— first approximation
- - - - - - second approximation
—— - —— third approximation
———— final approximation

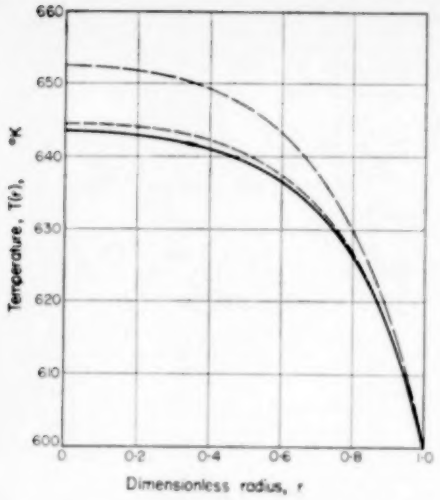

FIG. 4. Comparison of true and approximate temperature profiles for Example I.
——— Final solution, rigorous method
— — — First approximation, line 1
- - - - - - First approximation, line 2

Fig. 5 shows the graph of $q(T)$ vs. the temperature and two separate approximations, one by a single line and another by two straight lines

one line $\sim a - bT = 12{,}620 - 19{\cdot}01T$, °K

two lines $\sim a_c - b_c T = 25{,}530 - 38{\cdot}46T$, °K

$a_0 + b_0 T = -2194 + 4{\cdot}691T$, °K

Fig. 6 gives the temperature profiles calculated from the rigorous solution and the two first

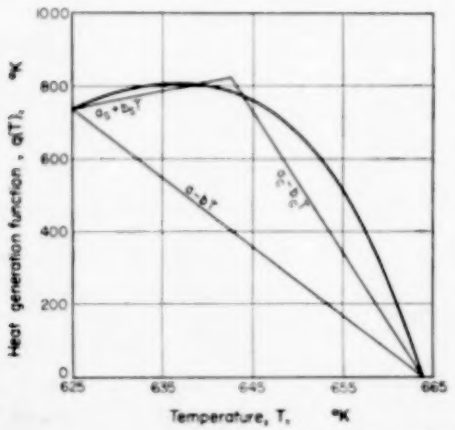

FIG. 5. Heat generation functions for Example II showing one- and two-line approximations.
$a_s + b_s T$, $a_c - b_c T$ } Linear approximations, two-line method
$a - bT$ Linear approximation, one-line method

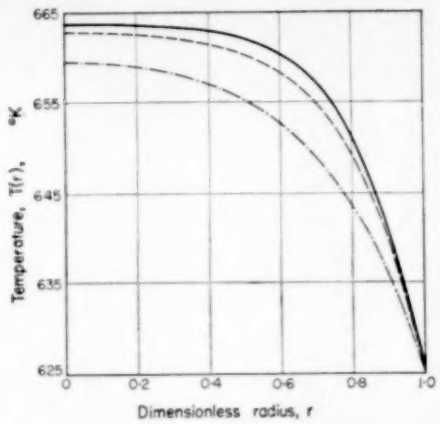

FIG. 6. Temperature profiles for Example II.
——— Final solution
- - - - - - First approximation, two-line method
— — — First approximation, one-line method

approximations, one using a one line approximation for $q(T)$ and the other for a two-line approxmation. It should be pointed out that even though the single straight line appears to be a poor approximation the final results by the two methods are essentially identical although twice as many successive substitutions are required in one than in the other.

	Two lines	*One line*
First approximation E.F.	0·712	0·531
Rigorous solution E.F.	0·709	0·713
Centre temperature (°K)	663·6	663·6

In the two-line method the first approximation is almost as good as the third approximation, while the third differs almost imperceptibly from the ninth.

Example III. $2A \rightarrow B$

$\Delta H_T = -160{,}000$ cal/g mole B $R = 0{\cdot}25$ cm

$m_A = 36$ $\bar{r} = 200$ Å

$T_s = 400$ °K $\gamma = 0{\cdot}400$

$p_{As} = 1{\cdot}0$ atm $k_s = 8 \times 10^{-4}$ cal/sec cm °K

$f_A = 0{\cdot}702\,(10^{11}) \exp(-20{,}000/T)\, p_A^2$, g mole A/cm² sec

$D_A = 3{\cdot}941\,(10^{-7})$, g mole/atm cm sec (assumed constant)

$p_A = 7{\cdot}090 - 0{\cdot}01523\,T$, atm

$q(T) = 2{\cdot}925\,(10^{23}) \exp(-20{,}000/T)\, p_A^2$, °K

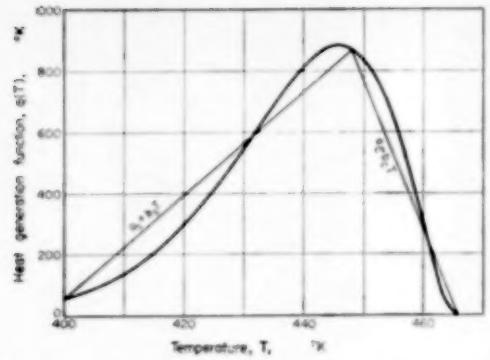

Fig. 7. Heat generation function and two-line approximation for Example III.

$a_c - b_c T$, $a_s + b_s T$ } Linear approximations, two-line method

Fig. 7 gives the graph of $q(T)$ vs T, and it appears that $q(T)$ can only be approximated by two straight lines

$$a_c - b_c T = 22{,}863 - 49{\cdot}10T, \ ^\circ\text{K}$$
$$a_0 - b_0 T = -6706{\cdot}5 + 16{\cdot}91T, \ ^\circ\text{K}$$

and the intersection point is $T_x = 448\ ^\circ\text{K}$. The distance r_x can be computed for the first approximation and is 0·665. After a few approximations r_x was recalculated and was found to be 0·672. From the first approximation the effectiveness factor was 7·65 while for the rigorous solution it was 7·29. Fig. 8 shows how closely the temperature profiles of the first approximation and the rigorous solution agree.

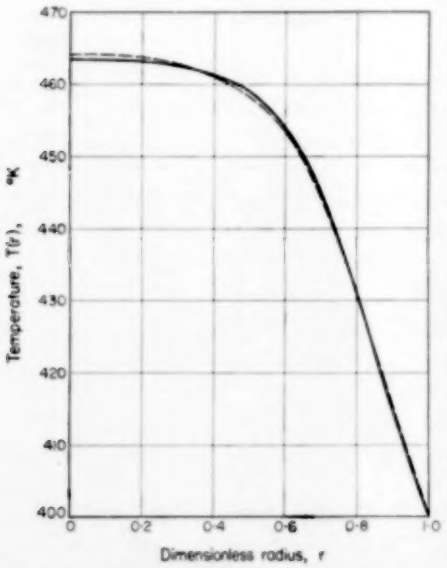

Fig. 8. True and approximate temperature profiles in Example III.

——— Final solution

– – – – – – First approximation

Example IV. $2A \rightarrow B$

$\Delta H_T = 160{,}000$ cal/g mole B — $R = 0{\cdot}5$ cm

$m_A = 40$ — $r = 200$ Å

$T_s = 600\ ^\circ\text{K}$ — $\gamma = 0{\cdot}500$

$p_{As} = 2{\cdot}0$ atm — $k_g = 6{\cdot}0 \times 10^{-4}$ cal/sec cm °K

$$f_A = -0{\cdot}775\,(10^{-3}) \exp(-10{,}000/T)\, p_A^2, \ \text{g mole A/cm}^2 \text{ sec}$$
$$p_A = -1{\cdot}931 + 2{\cdot}675\,(10^{-4})\, T^{3/2}, \text{ atm}$$
$$q(T) = -2{\cdot}583\,(10^{22}) \exp(-10{,}000/T)\, p_A^2, \ ^\circ\text{K}$$

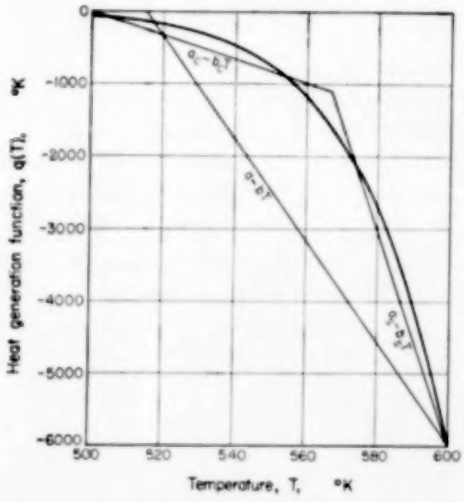

Fig. 9. Heat generation function and two approximations for Example IV.

$a - bT$ Linear approximation, one-line method

$a_c - b_c T$, $a_s - b_s T$ } Linear approximations, two-line method

Fig. 9 gives $q(T)$ vs. T and shows possible one and two line approximations. Suitable equations are

$$\text{one line} = a - bT = 36{,}180 - 70{\cdot}25T, \ ^\circ\text{K}$$
$$\text{two lines} \sim a_c - b_c T = 8209 - 16{\cdot}42T, \ ^\circ\text{K}$$
$$a_0 - b_0 T = 82{,}600 - 147{\cdot}6T, \ ^\circ\text{K}$$

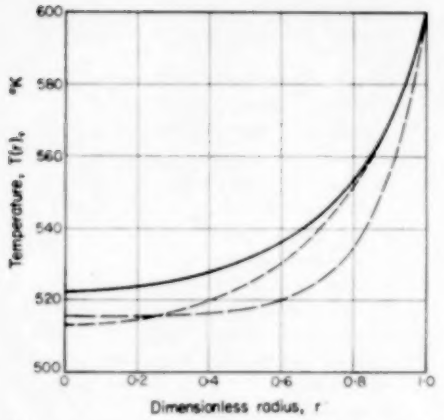

FIG. 10. Temperature profiles in Example IV.
——— Final solution
— — — First approximation, one-line method
- - - - - - First approximation, two-line method

with $r_s = 0.889$ and $T_s = 567$ °K. Fig. 10 gives the usual comparison of the temperature profiles. The effectiveness factors are 0·241, 0·315 and 0·240 for the rigorous solution, the one line first approximation, and the two line first approximation, respectively.

SUMMARY AND CRITIQUE

Techniques have been presented which enable one to treat the problem of non-isothermal reaction within a porous catalyst pellet. The most important result is that the two approximation methods presented, either the one-line or two-line methods, give results which indicate that for single reactions, at least, a more detailed solution is not essential. The pertinent point here is that the heat generation function, $q(T)$, must be examined and it was apparent that in spite of the fact that it appeared to be rather complex it could here be satisfactorily approximated to in the four numerical examples presented. Problems with more complicated kinetic expressions involving adsorption denominators have been investigated and as yet no case has been confronted which could not be treated by one of the two techniques.

The problem with a film resistance at the boundary may be treated in the same way except that the details of the computations differ. Obviously, the problem of the isothermal particle with complicated chemical kinetics follows directly also from the above analysis.

One point which needs some elucidation is the method of numerical solution for what has been called above the rigorous solution, although one result of this paper is that such calculations need not be made. In order to solve the differential equation (10), it was changed to an integral equation but first subtracting out a first approxation. The integral in the integral equation was then changed to a sum and the set of nonlinear transcendental equations was solved by successive substitutions. Although no formal proof was presented the successive substitutions seemed to converge and it was assumed that the desired temperature profile was obtained. Now there are many other methods of solving such a set of equations; however, many that were tried were not successful and some diverged badly even with a good first approximation.

When one is presented with an ordinary differential equation today the analogue computer immediately comes to mind and this was tried here, albeit not exhaustively. These problems are two-point boundary value problems and so in order to use the analogue computer the value of the derivative must be estimated at the particle surface or the temperature must be estimated at the centre of the particle. While conceptually this is very simple, there are difficulties. It is found that the equations are so unstable numerically that there is no value of the derivative at the particle surface which will enable the equations to be integrated by a marching technique. Solution on the analogue computer starting at the centre of the particle where the gradient is zero may be accomplished in some cases. With this procedure the temperature must be estimated at the centre and revised until the solution agrees at the surface with the prescribed surface temperature. This phenomenon is not peculiar to these problems, but from the experience of the writers, it does occur in many problems which involve combined chemical reaction, heat release and diffusion. The mathematical problem is extensively discussed in the book by Fox [19].

One further point needs discussion. The definition of the effectiveness factor given by THIELE

implies that it will always lie between zero and one. In problem III of this paper an E.F. of over seven was obtained and it is apparent that this is possible since the high temperature within the particle produces an abnormally high rate of reaction.

Acknowledgements—This paper was supported by grants in aid from the Proctor and Gamble Company, The Eastman Kodak Company, the Standard Oil Foundation (Indiana), The Minneapolis-Honeywell Regulator Company and by the National Science Foundation.

NOTATION

a, b	constants in linearization of $q(T)$
a_0, b_0	constants in linearization of $q(T)$, outer section
a_c, b_c	constants in linearization of $q(T)$, centre section
a_i, a_j	stoichiometric coefficients
D_i	Knudsen diffusivity multiplied by $\gamma/2$
E_i	temperature independent part of D_i
f_i	rate of production of M_i in moles per unit area per unit time
$G(r, t)$	Green's function in solution for temperature profile
$\overline{H}_i$	heat carried by M_i per mole
$\widetilde{H}_i$	partial molar enthalpy of M_i
ΔH_T	heat of reaction for $\sum_{i=1}^{n} a_i M_i = 0$ at temperature T
i, j	component designating variables
k_s	thermal conductivity of catalyst
m_i	molecular weight of M_i
M_i	ith chemical specie
n	number of chemical species
p_i	partial pressure of M_i
p_{is}	partial pressure of M_i at the surface
$q(T)$	heat generation function
$Q(r)$	residual heat generation function
r	dimensionless radius variable
$\overline{r}$	average pore radius
r_x	radius at intersection of two-line approximation
R	particle radius
T	temperature in particle
T_c	temperature in two-line approximation, centre section
T_0	temperature in two-line approximation, outer section
T_s	surface temperature
T_L	limiting temperature
$T_j(v)$	jth temperature profile in successive substitution
t	dimensionless dummy radius variable
γ	fractional void volume
ρ	radius variable
ρ_p	particle density

REFERENCES

[1] THIELE E. W. *Indstr. Engng. Chem.* 1939 **31** 916.
[2] ZELDOWITSCH J. B. *Acta Physicochim. URSS* 1939 **10** 583.
[3] WHEELER A. *Advances in Catalysis*, Vol. 3 p. 249. Academic Press, New York 1951 : *Catalysis* Edited by EMMETT P. H. Vol. 2, Reinhold, New York 1955.
[4] PRATER C. D. and WEISZ P. B. *Advances in Catalysis*, Vol. 3, p. 249. Academic Press, New York 1951.
[5] ARIS R. *Chem. Engng. Sci.* 1957 **6** 262.
[6] WICKE E. *Z. Electrochem.* 1956 **60** 774.
[7] WICKE E. and BROTZ W. *Chem. Engng. Tech.* 1949 **21** 219.
[8] WICKE E. and HEDDEN K. *Z. Electrochem.* 1953 **57** 636.
[9] WICKE E. and KALLENBACH R. 1941 *Kolloid Z.* **97** 135.
[10] SEHR R. A. *Chem. Engng. Sci.* 1958 **9** 145.
[11] WEISZ P. B. *Chem. Engng. Prog.* **55** Symposium Series No. 25.
[12] WEISZ P. B. *Gordon Research Conf. Colby, June* 1952.
[13] WEISZ P. B. *Z. Phys. Chem.* 1957 **11** 1.
[14] WEISZ P. B. *Conf. on Chem. Reactor Dynam., Princeton Univ., April* 1957.
[15] WEISZ P. B. and PRATER C. D. *Advances in Catalysis*, Vol. 9. p. 575. Academic Press, New York 1957.
[16] WEISZ P. B. and SWEGLER E. W. *J. Phys. Chem.* 1955 **59** 823.
[17] WEISZ P. B. *Science* 1957 **126** 31.
[18] WEISZ P. B. *Science* 1956 **123** 887.
[19] FOX L. *The Numerical Solution of Two-Point Boundary Problems in Ordinary Differential Equations*. Clarendon Press, Oxford 1957.

Chemical Engineering Science, 1961, Vol. 13, pp. 237 to 244. Pergamon Press Ltd., London. Printed in Great Britain

Intraparticle diffusion and conduction in porous catalysts—II

Complex reactions

ROBERT E. SCHILSON* and NEAL R. AMUNDSON
University of Minnesota, Minneapolis 14, Minnesota, U.S.A.

(*Received* 10 *August* 1960)

Abstract—The problem of intraparticle diffusion and conduction is considered for complex reactions taking place in porous catalytic spheres. It is assumed that Knudsen diffusion prevails and that heat generated in the reaction is conducted through the porous structure to the catalyst surface. Equations are written for an arbitrary number of reactions and criteria are developed to determine the number of conservation equations for complex systems. A particular numerical example is worked both approximately and exactly by the same technique as used in the previous paper; the term exactly meaning that partial pressure and temperature profiles may be calculated numerically as accurately as desired. The approximate method should be satisfactory for almost all industrial work.

Résumé—Le problème de la diffusion et de la conduction à l'intérieur d'une particule est considéré pour des réactions complexes se produisant avec des catalyseurs poreux de forme sphérique. On suppose que la diffusion de Knudsen prévaut et que la chaleur dégagée par la réaction est conduite jusqu'à la surface du catalyseur à travers la structure poreuse de celui-ci. Des équations sont posées pour un nombre arbitraire de réactions et des critéria développés pour déterminer le nombre d'équations de conservation pour des systèmes complexes. Un exemple numérique particulier est étudié à la fois approximativement et exactement par la technique utilisée dans les précédents articles. Le terme exact montre que la pression partielle et le profil de température peuvent être calculés numériquement de façon aussi précise que l'on veut. La méthode approximative devrait être satisfaisante pour la plupart des cas industriels.

Zusammenfassung—Das Problem der intrapartikulären Diffusion und Leitung wird für komplexe Reaktoinen betrachtet, die in porösen Katalysatorkugeln stattfinden. Dabei wird angenommen, dass Knudsen-Diffusion vorherrscht und dass die Reaktionswärme durch die poröse Struktur zur Katalysatoroberfläche geleitet wird. Für eine willkürliche Zahl von Reaktionen werden Gleichungen angegeben und Kriterien entwickelt, um die Zahl der Bilanzgleichungen für komplexe Systeme zu bestimmen. Ein numerisches Beispiel ist sowohl angenähert als auch exakt mit der gleichen Methode durchgerechnet, die in der vorhergehenden Arbeit benutzt wurde; mit Hilfe des exakten Ausdrucks können Partialdruck und Temperaturprofil numerisch beliebig genau berechnet werden. Die Näherungsmethode sollte für die meisten industriellen Arbeiten genügen.

INTRODUCTION

IN A previous paper [1] the authors considered the problem of a chemical reaction taking place inside a single porous catalyst sphere. It was shown how the temperature and partial pressure profile could be calculated and how the effectiveness factor could be estimated. An approximate method was developed and it was shown that the approximation made by a suitable linearization gave results of satisfactory accuracy. It is the purpose of this paper to generalize the methods of the previous paper to complex reactions. An arbitrary system of chemical reactions will be considered [2].

The chemical species will be denoted by M_i and the stoichiometric coefficient of the ith species in the jth reaction will be a_{ij}. Suppose there are m reactions

$$\sum_{i=1}^{n} a_{ij} M_i = 0; \quad j = 1, 2, \ldots, m$$

where in a particular reaction a_{ij} is positive for a product and negative for a reactant. The heat of reaction for the jth reaction is ΔH_j and f_{ij} is

* Present address: The Ohio Oil Company, Littleton, Colorado, U.S.A.

the rate of formation of the ith species in the jth reaction in moles per unit of catalytic surface area per unit of time. The quantity f_{ij} may be a function of all n partial pressures, the temperature and the total pressure. We suppose that the set of chemical species $\{M_i\}$ contains all of the species in the reaction system.

It is proposed to show how the partial pressure and temperature profile may be computed both exactly and approximately. The same methods may be used if the conductivity of the particles is great enough so that temperature gradients may be neglected.

DERIVATION OF EQUATIONS*

It is assumed that Knudsen diffusion obtains within the particles so that the diffusion coefficient is given by

$$D_i = \frac{\gamma}{2} \cdot \frac{8}{3} \frac{\bar{r}}{\sqrt{(2\pi\, R m_i T)}} = \frac{E_i}{\sqrt{T}}$$

for the ith chemical species. E_i is independent of the temperature and depends on the pore properties as well as the molecular weight. Assuming that all flow is by molecular diffusion a mass balance on a single particle is given by

$$\frac{d}{d\rho}\left(\rho^2 D_i \frac{dp_i}{d\rho}\right) = -\rho^2 \rho_p S_g \sum_{j=1}^{m} f_{ij}\,; \qquad i = 1, 2, 3, \ldots n$$

From the stoichiometry of the reaction it follows that

$$\frac{f_{ij}}{a_{ij}} = \frac{f_{kj}}{a_{kj}} = \bar{f}_j \qquad \text{for all } j$$

so that

$$\frac{d}{d\rho}\left(\rho\, D_i \frac{dp_i}{d\rho}\right) = -\rho^2 \rho_p S_g \sum_{j=1}^{m} a_{ij} \bar{f}_j\,; \quad i = 1, 2, 3, \ldots n \qquad (1)$$

The question now arises as to the number of these equations which are independent. This set of equations may be written in vector form as

$$\frac{d}{d\rho}(\rho_2 \bar{\mathbf{q}}) = -\rho^2 \rho_p S_g \bar{A}\, \bar{\mathbf{f}}$$

where $\bar{\mathbf{q}}$ and $\bar{\mathbf{f}}$ are vectors,

$$\bar{\mathbf{q}} = \begin{bmatrix} D_1 \dfrac{dp_1}{d\rho} \\ D_2 \dfrac{dp_2}{d\rho} \\ \cdot \\ \cdot \\ \cdot \\ D_n \dfrac{dp_n}{d\rho} \end{bmatrix}\,; \quad \bar{\mathbf{f}} = \begin{bmatrix} \bar{f}_1 \\ \bar{f}_2 \\ \cdot \\ \cdot \\ \cdot \\ \bar{f}_m \end{bmatrix}$$

and $\bar{A}$ is the matrix

$$\bar{A} = \begin{bmatrix} a_{11} & a_{12} \cdots a_{1m} \\ a_{21} & a_{22} \cdots a_{2m} \\ \cdot & \cdot \quad \cdot \\ \cdot & \cdot \quad \cdot \\ \cdot & \cdot \quad \cdot \\ a_{n1} & a_{n2} \cdots a_{nm} \end{bmatrix}$$

Consider the matrix $\bar{A}^T$, the transpose of $\bar{A}$

$$\bar{A}^T = \begin{bmatrix} a_{11} & a_{21} \cdots a_{n1} \\ a_{12} & a_{22} \cdots a_{n2} \\ \cdot & \\ \cdot & \\ \cdot & \\ a_{1m} & a_{2m} \cdots a_{nm} \end{bmatrix}$$

and suppose $\bar{A}$ has rank s. For the sake of convenience, suppose the nonzero determinant of order s is in the upper left hand corner. If it is not, the species may be renumbered to make it so. Now if the columns of $\bar{A}^T$ are considered as vectors it follows that each of the last $n-s$ columns may be expressed as a linear combination of the first s columns. Therefore, there is a matrix $\bar{B}^T$ of the form

$$\bar{B}^T = \begin{bmatrix} 1 & 0 & 0 \ldots . 0 & \gamma_{s+1,1} & \cdots & \gamma_{n,1} \\ 0 & 1 & 0 \ldots . 0 & \gamma_{s+1,2} & & \gamma_{n,2} \\ 0 & 0 & 1 \ldots . 0 & \cdot & & \cdot \\ \cdot & & & \cdot & & \cdot \\ \cdot & & & \cdot & & \cdot \\ \cdot & & & \cdot & & \cdot \\ 0 & 0 \ldots \ldots . 1 & & \gamma_{s+1,s} & & \gamma_{n,s} \end{bmatrix}$$

* Notation will be the same as in the first paper.

VOL. 13 1961

and $\bar{\bar{B}}^T$ may be obtained from $\bar{\bar{A}}^T$ by operations on rows above, as by the Simplex Method of linear programming. In short, there is a matrix operator $\mathscr{P}$ such that

$$\bar{\mathscr{P}}\,\bar{\bar{A}}^T = \bar{\bar{B}}^T$$

or

$$\bar{\mathscr{P}}^*\,\bar{\bar{A}} = \bar{\bar{B}}$$

where $\bar{\mathscr{P}}^*$ is the matrix operator which operates on the columns of $\bar{\bar{A}}$. Note that the last n–s columns of $\bar{\bar{B}}^T$ represent the coefficients in the expansion of the last n–s columns of $\bar{\bar{A}}^T$ in terms of the first s columns of $\bar{\bar{A}}^T$, the first s columns being considered as a basis in a vector space.

If one now writes

$$\bar{\bar{A}}\,\bar{\mathbf{f}}$$

it is clear that this is a column vector with elements $\sum_{j=1}^{m} a_{ij}\bar{f}_j$ and hence each of the last n–s elements in the vector is a linear combination of the first s elements as

$$\sum_{j=1}^{m} a_{s+p,j}\,\bar{f}_j = \sum_{q=1}^{s} \gamma_{s+p,q} \sum_{j=1}^{m} a_{qj}\,\bar{f}_j, \quad p = 1 \text{ to } n\text{–}s$$

or from equation (1)

$$\frac{d}{d\rho}\left(\rho^2 D_i \frac{dp_i}{d\rho}\right) = \sum_{q=1}^{s} \gamma_{iq} \frac{d}{d\rho}\left(\rho^2 D_q \frac{dp_q}{d\rho}\right); \qquad i = s+1 \text{ to } n$$

This may be integrated once to give

$$D_i \frac{dp_i}{d\rho} = \sum_{q=1}^{s} \gamma_{iq} D_q \frac{dp_q}{d\rho}, \quad i = s+1 \text{ to } n \qquad (2)$$

where use has been made of the fact that the gradients are zero at the centre of the particle. Since $E_i = D_i\sqrt{T}$ the latter equation may be integrated to give

$$E_i(p_i - p_{is}) = \sum_{q=1}^{s} \gamma_{iq} E_q (p_q - p_{qs}), \qquad i = s+1 \text{ to } n \qquad (3)$$

Therefore inside the particle there are s independent partial pressures since the remaining $(n$–$s)$ may be eliminated from the rate expressions, and hence also there are s equations of the type given by equation (1).

Equation (2), of course, may be written in the form

$$\bar{\mathbf{q}} = \bar{\bar{B}}\,\bar{\mathbf{q}}' \qquad (4)$$

where

$$\bar{\mathbf{q}}'^T = \left[D_1 \frac{dp_1}{d\rho}\; D_2 \frac{dp_2}{d\rho} \ldots D_s \frac{dp_s}{d\rho}\right]$$

The essential result of this development is that if the rank of the stoichiometric matrix is s there are s independent mass conservation equations, the remaining partial pressures having been eliminated by equation (3).

Now the heat balance must be considered. The same assumptions are made here as in the previous paper so that the energy conservation equation is formally the same

$$\frac{d}{d\rho}\left(\rho^2(1-\gamma)k_s\frac{dT}{d\rho}\right) + \frac{d}{d\rho}\left(\rho^2 \sum_{i=1}^{n} D_i \hat{H}_i \frac{dp_i}{d\rho}\right) = 0 \qquad (5)$$

Here again $\hat{H}_i$ is the partial molar enthalpy and the heat of transport $(-\frac{1}{2}RT)$ will be neglected. One integration can be made directly to give

$$(1-\gamma)\,k_s\frac{dT}{d\rho} + \sum_{i=1}^{n} D_i \hat{H}_i \frac{dp_i}{d\rho} = 0$$

Define now a vector $\bar{\mathbf{H}}$ in which $\hat{H}_i$ is the ith element, then

$$(1-\gamma)\,k_s\frac{dT}{d\rho} + \bar{\mathbf{H}}^T\bar{\mathbf{q}} = 0 \qquad (6)$$

A vector $\overline{\Delta\mathbf{H}}$ of the heats of reaction may be defined where the ith element is the heat of reaction of the ith reaction. Hence

$$\bar{\bar{A}}^T\,\bar{\mathbf{H}} = \overline{\Delta\mathbf{H}}$$

Also the reaction system itself may be written

$$\bar{\bar{A}}^T\,\bar{\mathbf{M}} = \bar{\mathbf{0}}$$

where $\bar{\mathbf{M}}$ is the vector of chemical species. The operator $\bar{\mathscr{P}}$ operating as

$$\mathscr{P}\,\bar{\bar{A}}^T\,\bar{\mathbf{M}} = \bar{\mathbf{0}}$$

will give another set of chemical reactions where the heat of reaction vector will be

$$\bar{\mathscr{P}}\,\bar{\bar{A}}^T\,\bar{\mathbf{H}} = \overline{\Delta\mathbf{H}}' = \bar{\bar{B}}^T\,\bar{\mathbf{H}} \qquad (7)$$

where a typical element of $\overline{\Delta \mathbf{H}}'$ is

$$\Delta H_r' = \hat{H}_r + \gamma_{s+1,r}\,\hat{H}_{s+1} + \cdots + \gamma_{nr}\,\hat{H}_n\,; \qquad r = 1 \text{ to } s$$

and also where the elements $\Delta H_r'$ are a linear combination of the original ΔH_r. From equations (4), (6) and (7) one may write

$$(1-\gamma)\,k_s\frac{dT}{d\rho} + \overline{\mathbf{H}}^T\,\overline{B}\,\overline{\mathbf{q}}' = 0$$

The transpose may be taken to give

$$(1-\gamma)\,k_s\frac{dT}{d\rho} + \overline{\mathbf{q}}'^T\,\overline{B}^T\,\overline{\mathbf{H}} = 0$$

or

$$(1-\gamma)\,k_s\frac{dT}{d\rho} + \overline{\mathbf{q}}'^T\,\overline{\Delta \mathbf{H}}' = 0$$

If $\overline{\Delta \mathbf{H}}'$ is assumed to be a constant vector, then

$$\frac{2}{3}(1-\gamma)\,k_s\,(T^{3/2} - T_s^{3/2}) = -\sum_{i=1}^{s} E_i\,\Delta H_i'\,(p_i - p_{is})$$

or if D_i is taken a as constant

$$(1-\gamma)\,k_s\,(T - T_s) = -\sum_{i=1}^{s} D_i\,\Delta H_i'\,(p_i - p_{is})$$

and hence the temperature or one of the independent p_i's can be eliminated from the rate expression.

Hence of the original $n+1$ conservation equations there are only s conservation equations which need integrating. Which equations in a particular case will be integrated depends on what is desired. In the example to follow in which ΔH_j and D_j are assumed temperature independent, a partial pressure and the temperature will be used as independent variables.

EXAMPLE

We will consider a reaction system

1. $A + B \rightarrow C$
2. $2C \rightarrow D + E$

in which the reactions are irreversible and second order in the forward direction. The reaction is carried out in a porous pellet with the following information available.

$\Delta H_1 = -80{,}000$ cal/g mole
$\Delta H_2 = 60{,}000$ cal/g mole
$m_A = 25$ g/g mole
$m_B = 36$ g/g mole
$m_C = 61$ g/g mole
$m_D = 72$ g/g mole
$m_E = 50$ g/g mole
$T_s = 550°\text{K}$
$p_{As} = 1.50$ atm
$p_{Bs} = 1.50$ atm
$p_{Cs} = .010$ atm
$p_{Ds} = p_{Es} = 0.0$ atm
$R = 0.5$ cm
$\bar{r} = 200$ Å
$\gamma = 0.40$
$k_s = 8 \times 10^{-4}$ cal /sec cm °K
$D_A = 3.892\,(10^{-7})$ g mole/atm cm sec
$D_B = 3.244\,(10^{-7})$ g mole/atm cm sec
$D_C = 2.492\,(10^{-7})$ g mole/atm cm sec
$D_D = 2.293\,(10^{-7})$ g mole/atm cm sec
$D_E = 2.752\,(10^{-7})$ g mole/atm cm sec

$$f_{A1} = 3.36\,(10^{-8})\exp\left(-\frac{7500}{T}\right)p_A p_B \frac{\text{g mole } A}{\text{cm}^2\,\text{sec}}$$

$$f_{C2} = 1.430\,(10^{4})\exp\left(-\frac{20{,}000}{T}\right)p_C{}^2 \frac{\text{g mole } C}{\text{cm}^2\,\text{sec}}$$

In this problem the rank of the stiochiometric matrix is two so that there are two conservation equations. The detailed manipulations will not be given here but on the assumption that $\Delta \mathbf{H}$, k_s, and the diffusivities are constant the following relations may be derived.

$$p_C = \left(p_{Cs} + \frac{D_A}{D_C}p_{As} + \frac{2D_D}{D_C}p_{Ds}\right) - \frac{D_A}{D_C}p_A - \frac{2D_D}{D_C}p_D$$

$$p_B = \left(p_{Bs} - \frac{D_A}{D_B}p_{As}\right) + \frac{D_A}{D_B}p_A$$

$$p_D = \left(p_{Ds} - \frac{D_A\,\Delta H_1}{D_D\,\Delta H_2}p_{As} + \frac{k_s(1-\gamma)}{D_D\,\Delta H_2}T_s\right) + \frac{D_A}{D_D}\frac{\Delta H_1}{\Delta H_2}p_A - \frac{k_s(1-\gamma)}{D_D\,\Delta H_2}T$$

VOL 13 1961

The two conservation equations may be written

$$\frac{d_2 p_A}{dr^2} + \frac{2}{r}\frac{dp_A}{dr} + w(T, p_A) = 0$$

$$\frac{d^2 T}{dr^2} + \frac{2}{r}\frac{dT}{dr} + q(T, p_A) = 0$$

with

$$q(T, p_A) \quad \frac{R^2 \rho_p S_g}{k_s (1-\gamma)}\left[f_{A1}(\Delta H_1) + \frac{f_{C2}}{2}(\Delta H_2)\right]$$

$$w(T, p_A) = \frac{R^2 \rho_p S_g}{D_A} f_{A1}$$

The solution of this set of equations follows in principle the solution for a single equation except that it is more complicated. Our purpose here is to sketch the solution not to present the detailed technique. A particular example will be solved rather than a general one but it will be obvious what changes need be made for other cases. It will be recalled that a certain linear approximation was made and that will be done here. Let

$$a_{00} + a_{10} p_A + a_{11} T$$

and

$$b_{00} + b_{10} p_A + b_{11} T$$

be linear approximations to $q(T, p_A)$ and $w(T, p_A)$ respectively. Then the solution of the equations

$$\frac{d^2 T}{dr} + \frac{2}{r}\frac{dT}{dr} + a_{00} + a_{10} p_A + a_{11} T = 0$$

$$\frac{d^2 p_A}{dr^2} + \frac{2}{r}\frac{dp_A}{dr} + b_{00} + b_{10} p_A + b_{11} T = 0$$

with

$$\frac{dT}{dr} = 0 = \frac{dp_A}{dr} \qquad \text{at } r = 0$$

$$\left.\begin{aligned} T &= T_s \\ p &= p_{As} \end{aligned}\right\} \qquad \text{at } r = 1$$

should give an approximation to the temperature and partial pressure profiles, say the first approximation. This solution may be found by direct methods and it is

$$T_1(r) = X(r) - Y(r)$$

$$p_{A1}(r) = \beta X(r) - \alpha Y(r)$$

where

$$X(r) = \frac{b_{00} - \alpha a_{00}}{\mu^2(\beta - \alpha)} + \frac{(\mu^2 p_{As} - b_{00}) - \alpha(\mu^2 T_s - a_{00})}{\mu^2(\beta - \alpha)\sinh \mu} \frac{\sinh \mu r}{r} \tag{8}$$

$$Y(r) = \frac{b_{00} - \beta a_{00}}{\lambda^2(\beta - \alpha)} + \frac{\mu^2 p_{As} - b_{00}) - \beta(\lambda^2 T_s - a_{00})}{\lambda^2(\beta - \alpha)\sinh \lambda} \frac{\sinh \lambda r}{r} \tag{9}$$

with

$$\lambda = \frac{1}{\sqrt{2}}\left[-u + \sqrt{(u^2 - 4v)}\right]^{1/2}$$

$$\mu = \frac{1}{\sqrt{2}}\left[-u - \sqrt{(u^2 - 4v)}\right]^{1/2}$$

$$u = a_{11} + b_{10}$$

$$v = a_{11} b_{10} - b_{11} a_{10}$$

$$\alpha = \frac{\lambda^2 + a_{11} - b_{11}}{\lambda^2 + b_{10} - a_{10}}$$

$$\beta = \frac{\mu^2 + a_{11} - b_{11}}{\mu^2 + b_{10} - a_{10}}$$

With these functions the profiles may be plotted and this will be done.

As a generalization of the previous paper the two differential equations are now written

$$\frac{d^2 T}{dr^2} + \frac{2}{r}\frac{dT}{dr} + a_{10} p_A + a_{11} T = Q(r) - a_{00}$$

$$\frac{d^2 p_A}{dr^2} + \frac{2}{r}\frac{dp_A}{dr} + b_{10} p_A + b_{11} T = W(r) - b_{00}$$

where

$$Q(r) = a_{00} + a_{10} p_A + a_{11} T - g(T, p_A)$$

$$W(r) = b_{00} + b_{10} p_A + b_{11} T - w(T, p_X)$$

If it is assumed for the moment that $Q(r)$ and $W(r)$ are known functions of r, these two equations may be changed to integral equations by the method of variation of parameters to give

$$T(r) = X(r) - Y(r) + \int_0^1 \left[\alpha Q(\epsilon) - W(\epsilon)\right] G_\mu(r, \epsilon)\, d\epsilon - \tag{10}$$

$$- \int_0^1 [\beta Q(\epsilon) - W(\epsilon)] G_\lambda(r, \epsilon)\, d\epsilon$$

$$p_A(r) = \beta X(r) - \alpha Y(r) + \beta \int_0^1 [\alpha Q(\epsilon) - W(\epsilon)] G_\mu(r, \epsilon)\, d\epsilon - \alpha \int_0^1 [\beta Q(\epsilon) - W(\epsilon)] G_\lambda(r, \epsilon)\, d\epsilon \qquad (11)$$

with

$$G_\mu(r,\epsilon) = \begin{cases} \dfrac{\epsilon \sinh \mu(1-r) \sinh \mu\epsilon}{r(\beta-\alpha)\mu \sinh \mu}, & 0 \leqslant \epsilon \leqslant r \\ \dfrac{\epsilon \sinh \mu r \sinh \mu(1-\epsilon)}{r(\beta-\alpha)\mu \sinh \mu}, & r \leqslant \epsilon \leqslant 1 \end{cases}$$

and where $G_\lambda(r, \epsilon)$ is the same except λ is substituted for μ. Equations (10) and (11) are solved by successive substitutions to obtain a sequence of profiles which it is hoped will converge in the limit to the solution of the original set of differential equations. That is, the profiles $T_1(r)$ and $p_{A1}(r)$ are substituted into $Q(\epsilon)$ and $W(\epsilon)$ to obtain new profiles $T_2(r)$ and $p_{A2}(\epsilon)$ and this process is iterated to give a sequence of profiles $\{T_n(r), p_{An}(r)\}$.

From these equations the effectiveness factor may be computed from

$$\text{E.F.} = \frac{-3 D_a (dp_i/dr)_{r=1}}{R^2 \rho_p S_g \sum_{j=1}^{m} (f_{ij})_s} \frac{\text{moles of } M_i}{\text{unit of time}}$$

λ and μ could be complex numbers but this alters the method in detail rather than principle.

With the data presented at the beginning of this Section it may be shown that

$$q(T, p_A) = 5{\cdot}60\,(10^8) \exp\left(-\frac{7500}{T}\right) \cdot p_A(1{\cdot}1998\, p_A - 0{\cdot}2997) - 8{\cdot}92\,(10^{16}) \exp\left(-\frac{20{,}000}{T}\right) \cdot (2{\cdot}604\, p_A + 0{\cdot}06421\, T - 39{\cdot}12)^2$$

$$w(T, p_A) = -8{\cdot}632\,(10^6) \exp\left(-\frac{7500}{T}\right) \cdot p_A(1{\cdot}1998\, p_A - 0{\cdot}2997)$$

where use has been made of the formula $\rho_p S_g = 2\lambda/\tau$. In order to study the nature of the functions q and w calculations were made and three-dimensional models made which are shown in Figs. 1 and 2. These models are interesting but they must be analysed further to find the region in the T, p_A plane of interest. Since $q(T_s, p_{As})$ is positive it appears that there will be a net exothermic effect so that $T \geqslant 550°$ K in the particle. Since p_B and p_C must not be negative

$$p_A \geqslant 0{\cdot}2498$$

$$T \geqslant 609{\cdot}2 - 40{\cdot}55$$

In addition $p_A \leqslant 1{\cdot}50$. A further boundary line may be obtained from the condition that if the first reaction goes to completion and the second one is insignificant, then $p_C \leqslant 1{\cdot}50$ and therefore

$$T \leqslant 632{\cdot}6 - 40{\cdot}55\, p_A$$

The resulting region of interest is shown in Fig. 3. With this information the linear approximations can be found and in this problem these are

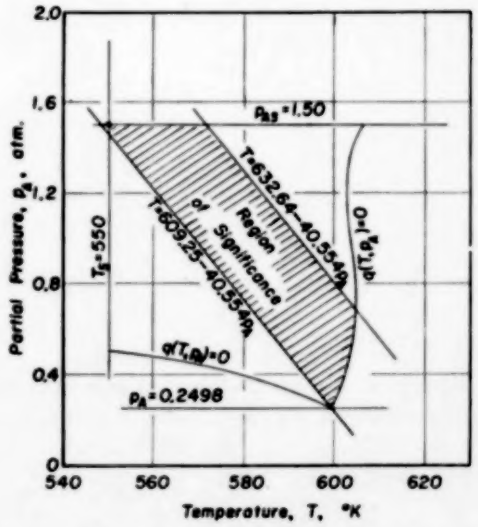

FIG. 3. Graph showing the region of interest in the T, p_A plane for the sample problem.

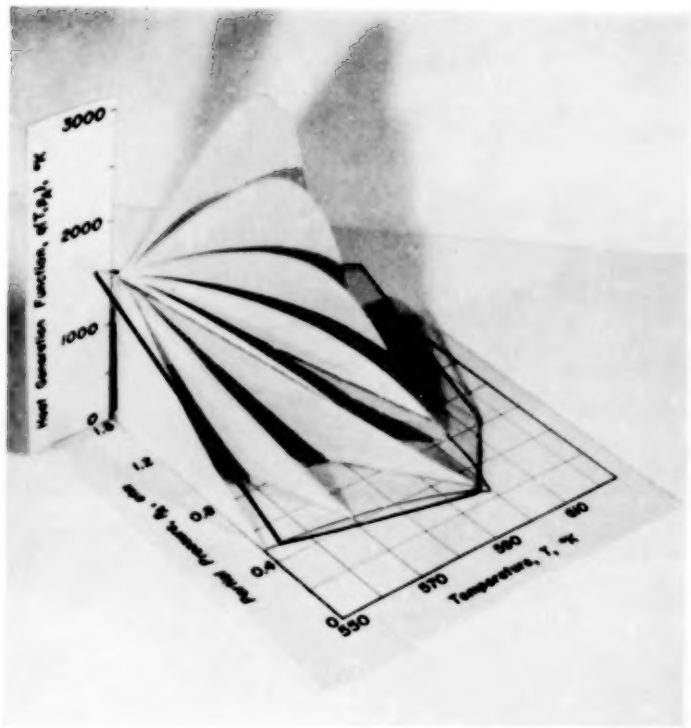

FIG. 1. Heat generation function of $q(T, p_A)$. Photograph of three-dimensional model.

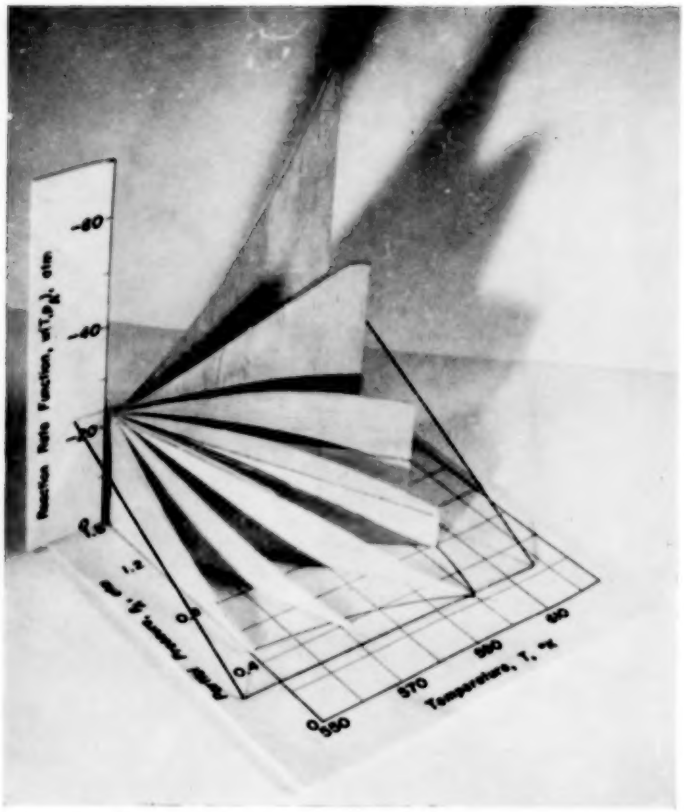

FIG. 2. Mass generation function $w(T, p_A)$. Photograph of three-dimensional model.

$$a_{00} + a_{10}p_A + a_{11}T = 8463 + 638{\cdot}7\,p_A - 14{\cdot}37\,T$$

$$b_{00} + b_{10}\,p_A + b_{11}T = 4{\cdot}676 - 18{\cdot}70\,p_A$$

Then

$$u = -33{\cdot}07$$
$$v = 268{\cdot}8$$
$$\lambda = 4{\cdot}325$$
$$\mu = 3{\cdot}791$$
$$\alpha = -0{\cdot}006784$$
$$\beta = 0{\cdot}000 \qquad (b_{11} = 0)$$

and

$$T(r) = 600{\cdot}0 + 6{\cdot}064\,\frac{\sinh \mu r}{r} - 4{\cdot}878\,\frac{\sinh \lambda r}{r} + \int_0^1 \left[\alpha\,K(\epsilon) - W(\epsilon)\right] G_\mu(r, \epsilon)\,d\epsilon + \int_0^1 W(\epsilon)\,G_\mu(r, \epsilon)\,d\epsilon$$

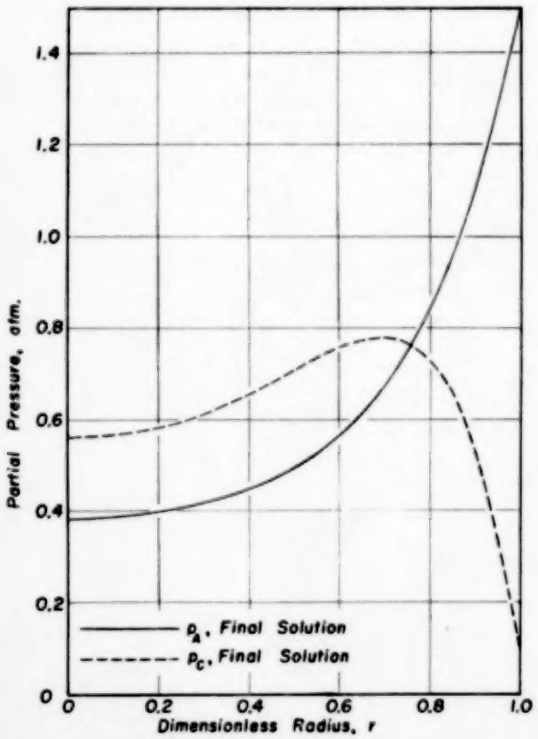

FIG. 4. Particle pressure profiles in particle for reactant A and product C (Exact solution).
—— p_A Final solution
- - - - p_C Final solution

$$p_A(r) = 0{\cdot}2500 + 0{\cdot}0331\,\frac{\sinh \lambda r}{r} - \alpha \int_0^1 W(\epsilon)\,G_\lambda(r, \epsilon)\,d\epsilon$$

The calculations were carried out as suggested earlier and the partial pressure and temperature profiles are shown in Figs. 4 and 5. What is called the final solutions on these curves is a result of several successive substitutions in the integral

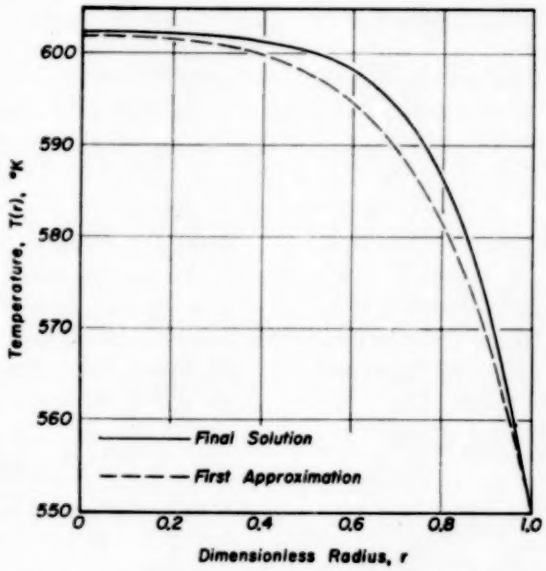

FIG. 5. Temperature profiles within particle showing effect of linear approximation.
—— Final Solution
- - - - p_C First approximation.

equations. The essential point here, however, is not the number of calculations made but rather the excellence of the results with the linear approximation, equations (8) and (9). Effectiveness factors are as follows :

	Final solution	*Approximate solution*
E.F. (on A)	0·592	0·533
E.F. (on C)	0·412	0·364
T_c (°K)	603	602

These calculations were made on a desk calculator with the radius of the particle divided into twenty equal parts. The integrals were then computed using a simple trapezoidal rule. Some attempts were made to determine the effect of interval size but no conclusions were drawn. Attempts were also made to solve the problem on an analogue computer although these results were only partially successful. The equations tend to be unstable when proceeding from the surface inwards. Some success was achieved integrating the equations on an analogue computer starting at the particle centre and moving outwards. However, two values must be guessed, the partial pressure and temperature at the centre of the particle, and this can be inconveniently tedious.

SUMMARY AND CRITIQUE

This paper is a generalization to complex systems of reactions of the previous paper on simple reactions. It was shown that the rank of the stoichiometric matrix gives the number of conservation equations which need integrating. An approximate method was devised for solving the equations and a technique was described which could be used to obtain temperature and partial pressure profiles as rigorously as desired. The approximation method may break down in some cases but it is recalled that for simple reactions it worked remarkably well.

It must be stated that the methods used in this paper for numerical computations while satisfactory for two and possibly three reactions will probably not be suitable for larger numbers of reactions. Analogue computer solutions for three or more reactions may be less inconvenient but this remains to be shown. It has been suggested that grid methods, that is the transformation to finite difference approximations for the derivations, be tried but there are considerable difficulties with this because of the nonlinearity of the finite difference equations and lack of information on convergence of the resulting iterative process. It would seem that some simpler approximation scheme is needed.

Acknowledgements—This work was supported by grants-in-aid from the Procter & Gamble Company, the Eastman Kodak Company, the Standard Oil Foundation (Indiana), the Minneapolis–Honeywell Regulator Company, and by support from the National Science Foundation.

REFERENCES

[1] SCHILSON R. E. and AMUNDSON N. R. *Chem. Engng. Sci.* (In press).

[2] SCHILSON R. E., Ph.D. Thesis, University of Minnesota, December 1957.

Chemical Engineering Science, 1961, Vol. 13, pp. 245 to 262. Pergamon Press Ltd., London. Printed in Great Britain

An investigation of laws governing the spouting of coarse particles*

H. A. Becker

(*Received* 5 *May* 1960)

Abstract—The relationships between the variables involved in the spouting of coarse particles are considered. The dependent variables are divided into four categories: those dependent only on the gas and particle properties, those dependent also on the column geometry, those additionally dependent on the bed depth, and those moreover dependent on position within the bed. General correlations are presented for variables of the first three categories (the minimum spouting velocity and its maximum and the maximum spoutable bed depth), and for one of the fourth category (the frictional pressure gradient). Restricted correlations are given for other variables of the fourth category (the rate of agitation and the local gas velocity).

Résumé—L'auteur considère les relations entre les variables qui interviennent pour maintenir en suspension des grosses particules. Il distingue 4 catégories de variables dépendantes: Celles qui dépendent seulement des propriétés des gaz et des particules. Celles qui dépendent aussi de la forme de la colonne, celles qui dépendent en plus de la profondeur du lit, et celles dépendant en outre de la position à l'intérieur du lit. Des relations générales sont données pour les variables des 3 premières catégories (vitesse min. de fluidisation et épaisseur min. et max. de lit fluidisé) et pour une variable de la 4ème catégorie (gradient de pression de friction). Des relations restrientes sont données pour les autres variables de la 4ème catégorie. (Vitesse d'agitation et vitesse locale du gaz).

Zusammenfassung—Die Beziehungen zwischen den Variablen beim Wirbeln von groben Teilchen werden betrachtet. Die abhängigen Variablen werden in vier Gruppen eingeteilt: solche, die nur von den Eigenschaften des Gases und der Teilchen abhängen, solche, die auch noch von den Säulenabmessungen abhängen, solche, die zusätzlich von der Höhe des Wirbelbettes abhängen, und solche, die ausserdem von der Lage innerhalb des Bettes abhängen. Für die Variablen der ersten drei Gruppen (minimale Wirbelgeschwindigkeit, ihr Maximum sowie die maximale Wirbelbetthöhe) und für eine der vierten Gruppe (der Druckgradient infolge Reibung) werden allgemeine Beziehungen angegeben. Restriktive Korrelationen sind für die anderen Variablen der vierten Gruppe (Rührgeschwindigkeit und örtliche Gasgeschwindigkeit) angegeben.

Introduction

The spouted bed technique of agitating beds of coarse particles was discovered by Mathur and Gishler [1]. They also made an exploratory study of the drying of wheat as a possible practical application of the new gas–solids contacting technique [2]. This study was continued and completed by the present author and Sallans [3]. In the course of the investigation it became clear that a knowledge of the general laws governing spouting was needed to guide the rational scale-up and design of dryers, and the research herein described was accordingly undertaken. The studies perforce transcended their primary aim and the generalizations to which they led are applicable to a variety of systems in broad ranges of the important variables, and have bearing as well on related aspects of aggregative fluidization.

Apparatus

The type of column used in spouting consisted of an upright, circular cylinder with a conical base terminating in a gas inlet pipe (see Fig. 1b). Geometrically this type of column is completely described by specifying the column diameter, D_c, the gas inlet pipe diameter, D_0, and the angle included by the base cone, β. Table 1 lists these dimensions for the five columns used in the present study.

Materials

Table 2 summarizes the physical properties of the particles spouted. Densities were determined pycnometrically

* Contribution from the National Research Council of Canada, Prairie Regional Laboratory, Saskatoon, Saskatchewan. Issued as N.R.C. No. 6139.

with toluene. Particle diameters are expressed as the diameter, D_v, of an equi-volumed sphere, calculated from the density and average weight of a particle. The cereal grains can be regarded as uniform particles; the kernel size distribution of wheat has recently been described [4]. The Ottawa sand was from a standard Tyler sieve fraction.

Definitions of Some Variables and Notes on Experimental Methods

1. *Bed Depth L*

The bed depth was measured (and enters the subsequent correlations) as the settled bed depth observed after strongly agitating a bed and then gradually shutting off the gas flow. (The gas used was air at room temperature.)

2. *Maximum spoutable bed depth (m.s.b.d.), L_m*

Mathur and Gishler [1] found that for a given system of column, gas and particles there is a maximum bed depth which can be spouted. This maximum is quite sharply defined and is usually reproduceable within ± 5 per cent.

3. *Average fraction void, ϵ*

The average fraction void of a bed under given conditions was calculated from the volume of the bed, the weight of material in it and the absolute density of the material.

4. *Fraction void at the point of incipient particulate fluidization, ϵ_{mf}.*

This characteristic, 'static' fraction void was measured, and is uniquely defined, as the fraction void of a quiescent bed naturally consolidated by gradual reduction of agitation, as described above under 'bed depth.'

5. *Maximum fraction void, ϵ_m.*

This characteristic 'dynamic' fraction void was measured, and is uniquely defined, as the fraction void observed when the gas flow through a bed is increased to the point of maximum, coherent, dense-phase expansion of the bed, i.e. to the point of incipient aggregative fluidization.

6. *Minimum spouting Velocity, v_s.*

The admission of an increasing flow of gas to a bed of particles resting in a column suitable for spouting causes no visible change until a central cone of particles with apex at the gas inlet is effectively suspended in the rising gas stream. The bed then expands slightly while the gas flow is increased a further 30 per cent or less, on which the entering gas jet becomes sufficiently intense to project a sharply bounded stream of particles upward through its core, forming a gas–solids jet, the 'spout.' The superficial gas velocity at this critical point is not reproduceable to the extent that the 'yield shear strength' of the bed is variable, the more so when the particles are nonspherical or rough and the particle-to-column diameter ratio is high, promoting bridging. If, on the other hand, the gas flow rate through a spouting bed is gradually reduced until the spout just fails, the superficial velocity at that point is less subject to unpredictable constraints on the bed, and is a precisely determineable quantity which Mathur and Gishler [1] call the 'minimum spouting velocity.'

7. *Maximum of the minimum spouting velocity, v_m.*

The minimum spouting velocity increases with increasing bed depth and becomes maximum at the maximum spoutable bed depth. The experimental evidence shows (as will be seen) that this maximum is identical with the minimum superficial gas velocity causing onset of aggregative (two-phase) fluidization.

8. *Minimum superficial velocity for onset of particulate fluidization, v_{mf}.*

This characteristic velocity is commonly defined as the superficial fluid velocity at which the extrapolated relation between frictional pressure drop and fluid velocity for a quiescent bed intersects the ordinate of equality between the drag and weight forces. The definition is made unique (at least for smooth walled columns and low values of the particle-to-column diameter ratio) by specifying that the quiescent bed is consolidated by gradual reduction of agitation. Then

$$v = v_{mf} \text{ at } (-\Delta P)_{f,\text{ext.}} = gL(\rho_s - \rho)(1 - \epsilon_{mf})$$

9. *Absolute local gas velocity, u*

The term "absolute" local gas velocity is here only meant to imply some direct, average measure of the local gas velocity in a bed, to be contrasted with an indirect measure such as the superficial velocity. The problem of obtaining such an 'absolute' measure in so complex a situation as that prevailing in an agitated bed of particles has obvious difficulties, an evidently satisfactory solution of which was found by using the following Pitot-type instrument: separate impact and static pressure probes were constructed from $\frac{3}{64}$ in. stainless steel tubing and were mounted in lengths of heavy-walled brass tubing. The brass tubes were rigidly coupled, bringing the impact and static openings into apposition about 2 in. apart. This instrument was mounted in suitable carriers to probe any position in the 0·5 ft and 0·75 ft diameter columns. Only beds of wheat were investigated, but measurements could as easily be made in beds of larger particles. With smaller particles, the differential pressures developed would be rather low, besides which the impact probe Reynolds number might be too small for accurate measurements (it is well known that in a free gas stream this Reynolds number must be held above 100 if the probe is to be used without calibration for viscous effects). The diameter of the impact tube for the present work was chosen to be comparable with the particle diameter, (but slightly smaller, to prevent clogging). Larger probes could be used, if screened, but might upset the gas and particle flow patterns excessively.

Respecting successful use of this instrument, a spouted

bed has the saving grace that all the particles are in continuous and rapid movement. The fluctuations sensed as changing configurations of particles pass the probe tip are significantly averaged, owing to the inertia of the micromanometer used to sense the differential pressures, and a constant reading is observed. The situation may not be much worse than when a Pitot tube is used to measure average velocities in a stream of high turbulence intensity. A wholly correct interpretation of such measurements cannot be hoped for, but interpretation in a relative sense can nevertheless be undertaken without qualms, since the nonideality of the measurements probably varies little.

Results

1. *The four categories of dependent variables*

Mathur and Gishler [1, 2] have described the general characteristics of the spouted bed technique of agitating beds of particles. The problem of quantitatively predicting the behaviour of spouted beds will therefore be broached at once, without further preamble. What follows is, in essence, a development and presentation of correlations for predicting the more important of the dependent variables involved in spouted systems. These variables are formally separable into four categories:

(i) Those dependent only on the properties of the gas and particles: the maximum of the minimum spouting velocity, v_m, and the maximum fraction void, ϵ_m;

(ii) Those also dependent on the column geometry: the maximum spoutable bed depth, L_m;

(iii) Those additionally dependent on the bed depth: the minimum spouting velocity, v_s, the integral frictional pressure drop, $(-\Delta P)_f$, and the maximum duration of the bed turnover cycle, θ_c;

(iv) Those moreover dependent on position within the bed; the frictional pressure gradient, $(-dP/dz)_f$, the particle velocity at the wall, u_p, the local gas velocity, u, etc. It will be seen that this classification delineates the most profitable order of consideration, that discussion of the variables in each category presupposes knowledge of those preceding it. Other approaches are possible but appear likely to obscure some basic features of spouted systems.

2. *The maximum of the minimum spouting velocity*

2.0 *Introductory note.* The maximum of the minimum spouting velocity (by Section 1) belongs in the first category of dependent variables, being a function only of the properties of the gas and the particles. The reason for this characteristic is easily appreciated on examining the relation between the drag forces, the weight forces, the reduced superficial gas velocity v/v_m and the reduced bed depth L/L_m, typified by Fig. 1 (a). It is seen that at the maximum spoutable bed depth ($L/L_m = 1$) the minimum spouting velocity slightly exceeds the velocity (v_{mf}) equalizing the drag and weight forces in a quiescent bed, thus

Table 1. *Characteristics of columns*

Material of construction	D_c, (ft.)	D_0/D_c	β
Black iron	0·50	0·175	90°, 120°
Black iron	0·75	0·179	90°, 120°
Black iron	1·00	0·172	90°,
Aluminium	2·00	0·167	90°, 180°
Glass	0·49	0·065 0·086 0·155 0·196 0·285 1·000*	180°

* This arrangement was used in studying the onset of fluidization. A calming section preceded the support screen holding the bed.

indicating the existence of a terminal condition. Indeed, the experimental evidence (more of which is produced in the following Sections) uniformly indicates that the maximum of the minimum spouting velocity is identical with the minimum superficial gas velocity causing onset of aggregative fluidization.

2.1 *Direct correlation of the terminal drag coefficient.* The aforementioned characteristics of the maximum of the minimum spouting velocity indicate that the total drag coefficient based upon

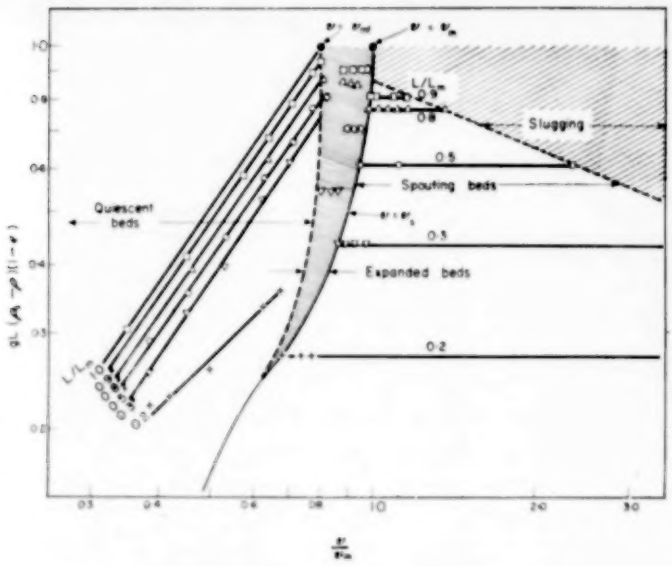

Fig. 1(a). A typical relation between the reduced drag force, the reduced gas velocity and the reduced bed depth for a bed of particles contained in a column shaped for spouting. This constitutes a "phase diagram" for such a bed. Data on wheat in the 0·5 ft dia. glass column with $\beta = 180°$.

equality between the drag and weight forces, $C_D = 4\,D_v\,g\,(\rho_s - \rho)/3\rho v_m^2$, and the corresponding Reynolds number, $\mathrm{Re}_m = D_v\,v_m\,\rho/\mu$, should be be uniquely related for particles of similar shape, (the choice of a characteristic particle dimension in these definitions is arbitrary, but the diameter, D_v, of an equi-volumed sphere is convenient and unambiguous). The limited data so far obtained are in reasonable agreement thereon; Fig. 2 indicates that the loci of data on similarily-shaped particles are smooth curves whose displacement with increasing nonsphericity of shape is in the expected direction of an increasing drag coefficient. The data on spheres are closely represented by the equation

$$C_D = 22 + \frac{2600}{\mathrm{Re}_m} \qquad (1)$$

The (broken) curves for the nonspherical particles are based on the assumption (good for moderate

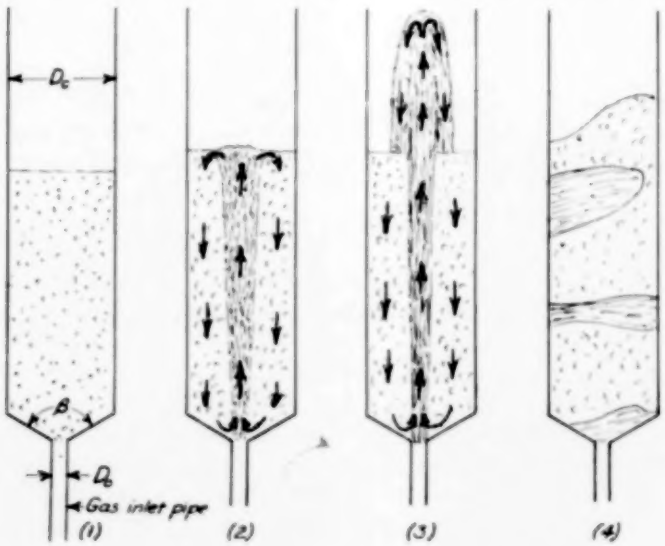

Fig. 1(b). Sketches of beds in some of the states represented in Fig. 1(a):

(1) A quiescent bed resting in a column shaped for spouting.

(2) A spouting bed at the point of minimum spouting; i.e. at the point of extinction of the spout, at which $v = v_s$.

(3) A spouting bed at a higher gas velocity; $v > v_s$.

(4) A slugging bed showing the passage of massive pockets of gas in a pattern unproductive of particle turnover; $v \gg v_s$.

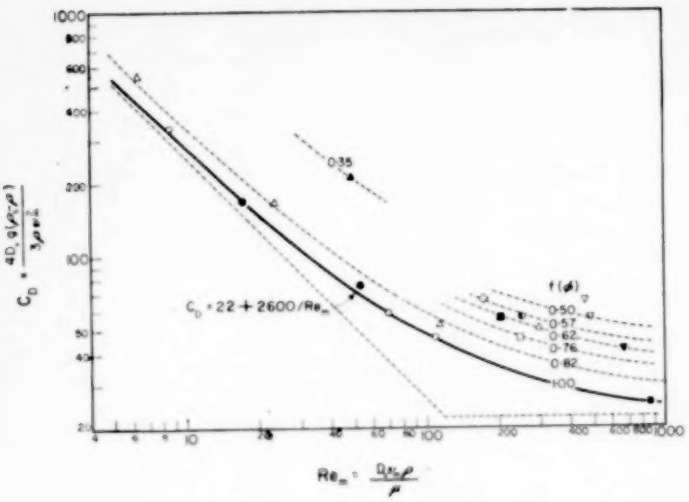

FIG. 2. A correlation of the maximum of the minimum spouting velocity.

Present data ● ■ ▲ ▼ ◐

MATHUR and GISHLER ○ □ △ ▽ ◇

Spheres* ● ○ Flax seed ▲

Wheat Barley ◐

Corn Oats ◇

Sunflower seeds, Coffee beans ▽

Brucite, Shale, Gravel △

* Spheres: peas, rape seed, mustard seed, Ottawa sand.

ranges of Reynolds number) that the fractional excursion of the ordinate (C_D) with change in particle shape is independent of the Reynolds number, and is therefore representable in equation (1) by inserting an experimental shape factor $f(\phi)$:

$$C_D f(\phi) = 22 + \frac{2600}{Re_m} \qquad (2)$$

Appropriate values of this shape factor are given as the parameter in Fig. 2.

Table 2. Characteristics of particles

Particle	D_v (ft)	ρ_s* (lb/ft^3)	Ψ
Corn	0·0227	78·7	0·75
Peas	0·0218	86·0	1·00
Barley	0·0131	82·4	—
Wheat	0·0111	86·0	0·91
Flax seed	0·0071	71·2	—
Rape seed	0·0053	69·9	1·00
Ottawa sand	0·0025	166·0	0·98

* The densities of the cereal grains are quoted for a moisture content of about 0·10 lb/lb, the natural moisture content at the time of the experiments.

2.2 *Correlations based on drag equations for quiescent beds.* Since the maximum of the minimum spouting velocity is evidently identical with the minimum superficial gas velocity causing onset of aggregative fluidization, it may be anticipated that it can be predicted from the drag equations for quiescent beds, (the term "quiescent bed" is in this paper used synonymously with the descriptively inferior, but commoner, terms "packed bed" and "fixed bed"). Here the fraction void should be taken as the "dynamic" maximum fraction void, ϵ_m, and the drag forces equated with the weight forces,

$$(-\Delta P)_f = gL_m(\rho_s - \rho)(1 - \epsilon_m) \qquad (3)$$

When this was done the above expectation was indeed precisely satisfied by the nonspherical particles. The spheres (peas and rape-seed), however, failed in the expanded (bed) state to follow their drag equation for the quiescent state, due to a change in their fraction void function with the onset of bed expansion. This individuality of behaviour is immaterial in the present context, since equation (1) predicts v_m for spheres very adequately. The present concern is therefore satisfied by the fact that v_m can be accurately predicted for *nonspherical* particles, at least, given a reasonable value of ϵ_m, adequate information on particle shape and a reliable drag equation for the quiescent state.

The drag equations for quiescent beds can, however, be used for the same end in a slightly different way, such that the spherical particles also become obedient to a general rule. The minimum superficial gas velocity for the onset

of particulate fluidization, v_{mf}, can always be calculated from the drag equations given reasonable values of the appropriate fraction void, ϵ_{mf}. It is therefore of interest to inquire whether v_{mf} and v_m are not directly related, perhaps by a simple proportionality. Table 3 indicates that this is indeed the case and suggests the simple rule that

$$v_m = 1{\cdot}25\, v_{mf} \qquad (4)$$

The Table also gives the experimental values of the characteristic fractions void, ϵ_m and ϵ_{mf}.

Table 3. Critical data on the agitation of particles

Particle	Re_m	v_m/v_{mf}	ϵ_m	ϵ_{mf}
Peas	850	1·26	0·432	0·395
Corn	670	1·23	0·445	0·412
Barley*	254	1·33	—	—
Wheat	205	1·26	0·415	0·380
Rape seed	52	1·22	0·400	0·371
Flax seed	49	1·10	0·390	0·372
Ottawa sand	17	1·12	0·395	0·381

* The *effective* fraction void of a barley bed cannot be measured, owing to the peculiar structure of the barley kernel.

A rather exhaustive investigation of drag in quiescent beds of spheres, wheat and corn was made in the course of the present study, and it may be of interest to record the results here. The data on spheres ($\epsilon = 0{\cdot}35$–$0{\cdot}44$) are very well correlated by the equation (for $D_v/D_c < 0{\cdot}05$)

$$K\,\epsilon^2 \exp\left[-4{\cdot}2\,(1-\epsilon)\right] = 24\mathrm{Re} + 1{\cdot}8\,\epsilon^{3/2}\,\mathrm{Re}^2 \qquad (5)$$

The data on wheat ($\epsilon = 0{\cdot}37$–$0{\cdot}43$) and corn ($\epsilon = 0{\cdot}37$–$0{\cdot}46$) are well correlated by the equation

$$K\,\epsilon^2 \exp\left[-4{\cdot}2\,(1-\epsilon)\right]\psi^2 = C_V\,\mathrm{Re} + C_I\,\mathrm{Re}^2, \qquad (6)$$

as may be seen in Fig. 3, but can be more simply represented by the restricted equations

$$K\,\epsilon^2 \exp\left[-4{\cdot}2\,(1-\epsilon)\right] = 6{\cdot}4\,\mathrm{Re}^{1{\cdot}65}, \qquad 60 < \mathrm{Re} < 250 \qquad (7)$$

for wheat, and

$$K\,\epsilon^2 \exp\left[-4{\cdot}2\,(1-\epsilon)\right] = 3{\cdot}8\,\mathrm{Re}^{1{\cdot}79}, \qquad 150 < \mathrm{Re} < 1000 \qquad (8)$$

for corn.

The foregoing equations will not be justified here; the investigation of drag in quiescent beds is being continued and will be the subject of another article.

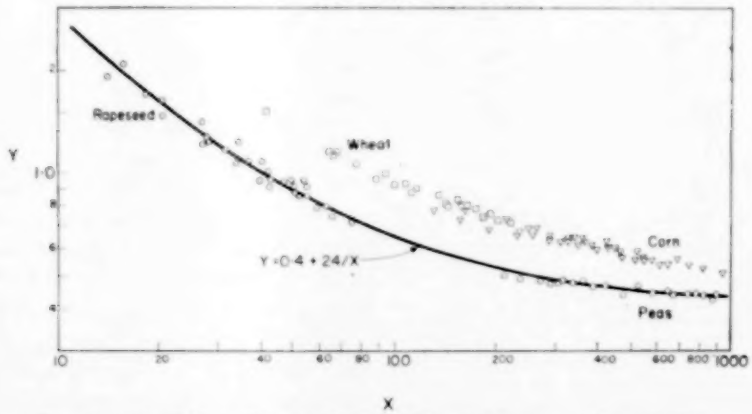

FIG. 3. A correlation of the maximum of the minimum spouting velocity.

$C_D = K/\mathrm{Re}^2$	X	Y
Spheres	$4{\cdot}5\,\epsilon^{3/5}\,\mathrm{Re}$	$C_D\,\epsilon^{1/2}\exp[-4{\cdot}2\,(1-\epsilon)]/4{\cdot}5$
Non-spheres	Re	$C_D\,\epsilon^2 \exp -[4{\cdot}2\,(1-\epsilon)\,\psi^2]$

3. *The maximum spoutable bed depth*

3.0 *Introductory note.* The maximum spoutable bed depth (m.s.b.d.) comprises the second category of dependent variables, according to Section 1; in contrast with the maximum of the minimum spouting velocity, the m.s.b.d. is dependent on the dimensions of the column used in spouting as well as on the properties of the gas and particles. Quantification of the attributes of the m.s.b.d. thus introduces the novel and interesting problem of the modelling of spouted beds.

3.1 *Phenomenological note.* The m.s.b.d. marks the closure of the stability of spouting with respect to changes in the gas flow rate. At lesser bed depths increases in the gas velocity above the minimum required for spouting augment the rate of bed turnover and cause the spout to mount higher above the bed, (see Fig. 1b). Ultimately, at an instability point characteristic of the bed depth they cause supersession of spouting by less organized agitational patterns such as slugging (with coarse particles) and aggregative fluidization (with fine particles). At small bed depths the gas velocity can be increased almost indefinitely without causing instability. But, as the m.s.b.d. is approached, the loci of the points of instability and minimum spouting draw together (Fig. 1a) and finally meet at the m.s.b.d. itself. The spouting bed may then be said to be at a critical phase transition point, as illustrated by MATHUR and GISHLERS' 'phase diagrams' [1] and by Fig. 1 (a).

The m.s.b.d. (enlarging on remarks in the preceding Section) also marks the point of maximum fractional expansion of beds, both prior to and during spouting. The physical appearance of a spouting bed is, to a first approximation, independent of the bed depth, and dependent only on the reduced level, z/L_m, at which the bed is observed. At low reduced levels the bed is in a compact state, the upward flow of gas being largely accommodated by the spout which is describable here as a high-velocity jet piercing the bed and supporting a thin population of particles. At values of z/L_m of 0·3–0·4 there is a noticeable loosening or expansion of the annulus of the bed. This loosening grows with increasing value of z/L_m, and becomes maximum at $z = L_m$. The condition of the bed at levels near $z = L_m$ is, in fact, that of incipient aggregative fluidization, the uppermost levels of the bed having reached the limit of coherent, dense-phase expansion. It is therefore evident that the gas flow must be nearly uniform at $z = L_m$ and that the superficial gas velocity must be practically identical with the minimum velocity for onset of aggregative fluidization.

The m.s.b.d. is therefore characterized by maximum gas loading of the annulus, by maximum solids loading of the spout, and by consequent degeneration of the agitational pattern into aggregative fluidization or slugging.

The foregoing deductions are further borne out by gas velocity profiles presented in Section 7. That the fractions void of spout and annulus approach each other at $z = L_m$ was clearly visible in high-speed photographs taken of two-dimensional spouting in a narrow, rectangular column.

3.2 *A hypothesis for correlating the maximum spoutable bed depth.* The m.s.b.d. can, in principle, be related to the independent variables through force and energy balances. However, an exact statement of any kind would involve knowledge of momentum and energy transformations in the spout difficult or impossible to acquire experimentally. One consequently seeks a simplification which retains the useful skelton of a force or energy balance but which excludes those elements containing dependent variables of higher order than the m.s.b.d. itself, (i.e., variables of the third and fourth categories in Section 1). The simplification used in this paper is formulated as follows.

It is noted that the formation of a spout is accompanied by a significant decrease in the frictional pressure drop through a bed. (At the m.s.b.d. the frictional pressure drop through a quiescent bed on the verge of spouting essentially equals the weight stress at the foot of the bed, Equation (3), but when the spout breaks through, the decrease in gas flow through the annulus coincident to partial venting of the total gas flow through the spout causes a notable fall in the pressure drop, Fig. 1a). Thus the notion of a force balance suggests the hypothesis that

$$\left\{\begin{matrix}\text{decrease in integral}\\ \text{pressure drop at the}\\ \text{advent of spouting}\end{matrix}\right\} \propto \left\{\begin{matrix}\text{change in gas}\\ \text{momentum in}\\ \text{the bed}\end{matrix}\right\} \quad (9)$$

This statement is at least qualitatively correct, and is of a type facilitating analysis of a situation sufficiently complex that unguided dimensional analysis is so ambiguous as to be nugatory.

The hypothesis may be written symbolically in the form (with reference solely to beds of maximum spoutable depth)

$$\{gL_m(\rho_s - \rho)(1 - \epsilon_m) - (-\Delta P)_f\} \propto \rho Q_m (u_0 - u_e) \quad (10)$$

The velocity of exit, u_e, is the momentum-mean velocity *within* the bed, just prior to exit, and will for this reason be expressed as $u_e \equiv k_e v_m$, where k_e is the factor times which the momentum-mean velocity exceeds the superficial velocity within the bed. Thus, rearranging equation (10) and putting $Q_m \equiv \pi D_0^2 u_0/4$ and $u_0 \equiv v_m D_c^2/D_0^2$ one obtains

$$\left[\frac{L_m}{D_v}\right]\left[\frac{D_0}{D_c}\right]^2 C_D \propto \frac{1 - k_e(D_0/D_c)^2}{(1 - \epsilon_m) \cdot \Phi} \quad (11)$$

This rather unwieldy expression can be relaxed by taking account of the following facts: (i) the present experimental data indicate that the reduced pressure decrement, Φ, is proportional to powers of the ratios D_c/D_0 and D_v/D_c; (ii) the drag coefficient C_D is given in terms of particle shape and Reynolds number by equation (2); and (iii) the fraction "unvoid" $(1 - \epsilon_m)$ is uniquely determined by particle shape and (possibly) Reynolds number. Hence equation (11) can be written, allowing for residual effects of the flow regime and particle shape,

$$\left[\frac{L_m}{D_v}\right]\left[\frac{D_v}{D_c}\right]^m\left[\frac{D_0}{D_c}\right]^n\left(22 + \frac{2600}{\mathrm{Re}_m}\right) \times [f(\phi)]^p = f(\mathrm{Re}_m) \quad (12)$$

3.3 *Correlation of experimental data on maximum spoutable bed depths.* Examination of the abundant experimental data on wheat, (Fig. 4), indicates that the exponent m in equation (12) has the value 1·76. Let it be assumed (as justified by the results) that this value of m is universal. Figs. 5 (a) and 5 (b) then indicate that the exponent n is expressible as

$$n = 1{\cdot}6 \exp(-0{\cdot}0072\ \mathrm{Re}_m) \quad (13)$$

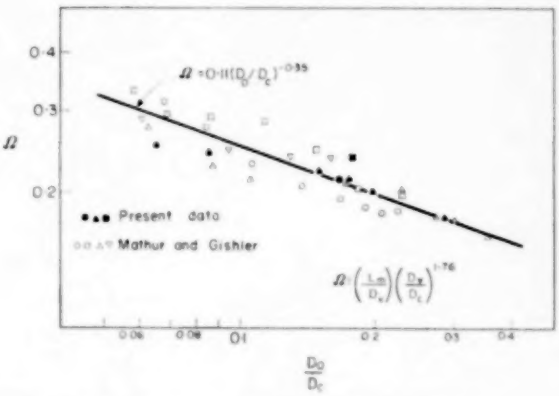

Fig. 4. A correlation of the maximum spoutable bed depth for wheat beds.
D_c = 4 in. ▽ 6 in. △ ▼ 9 in. □ ■ 12 in. ○●

The final correlation, Fig. 5 (c), then follows directly on determining the optimum exponent of the shape function, $f(\phi)$. The equation of the correlating curve is

$$\Omega\left(\frac{12{\cdot}2\ D_0}{D_c}\right)^n\left(22 + \frac{2600}{\mathrm{Re}_m}\right) \times [f(\phi)]^{2/3}\ \mathrm{Re}_m^{1/3} = 42 \quad (14)$$

The correlation is satisfactory for the range of particle shapes and Reynolds numbers so far investigated. Higher Reynolds numbers are probably uninteresting in practice, since extremely coarse particles would be involved. The limiting behaviour at low Reynolds numbers cannot be forecast with any accuracy, and data extending to Reynolds numbers as low as 0·5 are needed to fill this gap.

3.4 *A correlation for low Reynolds numbers.* An alternative interpretation of the present data, (Fig. 6), indicates a simplified behaviour at Reynolds numbers Re_m smaller than about 100 and leads to the correlating equation for spheres

$$\Omega^{-1} = 4{\cdot}4 + \frac{1{\cdot}6 \times 10^4}{\mathrm{Re}_0} \quad (15)$$

This equation is, to be sure, incompatible with

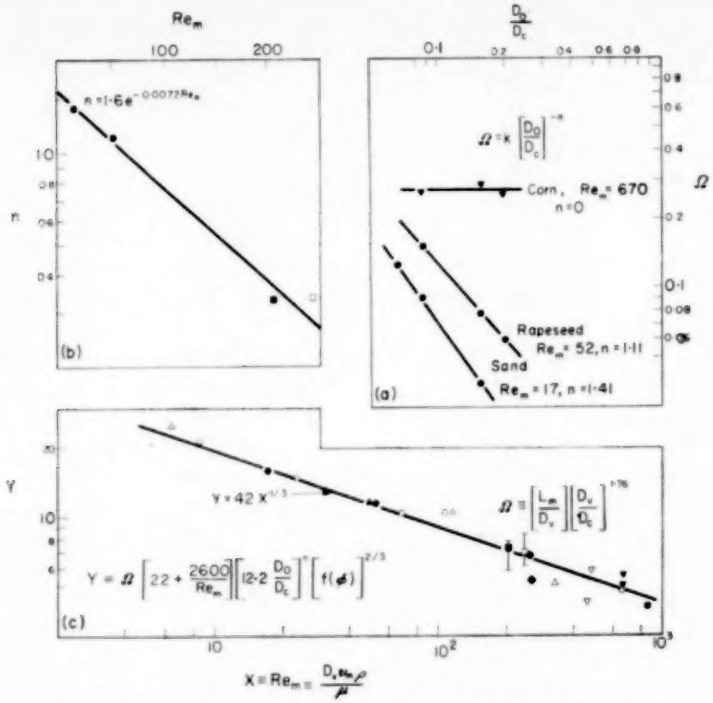

FIG. 5(a). Correlation of the maximum spoutable bed depth for corn, rape-seed and Ottawa sand. Data on the 0·5 ft dia. columns.

FIG. 5(b). Correlation of the exponent n.

FIG. 5(c). Generalized correlation of the maximum spoutable bed depth. For key to data see Fig. 2.

equation (14), and fails emphatically at Reynolds numbers above 100. Nevertheless, it gives an undeniably fair portrayal of the low Reynolds number behaviour and strongly suggests that the m.s.b.d. varies in direct proportion to the gas inlet particle Reynolds number Re_0 when the inlet flow regime is viscous with respect to the particles.

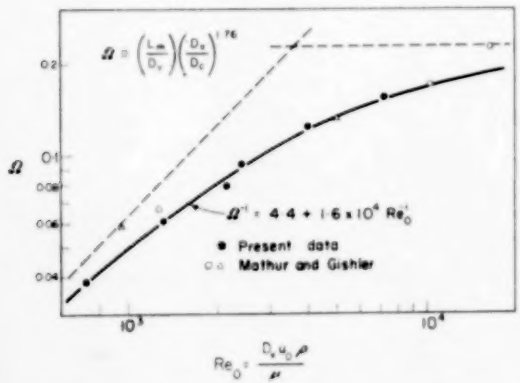

FIG. 6. A correlation of the maximum spoutable bed depth for Reynolds numbers Re_m smaller than about 100.

3.5 *The significance of the geometrical group* Ω. It can be plausibly argued that the group $\Omega = (L_m/D_v)(D_v/D_c)^{1.76}$, which appears in all the correlations, is a geometrical factor characterizing the ratio of the axial and radial resistances to gas flow in the spread of the gas from the spout through the annulus. This explanation has the necessary merit that it does not overtly contradict the constancy of the exponent, 1·76, on the ratio D_v/D_c.

3.6 *Limiting effects of the inlet-to-column diameter ratio.* The group $1 - k_t (D_0/D_c)^2$ in equation (11), eliminated from the foregoing analysis, has still an important significance with respect to the

stability of spouting. Clearly, if k_e is larger than unity this group will become zero at a value of D_0/D_c smaller than unity. In fact, evidence presented in Section 7.1 indicates that the value of k_e in a turbulent regime is approximately eight, giving a critical value of D_0/D_c of 0·35. This means that beds will not spout if D_0/D_c exceeds 0·35; at $D_0/D_c = 0{\cdot}35$ the m.s.b.d. is zero. A fairly accurate physical interpretation of this prediction is that with D_0/D_c greater than 0·35 the gas velocity in the bed exceeds the minimum velocity for onset of aggregative fluidization *before* the inlet velocity exceeds the free-fall velocity of the particles.

3.7 *Note on a Mathur and Gishler correlation.* It is of interest to note that MATHUR and GISHLER [1] have proposed a correlation for the minimum spouting velocity which should yield an expression for the m.s.b.d. if one substitues $L = L_m$ and $v_s = v_m$. The incorrelating equation gives, after rearrangement (see p. 164 of their article),

$$\left[\frac{L_m}{D_c}\right]\left[\frac{D_c}{D_c}\right]^2\left[\frac{D_0}{D_c}\right]^{2/3} C_D = \text{constant} \qquad (16)$$

This equation contains the basic elements of equation (14). The "constant" on the right is, however, a function of column diameter (private communication).

4. *The minimum spouting velocity*

4.0 *Introduction.* The third category of dependent variables, by Section 1, comprises those, such as the minimum spouting velocity and the integral frictional pressure drop, which are functions of the bed depth as well as of the column geometry and the properties of the gas and the particles. However, only the minimum spouting velocity will be discussed at this point as the integral pressure drop is most conveniently interpreted with the frictional pressure gradient in the fourth category of variables. The following discussion introduces a concept which is basic to the modelling of spouted beds.

4.1 *The similarity principle of spouted beds.* Investigation of variables of the third and fourth categories produced clear perception of the following similarity principle:

Beds of given particles spouted with a given gas in geometrically similar columns behave similarly when the reduced bed depths L/L_m are the same.

4.2 *The equation of the minimum spouting*

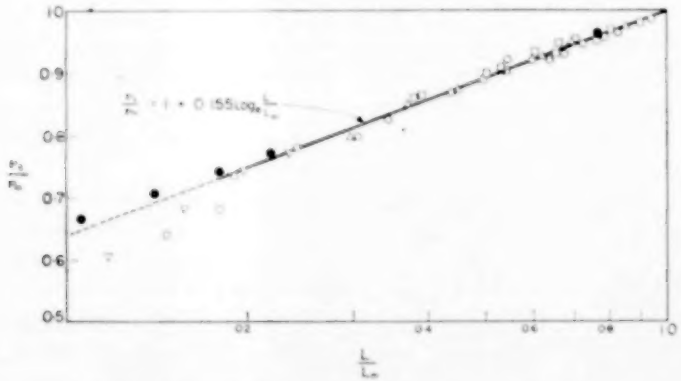

FIG. 7. A correlation of the minimum spouting velocity for wheat spouted in geometrically similar columns.

$D_0/D_c = 0{\cdot}172$

$D_c = 2{\cdot}00$ ft	$\beta = 180°$ ●
	$\beta = 90°$ ▽
$D_c = 1{\cdot}00$ ft	$\beta = 120°$ ○
$D_c = 0{\cdot}75$ ft	$\beta = 120°$ □
$D_c = 0{\cdot}50$ ft	$\beta = 120°$ △

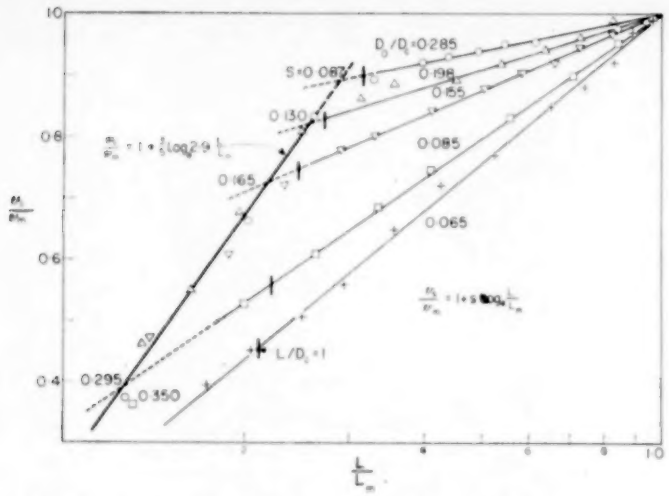

FIG. 8. A correlation of the minimum spouting velocity for wheat spouted in the 0·5 ft dia. glass column with $\beta = 180°$.

velocity. In the particular case of the minimum spouting velocity the above similarity principle predicts that for a given particle and gas and geometrically similar columns

$$\frac{v_s}{v_m} = f\left(\frac{L}{D_m}\right). \tag{17}$$

The validity of this relation is illustrated by Fig. 7, which shows a correlation of data on wheat (the m.s.b.d. in the 2 ft diameter column was too large to be determined experimentally and was therefore calculated from equation 14). The relation appears to be unaffected by variations in the base-cone angle between 90° and 180° (the m.s.b.d. was also unaffected by these variations).

Fig. 7 suggests the explicit form of equation (17)

$$\frac{v_s}{v_m} = 1 + s \ln\left(\frac{L}{L_m}\right) \tag{18}$$

This relation was universally exhibited by the present data, excepting those for very low bed

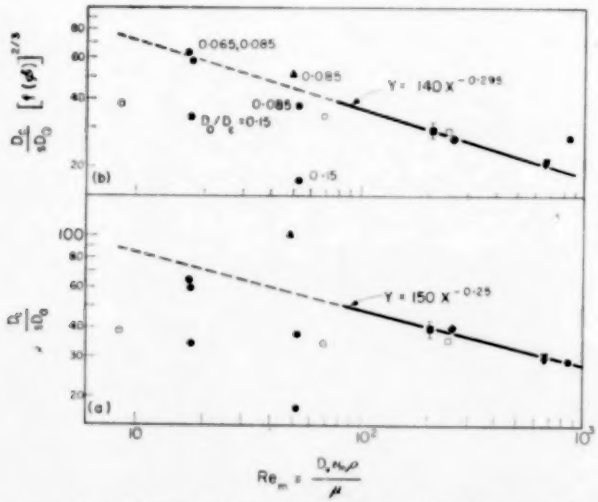

FIG. 9. A general correlation of the coefficient s. For key to data see Fig. 2.

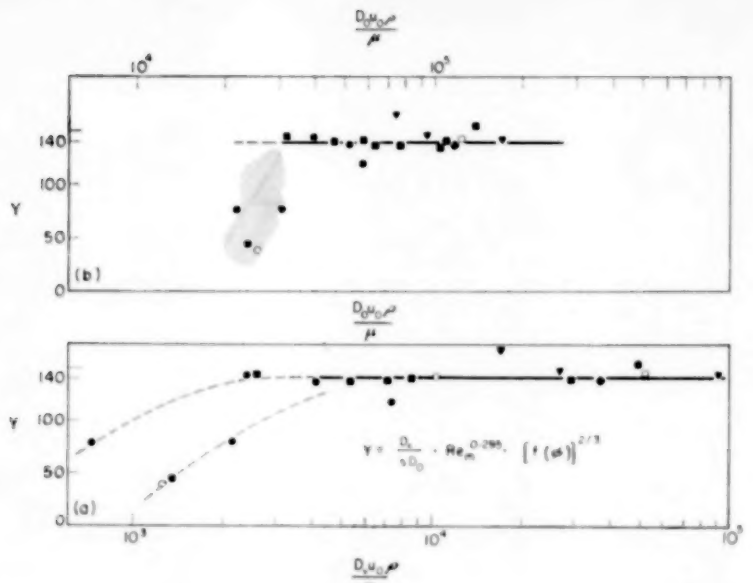

Fig. 10. A general correlation of the coefficient s. For key to data see Fig. 2.

depths; the lower limit of validity seems to be about $L/D_c = 1$. Thus the problem of correlating the minimum spouting velocity reduces to determining the behaviour of the numerical coefficient s in equation (18).

4.3 *Correlation of the coefficient, s.* The coefficient s decreased with increasing value of the geometrical ratio D_0/D_c, as may be seen in Fig. 8. Examination of the present data showed that the product sD_0/D_c is exactly constant for a given particle excepting certain of the data for low Reynolds numbers. Variations in this product depend on the Reynolds number Re_m (Fig. 9a) at least at Reynolds numbers above 100. The correlation is improved somewhat by postulating a 2/3 power dependence on the shape factor $f(\phi)$, Fig. 10b. Fig. 10a indicates that the gas inlet particle Reynolds number Re_0 is a possible criterion for deviation at low Reynolds numbers, but Fig. 10 (b) suggests that the inlet pipe Reynolds number may be a better one; the data for $D_0 u_0 \rho/\mu > 30000$ are uniformly well correlated by the equation

$$s = 0{\cdot}0071 \left(\frac{D_c}{D_0}\right) [f(\phi)]^{2/3} \mathrm{Re}^{0{\cdot}295} \qquad (19)$$

The validity of the Reynolds number criterion $D_0 u_0 \rho/\mu$ should, however, be further investigated at Reynolds numbers Re_m smaller than those in the present study.

Combination of equations (18) and (19) gives as the equation of the minimum spouting velocity

$$\frac{v_s}{v_m} = 1 + 0{\cdot}0071 \left(\frac{D_c}{D_0}\right) [f(\phi)]^{2/3} \mathrm{Re}_m^{0{\cdot}295} \ln (L/L_m) \qquad (20)$$

Figs. 9 and 10 (b) indicate that this equation is quite generally valid at $\mathrm{Re}_m > 100$, while at $10 < \mathrm{Re}_m < 100$ it is valid only if $D_0 u_0 \rho/\mu > 30000$. However, since no firm justification can, on the basis of the data so far obtained, be offered for the criterion $D_0 u_0 \rho/\mu$, perhaps Fig. 9 (b) should be interpreted in the following, simplest sense: Equation (19) is valid in the range $10 < \mathrm{Re}_m < 100$ if $D_0/D_c < 0{\cdot}1$.

4.4 *A correlation for very low bed depths.* The minimum spouting velocity seems to become independent of the properties of the particles as L/D_c falls below about unity. The following equation correlates data on all the particles as

spouted in the 0·5 ft diameter glass column with $\beta = 180°$:

$$\frac{v_s}{v_m} = 1{\cdot}2\left(\frac{L}{D_c}\right)\exp\left(-\frac{0{\cdot}038\,D_c}{D_0}\right) \qquad (21)$$

Other data indicated that increasing the cone angle to 90° increases the numerical coefficient of the r.h.s. slightly.

There should be little practical interest in beds with $L/D_c < 1$, for at such low bed depths agitation is feeble and of poor quality and the greater part of the gas flow is localized in the region of the spout.

5. *The frictional pressure gradient*

5.0 *Note on variables of the fourth category.* The remaining Sections consider variables of the fourth category, i.e. variables which are not only functions of the gas and particle properties, the column geometry and the bed depth, but also of position within the bed. In the cases of the frictional pressure gradient and the particle velocity at the wall position in the bed is adequately specified by stating the level in the bed, expressed by the reduced height z/L_m above the gas inlet. But for the local gas velocity radial variations are not negligible and one must also specify the reduced radial position r/r_c.

5.1 *A hypothesis for the gas flow in the annulus.* The frictional pressure gradient reflects the local gas flow in the annulus, and is determined by the drag equations for quiescent beds when the fraction void and superficial gas velocity in the annulus are known as a function of bed level. The present data show that the frictional pressure gradient is satisfactorily accounted for by the following simple hypothesis as to the gas flow in the annulus:

The mean superficial gas velocity at any level in the annulus is approximated by the equation of the minimum spouting velocity (equation 20) on substituting v_a for v_s and z for L:

$$\frac{v_a}{v_m} = 1 + 0{\cdot}0071\left(\frac{D_c}{D_0}\right)\times \times\left[f(\phi)\right]^{2/3}\mathrm{Re}_m^{\,0{\cdot}295}\ln\left(\frac{z}{L_m}\right) \qquad (22)$$

5.2 *A simplified equation for the frictional pressure gradient.* With the above hypothesis the equation can be written, linking the gas velocity in the annulus with the frictional pressure gradient,

$$-\frac{1}{g(\rho_s-\rho)(1-\epsilon)}\frac{dP}{dz} = \left(\frac{v_a}{v_m}\right)^b \qquad (23)$$

where ϵ is an average value of the fraction void (say, $[\epsilon_{mf} + \epsilon\ ]/2$) and the exponent b is given by the drag equations for quiescent beds; e.g. by equation (6), $b = 1{\cdot}65$ for wheat. Equation (23) is approximate, not exact, since the effects of gradients in the fraction void and in the superficial gas velocity are neglected.

Nevertheless, it provides reasonable estimates of the frictional pressure gradient when equation (22) is substituted for v_a/v_m.

5.3 *The integral frictional pressure drop.* The integral frictional pressure drop (a variable of the third category) is easily calculated from the frictional pressure gradient and, as noted earlier, is always somewhat smaller than the weight of the bed on unit area. A practically significant fact, however, is that a pressure drop *equal* to weight of the bed on unit area must be allowed for to start a bed spouting, this being the maximum pressure drop attained prior to formation of the spout.

6. *The rate and quality of agitation*

6.0 *Introductory note.* An idealized definition of spouting might specify a short, uniform bed turnover cycle consisting of downward flow of the annulus, capture of particles by the spout at the base of the bed, nearly instantaneous upward projection of these particles in the spout and their fall back into the annulus at the top of the bed. In actuality, however, particles enter the spout at all levels in a bed, and the rate of turnover therefore decreases from top to bottom of the bed. This may be an adverse factor under some conditions, and it is well to know the conditions which favour approach to ideality.

Bed turnover can be studied in two simple ways: (i) the particle velocity at the wall may be directly observed, and (ii) a marked pellet (or pellets) may be dropped into the bed adjacent to the wall and the lapse of time to its

reappearance at the top of the bed noted. The particle velocity at the wall measures the velocity of the annulus there (radial variations in the annular particle velocity should be small, since they require shearing of the annulus), and the decrease in annular velocity with decreasing height above the gas inlet measures the local flow of particles into the spout. The tracer method, on the other hand, measures the maximum cycle time in the bed (a variable of the third category). Both these methods were used in the present work to study turnover in beds of wheat. Further studies are needed to determine the generality (and possible modifications) of the following correlations.

6.1 *Correlation of the particle velocity at the wall.* The particle velocity at the wall of wheat beds spouted in the 0·5 ft diameter glass column was correlated using the similarity principle of Section 4.1 and the hypothesis as to gas flow in the annulus in conjunction with plausible

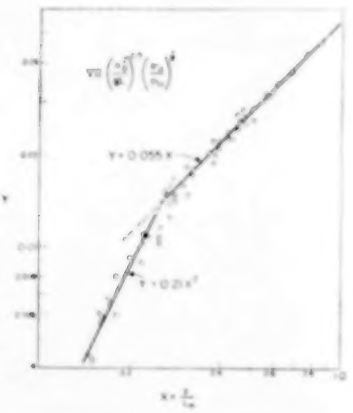

Fig. 11. A correlation of the particle velocity at the wall for wheat spouted in the 0·5 ft dia. glass column with $\beta = 180°$ and $D_0/D_c = 0{\cdot}065$–$0{\cdot}285$.

dimensionless groupings of the variables (Fig. 11). The correlating equation is

$$\left[\frac{u_p^2}{gL}\right]^{0.4}\left[\frac{v_a}{v_m}\right]^2 = B\left[\frac{z}{L_m}\right]^b \qquad (24)$$

where $B = 0{\cdot}055$ and $b = 1$ at $z/L_m > 0{\cdot}25$, and $B = 0{\cdot}21$ and $b = 2$ at $z/L_m > 0{\cdot}25$. Substitution of equation (22) for v_a/v_m gives

$$\frac{u_p}{\sqrt{gL}} = 0{\cdot}027\left(\frac{z}{L_m}\right)^{5/4} \times \left\{1 + 0{\cdot}0071\left(\frac{D_c}{D_0}\right)[f(\phi)]^{2.3}\mathrm{Re}_m^{\,0.295}\ln\left(\frac{z}{L_m}\right)\right\}^{5/2} \qquad (25)$$

for $z/L_m > 0{\cdot}25$. For $z/L_m < 0{\cdot}25$, the numerical coefficient of the r.h.s. is 0·142, and the exponent of z/L_m is 5/2.

Equation (25) should provide a safe basis for gauging the effects of the independent variables on the agitation of *any* given particles in a given column. It may not, however, predict fully the effects of the Reynolds number Re_m and the particle-to-column diameter ratio D_c/D_c.

6.2. *Correlation of the maximum turnover cycle time.* The maximum period of the bed turnover cycle, θ_c, was studied in wheat beds 2–6 ft deep spouted in all the columns listed in Table 1, with $D_0/D_c = 0{\cdot}17$ and $\beta = 90°$ and 180°. The data are satisfactorily correlated by the equation

$$\theta_c = 21\sqrt{(L/g)}\left(\frac{L_m}{D_c}\right) \qquad (26)$$

This equation was developed merely to provide a basis for treating certain problems encountered in the design of spouted wheat dryers, but probably contains the germ of a more general correlation. The maximum cycle time can be computed from the particle velocity at the wall but difficulties are encountered at the base of the bed, where the movement is chiefly inward and the downward velocity approaches zero However, it can be shown that equations (25) and (26) are roughly compatible.

6.3 *The effect of gas flow rate on agitation.* The foregoing correlations are for the condition of minimum spouting. Increasing the gas flow rate above the minimum increases the rate of agitation roughly in proportion to the gas flow ratio v/v_s.

7. *Local gas velocity patterns*

7.0. *Introductory note.* Although the basic gas flow pattern in a spouted bed is intuitively obvious, it is still of interest to study its details quantitatively. Basic data may be obtained for analysing the spread of the gas into the annulus, the local effectiveness of gas–solids contact may be judged and subtle effects of changes in the operating variables may be observed.

7.1. *Some observations on the measured local velocities.* The experimental data on wheat (no other particles were studied) indicate that the measured local velocity in a spouted bed at levels approaching $z = L_m$ is of the same magnitude as the terminal free-fall velocity of the particles in an infinite fluid. Hence local velocities are appropriately expressed in terms of the ratio u/u_t. Remembering that bed levels near $z = L_m$ are in a state of incipient aggregative fluidization this fact is striking. The identical situation must exist in the dense phase of fluidized beds. However, the finding may well prove to be valid only for non-viscous flows.

For the present case (of non-viscous flow) it is of interest to compare the terminal, free-fall velocity with the maximum of the minimum spouting velocity and to determine the compatibility of their measured ratio with several hypotheses as to the effective local value of the gas velocity in a quiescent bed. The terminal velocity of the wheat was found to be 24 ft/sec (calculated from the author's correlation [5] after experimentally checking the shape factor by free-fall experiments in alcohol and water) and the maximum of the minimum spouting velocity was 3·1 ft/sec, giving a ratio u_t/v_m of eight. If volume effects alone are considered, the effective local velocity should be $1/\epsilon_m \simeq 5/2$ times the superficial velocity. If, however, the local velocity is determined by the minimum free-flow area between contiguous spheres, the maximum velocity ratio is $\sqrt{3}\left[\sqrt{(3)} - (\pi/2)\right] = 11$. The measured local velocities are thus seen to be of the correct order of magnitude, the second hypothesis being in best accord with experiment.

In view of the foregoing, it can be plausibly argued that the measured local velocities closely approximate both the momentum-mean and residence time mean velocities in a turbulent regime. Certainly much of the void volume of a bed must be nearly stagnant with respect to gas flow in a turbulent regime, i.e. in the sense that fluid is caught in wake regions of low velocity. The assumption sometimes made that the local velocity approximates the void space-mean velocity appears to be erroneous.

7.2 *The axial velocity decay.* Fig. 12 shows data on the decay of the axial velocity with increasing height above the gas inlet in beds of near-maximum spoutable depth. At these bed depths the data fall on a curve characteristic of the m.s.b.d.; at lower bed depths the initial

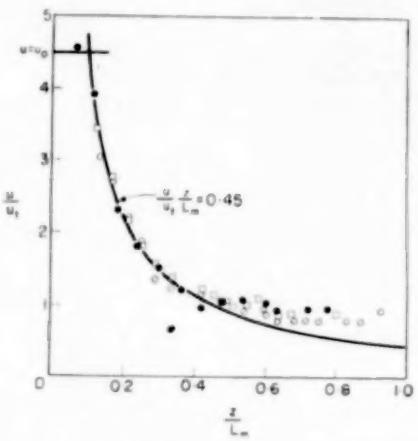

Fig. 12. Decay of the axial gas velocity in spouted wheat beds.
D_c = 9 in ● 6 in ○ □ L/L_m = 1·0 □ 0·8 ○ ●

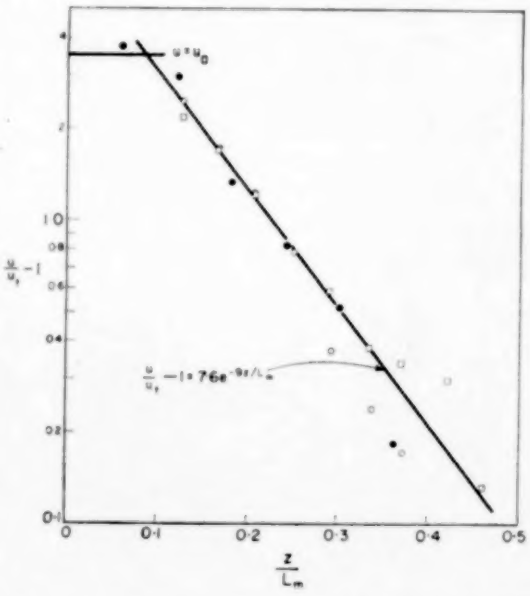

Fig. 13. Decay of the axial gas velocity excess in spouted wheat beds.
D_c = 9 in ● 6 in. ○ □ L/L_m = 1·0 □ 0·8 ○ ●

portion of the curve is depressed in proportion to the decrease in inlet velocity. The correlating equation for bed levels in the range $0{\cdot}1 < z/L_m < 0{\cdot}45$ is

$$\frac{u}{u_t} = \frac{0{\cdot}45}{z/L_m}, \tag{27}$$

and is (but not because of any very strong fluid-dynamical analogy) similar to the decay law [6] of a free jet

$$\frac{u}{u_0} = \frac{6{\cdot}6}{z/D_0} \tag{28}$$

Fig. 13 shows the form of the approach to an uniform velocity distribution at exit; the decay law of the axial velocity excess is exponential:

$$\frac{u}{u_t} - 1 = 7{\cdot}6 \exp\left(-9\frac{z}{L_m}\right) \tag{29}$$

7.3 *Radial velocity profiles.* Fig. 14 shows radial velocity profiles for beds of near-maximum spoutable depth spouted in the 0·5 ft diameter column. The behaviour exhibited is unremarkable excepting the development of a pronounced crest at the wall. Data on the 0·75 ft. diameter column (Fig. 15) however, show an unexpected complexity: each profile has an undulating shape ending at the higher bed levels with the same pronounced crest at the wall. When a series of closely-spaced profiles of this type are placed one above the other, the evolution of the standing wave forms is easily traced through the bed. There is no readily apparent explanation for this phenomenon which was completely absent in the 0·5 ft diameter column. Possibly it is something that is favoured by small values of the particle-to-column diameter ratio.

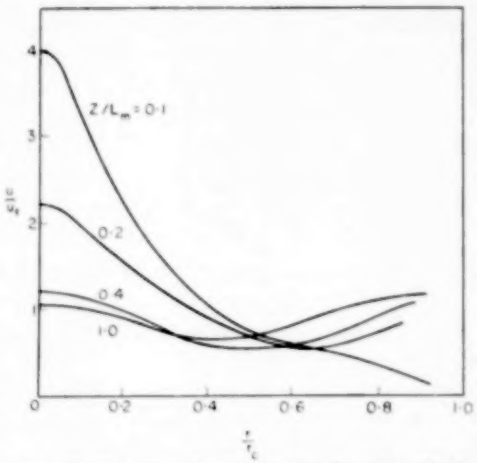

Fig. 14. Radial gas velocity profiles for wheat beds spouted in the 0·5 ft dia. column with $\beta = 180°$.

Velocity profiles for intermediate bed depths are nearly superimposable on those in Figs. 14 and 15 but the trough between the wall and the spout tends to be more pronounced. At low bed depths the gas velocity at the wall is markedly depressed.

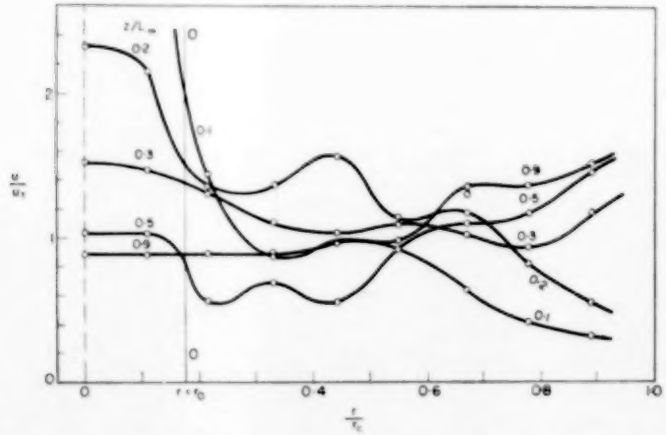

Fig. 15. Radial gas velocity profiles for wheat beds spouted in the 0·75 ft dia. column with $\beta = 120°$.

7.4 *Effects of the gas flow rate.* Data presented in the foregoing are for beds at the point of minimum spouting. The effect of increasing the gas velocity above the minimum is to increase the gas flow through the spout without significantly affecting the flow through the annulus (the constancy of the frictional pressure drop points to the same conclusion). The excess gas flow is therefore ineffectively contacted with the particles, and serves only to augment the rate of agitation.

Conclusion

The foregoing account is, hopefully, sufficiently complete to expedite design calculations for almost any feasible application of spouting that may arise in practice. Gas and particle properties will usually be given. The scale of the application, consideration of the qualities of agitation and gas-solids contact and an economic balance will usually determine the size of the column and the bed depth (the use of batteries of columns may be considered in place of one large one). The bed depth determines the maximum gas delivery pressure and the minimum spouting velocity. In practice, a gas flow up to 30 per cent in excess of the minimum should be available to ease the starting of agitation. The use of a 90° base cone will normally obviate stagnation of the bed around the gas inlet.

Spouting is, as suggested by Mathur and Gishler [1], primarily a technique for agitating particles too coarse to fluidize well. Indeed, there may be not competition with fluidization at all since it has not yet been shown that particles fine enough to fluidize really well will truly spout. It has been seen that spouting takes place at superficial gas velocities of the order of the minimum for the onset of aggregative fluidization and becomes unstable at velocities of the same order. Thus, with fine particles spouting would anyway yield to aggregative fluidization at all but perhaps uninterestingly low gas velocities. However, the use of a constricted gas inlet may still have a beneficial effect on fluidization *per se*. This does not preclude the manifestation of phenomena resembling spouting in beds of fine particles; these should simply not be confused with genuine spouting whose characteristics have been quantified in the preceding pages. (*Note*: Strongly oblate or prolate bodies have a marked tendency to channel. If such a tendency is present, a pseudo-spout (an internal channel) may form under any conditions. Such pseudo-spouts, unlike real spouts, have a peculiar, monotonous stability, e.g. they are insensitive to the inlet-to-column diameter ratio and are markedly insensitive to bed depth, showing no sharply defined "m.s.b.d.", tending merely to drift to the wall at some large, variable bed depth. This behaviour was actually observed in some beds of barley and flaxseed. Pseudo-spouting is a rather feeble form of agitation; the pseudo-spout is frequently nothing more than an empty vent owing its stability to the bridging tendency of the particles).

The concept of maximum spoutable bed depth provokes speculation as to the existence of a maximum fluidizable bed depth for aggregative fluidization. The m.s.b.d. decreases with decreasing Reynolds number as the viscous regime is entered. Should not the maximum fluidizable bed depth decrease with *increasing* Reynolds number as the viscous regime is departed from?

Finally, to emphasize that spouting and aggregative fluidization are fundamentally different phenomena, consider the basic mechanisms of agitation: in spouting agitation is caused by an intense, continuous jet of gas piercing a quiescent bed and yielding its energy to generate a well-defined stream of particles, the spout, whose upward motion is balanced by the downward motion of the surrounding annulus. In aggregative fluidization on the other hand, agitation is largely due to the stirring action of trains of gas cavities or bubbles rising through the continuum of loosely contiguous particles. In the former, jet momentum governs; in the latter, a buoyancy acting on gas volumes exceeding the saturation gas flow.

Acknowledgement—I am indebted to Mr. K. B. Mathur and to Dr. P. E. Gishler, then of the National Research Council of Canada, Ottawa for occasioning my first interest in spouting and for sending me reports on their work.

Notation

Dimensions in absolute units

M = mass
L = length
θ = time

D_c = column (inside) diameter L
D_0 = gas inlet pipe (inside) diameter L
D_v = particle diameter, expressed as the diameter of an equi-volumed sphere L
F_D = drag force on a particle ML/θ^2
$= \pi D_v^3 (-\Delta P)_f / 6L(1-\epsilon)$ in beds of particles
$= \pi D_v^3 g(\rho_s - \rho)/6$ at equality with the weight forces
g = local acceleration due to gravity L/θ^2
L = bed depth L
L_m = maximum spoutable bed depth L
P = pressure $M/L\theta^2$
$(-\Delta P)_f$ = frictional pressure drop $M/L\theta^2$
$Q_m = v_m \pi D_0^2/4$ = minimum gas flow rate causing spouting at the maximum spoutable bed depth L^3/θ
r = radial co-ordinate originating at the column axis L
$r_c = D_c/2$ = radius of column L
$r_0 = D_0/2$ = radius of gas inlet tube L
u = local gas velocity in a bed L/θ
$u_0 = v_m (D_c/D_0)^2$ = inlet gas velocity at $v = v_m$ L/θ
u_c = momentum-mean gas velocity at $z = L_m$ L/θ
u_t = terminal free-fall velocity of a particle L/θ
z = axial co-ordinate originating at the gas inlet L
θ_c = maximum duration of the bed turnover cycle θ
μ = gas viscosity $M/L\theta$
ρ = gas density M/L^3
ρ_s = particle density M/L^3
v = superficial gas velocity L/θ
v_a = superficial gas velocity in the annulus $L_f\theta$
v_m = maximum of the minimum spouting velocity L/θ
= minimum superficial gas velocity causing onset of aggregative fluidization
v_{mf} = minimum superficial gas velocity causing onset of particulate fluidization L/θ
v_s = minimum spouting velocity L/θ

Dimensionless variables

b, m, n, p = numerical exponents
B = numerical coefficient
C_V, C_I = coefficients in quadratic drag law
$C_D = F_D / \frac{1}{8}\rho v^2 (\pi D_c^2/4)$ = total drag coefficient
$K = 8\rho F_D / \pi \mu^2$ = drag number
$k_c = u_c/v_m$ = ratio of momentum-mean and superficial gas velocities
$\mathrm{Re} = D_v v\rho/\mu$ = particle Reynolds number
$\mathrm{Re}_m = D_v v_m \rho/\mu$
$\mathrm{Re}_0 = D_v u_0 \rho/\mu$
β = angle included by column base cone
ϵ = fraction void
ϵ_m = maximum fraction void, as exhibited by the dense phase of an aggregatively fluidized bed
= fraction void of a spouting bed near $z = L_m$
ϵ_{mf} = fraction void of a bed consolidated by gradual reduction of agitation
$\Phi = 1 - (-\Delta P)_f / gL_m(\rho_s - \rho)(1-\epsilon_m)$ = pressure deficiency factor for beds of maximum spoutable depth
$f(\phi)$ = experimental particle shape factor
$\psi = \pi D_v^2/S$ = particle sphericity (S = particle surface area)
$\Omega = (L_m/D_c)(D_c/D_v)^{1.76}$ = geometrical resistance factor for beds of maximum spoutable depth

References

[1] Mathur K. B. and Gishler P. E. *Amer. Inst. Chem. Engrs. J.* 1955 **1** 139.

[2] Mathur K. B. and Gishler P. E. *J. Appl. Chem.* 1955 **5** 624.

[3] Becker H. A. and Sallans H. R. *Chem. Engng. Sci.* 1961 **13** 97.

[4] Becker H. A. *J. Appl. Polymer Sci.* 1959 **1** 212.

[5] Becker H. A. *Canad. J. Chem. Engng.* 1959 **37** 95.

[6] Taylor J. F. Grimmett H. L. and Comings E. W. *Chem. Engng. Progr.* 1951 **47** 175.

Chemical Engineering Science, 1961, Vol. 13, pp. 263 to 267. Pergamon Press Ltd., London. Printed in Great Britain

Hold-up in packed liquid–liquid extraction columns

T. Sitaramayya and G. S. Laddha

Alagappa Chettiar College of Technology, University of Madras, India

(*Received* 26 *July* 1960)

Abstract—A generalized correlation for hold-up of dispersed phase in packed liquid extraction columns has been derived and used to correlate the data of the present investigation in 2 in. column along with the reported data in 3 in. to 12 in. columns for a wide variety of liquid systems using different sizes of Raschig rings, Berl Saddles and Lessing rings.

Résumé—Une relation générale exprimant la rétention de la phase dispersée dans une colonne à garnissage d'extraction liquide–liquide a été établie ; elle est utilisée pour comparer les données de la présente étude, obtenues avec une colonne de deux pouces, avec celles relatives à des colonnes de 3 à 12 pouces, pour une grande variété de systémes, et pour différents garnissages anneaux Raschig, selles Berl, et anneaux Lessing.

Zusammenfassung—Eine verallgemeinerte Beziehung für den hold-up der verteilten Phase in Füllkörperkolonnen der Flüssig-Flüssig-Extraktion wurde abgeleitet und dazu benutzt, die vorliegenden Ergebnisse in einer 2 in. Kolonne mit den Ergebnissen in 3–12 in. Kolonnen für einen weiten Bereich von flüssigen Systemen unter Verwendung von Raschigringen, Berl-Satteln und Lessingringen verschiedener Grösse zu korrelieren.

Introduction

The development of a satisfactory method for prediction of the performance of packed extraction columns will almost certainly involve the estimation of the interfacial area of the contact of the two phases. This may be estimated from the determination of the hold-up of the dispersed phase in the packing and of the mean droplet size. A study of droplet behaviour in packed columns has been made by Lewis *et al.* [1]. Hold-up in packed columns unlike that in spray columns cannot be determined accurately from the measurements of pressure drop since allowance must be made for the net thrust upwards or downwards on the packing. Very little information has appeared in the literature on the determination of hold-up in packed columns, although it has been observed that in the operation of liquid–liquid extraction columns a definite amount of dispersed phase is always present in the interstices of the packing and the amount of dispersed phase thus held up is dependent upon the flow of the two phases in the column. The earliest attempt on the measurement of hold-up was perhaps that of Appel and Elgin [2], carried out in the course of their work on the rate of extraction of benzoic acid from aqueous solutions. Gayler and Pratt [3, 4] have reported some data on hold-up and pressure drop in packed columns. Data on hold-up at flooding have been correlated by Venkataraman [5]. More recently Gayler, *et al.* [6] measured hold-up below loading and correlated the characteristic velocity in terms of the physical properties of the liquid systems and the packing characteristics. The present investigation was aimed at developing a satisfactory and generalised correlation for hold-up below flooding in packed liquid–liquid extraction columns.

Experimental

Apparatus

The extraction column used in the present investigation was a 2 in. i.d. pyrex glass tube, 3 ft in length fitted with expanded end pieces, 6 in. i.d. at the bottom and 4½ in. i.d. at the top, described by Venkataraman [5]. A schematic diagram of the experimental set-up is shown in Fig. 1 for ready reference.

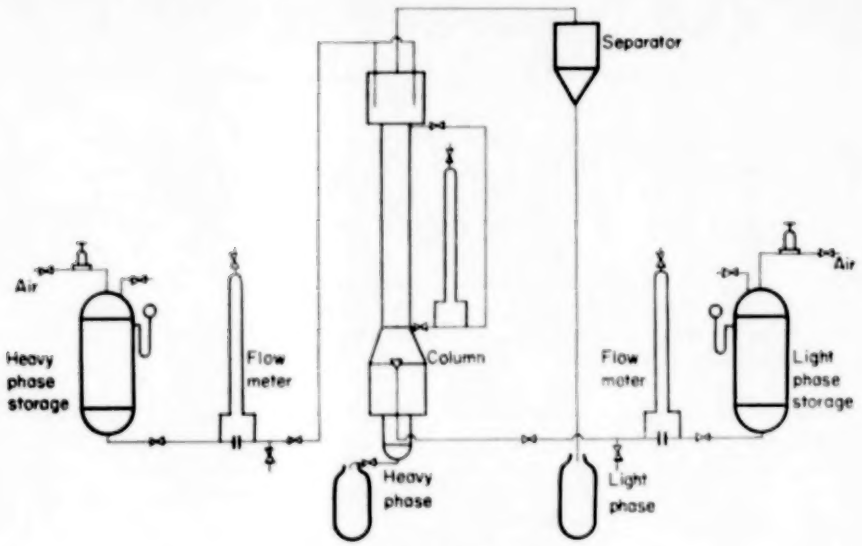

FIG. 1. Experimental set-up.

Packings

The physical characteristics of unglazed Raschig rings, Berl saddles and Lessing rings used as packings are given in Table 1.

Table 1. *Packing characteristics*

Packing	*Outside dia. (in.)*	*Inside dia. (in.)*	*Length (in.)*	*a*	*ε*
⅜ in. Raschig rings	0·365	0·194	0·363	158·2	0·632
¼ in. Raschig rings	0·25	0·123	0·245	206·0	0·58
⅜ in. Lessing rings	0·38	0·25	0·374	185·0	0·635
¼ in. Lessing rings	0·254	0·187	0·249	283·0	0·69
½ in. Berl Saddles	—	—	—	223·0	0·65

Liquid systems

Hold-up determinations were made in conjunction with the study of extraction of acetone from aqueous solutions by kerosene, butyl acetate and benzene. The aqueous phase (continuous phase) was always saturated with the solvent phase (dispersed phase). Similarly the solvents used were saturated with water. The average properties of the continuous phase and discontinuous phase are given in Table 2 for the various liquid systems studied in the present investigation.

Table 2. *Average physical properties of liquid phases at* 30 °C

Liquid system	ρ_c (g/cm³)	ρ_d (g/cm³)	μ_c cP	μ_d cP	γ (dyn/cm)
Kerosene–acetone–water	0·997	0·780	0·807	1·18	24·32
Butyl acetate–acetone–water	0·998	0·874	0·8065	0·656	12·32
Benzene–acetone–water	0·999	0·871	0·807	0·392	24·32

EXPERIMENTAL PROCEDURE

In order to ensure that each feed solvent was saturated with the other, a layer of water was maintained on the bottom of the solvent layer in the solvent feed tank and a layer of solvent on the top of the fluid in the aqueous feed tank. Feed flow of both phases was motivated by means of constant air pressure in the feed tanks. The column was filled with the continuous phase and the rate adjusted to the desired value as observed by the orifice meter in the line. The dispersed phase flow was next turned on and brought up to the desired value, the interface position having been stabilized in the middle of

the separating section at the top. When conditions became steady as evidenced by the constancy of the pressure drop readings, the aqueous and solvent flow rates were stopped simultaneously. It was observed that the interface at the top descended slowly due to the accumulation of the dispersed phase held up in the column pushing down the continuous phase. When no further movement of the interface was observed, the continuous phase supply was turned on gradually and the dispersed phase liquid collected at the top was allowed to be displaced out of the column in a receiver. The continuous phase supply was cut off exactly when the interface at the top regained its original level. The volume of the dispersed phase collected was determined and the ratio of the volume of the dispersed phase present in the interstices of the packing between the interface and the packing support to the actual free volume space in the column was calculated and expressed as hold-up of the dispersed phase.

Results and Interpretation of Data

By analogy with the results of an investigation by Steinour [7], Gayler *et al.* correlated the mean rate of rise v_r of the droplets of the discontinuous phase relative to the moving continuous phase by the following expression:

$$v_r = \frac{V_d}{\epsilon x} + \frac{V_c}{\epsilon (1-x)} = \bar{v}_0 (1-x) \qquad (1)$$

where $\bar{v}_0$ was defined as the limiting mean droplet velocity at zero continuous phase or the characteristic velocity. They indicated that this characteristic velocity could be determined by plotting

$$\left(V_d + \frac{x}{1-x} V_c \right)$$

against $x(1-x)$ on arithmetic co-ordinates. Straight lines of slope $\epsilon \bar{v}_0$ passing through the origin should be obtained. When data of the present investigation are plotted in this manner straightline correlationships result for specific packing and liquid systems giving the following basic correlation

$$\frac{V_d}{x} + \frac{V_c}{1-x} = m(1-x) \qquad (2)$$

where $m = \epsilon \bar{v}_0$. Fig. 2 shows such a plot for the system kerosene–acetone–water using $\frac{3}{8}$ in. Raschig rings as the packing. The data of the

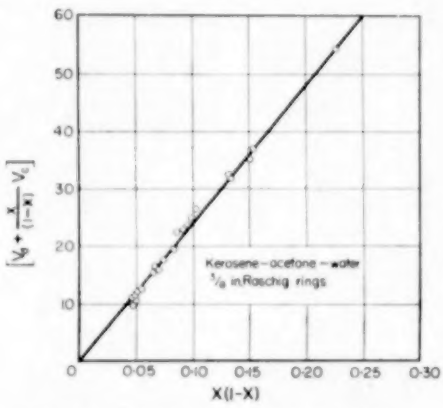

Fig. 2. Typical plot of hold-up data.

present investigation covering more than 300 experimental runs were first analysed by plotting

$$\left(V_d + \frac{x}{1-x} V_c \right) \text{ vs. } x(1-x)$$

and the values of m were determined by the method of least squares. These values of m are given in Table 3 along with the calculated values of m from the reported data of Gayler *et al.* [6] covering a wide range of tower diameters, liquid systems and different packings.

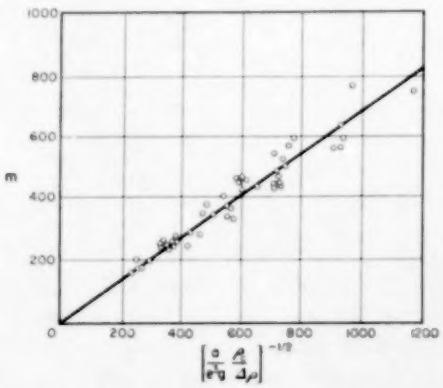

Fig. 3. Correlation of hold-up data.

Table 3. Calculated values for correlation of hold-up data

System	Tower dia. (in.)	Packing	$\left[\frac{a}{\epsilon^3 g}\frac{\rho_c}{\Delta\rho}\right]^{-1/2}$	m
Kerosene–acetone–water	2	¾ in. R	373·2	245
	2	½ in. R	288·6	192
	2	¾ in. L	348·6	293
	2	½ in. L	319·2	256
	2	½ in. B	328·8	237
Butyl acetate–acetone–water	2	½ in. L	240·6	198
Benzene–acetone–water	2	½ in. B	257·4	174
	2	½ in. L	250·2	175
	2	½ in. R	225·6	162
Methyl isobutyl ketone–water*	3	½ in. R	597·6	424
		¾ in. R	711·0	549
	6	½ in. R	550·8	371
		¾ in. R	720·0	468
		1 in. R	934·8	633
		½ in. B	475·2	380
		1 in. B	774·6	598
	12	½ in. R	561·6	351
		1 in. R	928·8	571
		1½ in. R	942·6	592
		1 in. B	765·0	573
Butyl acetate–water*	3	½ in. R	462·6	345
	6	½ in. R	426·6	282
		¾ in. R	537·4	363
		1 in. R	724·2	463
		½ in. B	368·4	240
		1 in. B	600·0	496
Benzene–water*	6	¾ in. R	564·6	329
		1 in. R	733·2	445
		1 in. B	607·8	454
	12	1 in. R	729·0	437
		1½ in. R	739·2	530
		1 in. B	600·0	466
Ethyl acetate–water*	6	½ in. R	381·6	256
		¾ in. R	498·6	339
		1 in. R	647·4	430
		½ in. B	329·4	245·5
		1 in. B	536·4	405·5
Iso-octane–water*	3	½ in. R	750·6	495
	6	½ in. R	602·4	398
		¾ in. R	904·2	567
		1 in. R	1174·2	752
		½ in. B	597·0	343
		1 in. B	973·2	774
Dibutyl ketone–water*	3	½ in. R	454·8	279
		½ in. B	377·4	273
	6	½ in. R	419·9	237
		¾ in. R	548·1	334
		1 in. R	711·6	440
		½ in. B	361·8	230
		1 in. B	589·8	450·6
	12	½ in. R	427·2	238
		1 in. R	707·4	426
		1½ in. R	717·6	479
		1 in. B	582·6	462
Iso-octane–20% glycerol*	6	¾ in. R	954·0	556

R = Raschig rings
B = Berl saddles
L = Lessing rings
* = Calculated values from the data of GAYLER *et al* [6]

The dependence of m on physical properties of the liquid systems and packing characteristics should now be evaluated. Neglecting the effect of viscosity and interfacial tension it may be assumed that m should vary with g, a/ϵ^3, ρ_c and $\Delta\rho$. The following relationship results by the application of dimensional analysis:

$$m \propto \left(\frac{a}{\epsilon^3 g}\right)^{-1/2}\left(\frac{\rho_c}{\Delta\rho}\right)^{-n} \qquad (3)$$

VOL 13 1961

The most useful value of n was found to be $\frac{1}{2}$ from the analysis of experimental data. The validity of the assumptions made may now be examined by plotting the calculated values of m vs. $[(a/\epsilon^3 g)(\rho_c/\Delta\rho)]^{-1/2}$ on arithmetic co-ordinates. This is shown in Fig. 3 where the calculated values of m from the experimental data as well as from the data reported by GAYLER *et al.* [6] for a wide variety of liquid systems, packing types and sizes and a wide range of tower diameters are plotted against $[(a/\epsilon^3 g)(\rho_c/\Delta\rho)]^{-1/2}$ It is observed that the data are satisfactorily correlated by the equation

$$m = 0{\cdot}683\left[\frac{a}{\epsilon^3 g}\frac{\rho_c}{\Delta\rho}\right]^{1/2} \qquad (4)$$

Average percentage deviation of the points from correlation is 10·97 per cent. Fifty-five per cent of the points lie within $\pm$ 10 per cent of the correlation and 80 per cent of the points fall within the range of 15 per cent.

The generalized correlations for hold-up in packed liquid–liquid extraction columns ranging from 2 in. to 12 in. in diameter packed with different sizes of Raschig rings, Berl saddles and Lessing rings and covering a wide variety of liquid system may be obtained by substituting the value of m from equation (4) into equation (2). The following correlation results:

$$\left[\frac{V_d}{x}+\frac{V_c}{1-x}\right]\left[\frac{a}{\epsilon^3 g}\frac{\rho_c}{\Delta\rho}\right]^{1/2} = 0{\cdot}683\,x\,(1-x)$$

which may be regarded as useful in predicting hold-up below flooding in liquid–liquid extraction columns.

Acknowledgment—The authors wish to express their deep gratitude to the University of Madras for the award of a Research Stipend for carrying out this investigation.

NOTATION

a	superficial area of packing	ft²/ft³
ϵ	fractional voids in packed tower	
g	gravitational acceleration	ft/hr²
v_r	rate of rise of droplets of discontinuous phase	ft/hr
v_0	characteristic velocity	ft/hr
V_c	superficial velocity of continuous phase (empty tower)	ft/hr
V_d	superficial velocity of discontinuous phase (empty tower)	ft/hr
x	fractional hold-up of dispersed phase in column for space	
ρ_c	density of continuous phase	lb/ft³
ρ_d	density of discontinuous phase	lb/ft³
$\Delta\rho$	density difference	lb/ft³

REFERENCES

[1] LEWIS J. B., JONES I. and PRATT H. R. C. *Trans. Inst. Chem. Engrs.* 1951 **29** 126.

[2] APPEL F. J. and ELGIN J. C. *Industr. Engng. Chem.* 1937 **29** 451.

[3] DELL F. R. and PRATT H. R. C *Trans. Instn. Chem. Engrs.* 1951 **29** 89.

[4] GAYLER R. and PRATT H. R. C. *Trans. Instn. Chem. Engrs.* 1951 **29** 110.

[5] VENKATARAMAN G. Ph.D. Thesis. Madras University 1957.

[6] GAYLER R., ROBERTS N. W. and PRATT H. R. C. *Trans. Instn. Chem. Engrs.* 1953 **31** 57.

[7] STEINOUR H. H. *Industr. Engng. Chem.* 1944 **36** 618.

Chemical Engineering Science, 1961, Vol. 13, p. 268. Pergamon Press Ltd., London. Printed in Great Britain

Book Reviews

Gas Chromatography Abstracts 1958. Edited by C. E. H. Knapman, Butterworths, London 1960, pp. 262. £2. 2. 0.

THE Gas Chromatography Discussion Group associated with the Institute of Petroleum was founded in 1955 and since then has been responsible for the organisation of regular bi-annual informal symposia and three biennial formal meetings of an international character. It is for these reasons that it is best known. However, among its other and less publicized activities it sponsors an abstracting service. The need for this has arisen through the quite remarkable acceleration in the rate of publication. At the end of 1959 something over 2100 papers had been published while at the present time between thirty and forty papers a month are appearing, often in journals of limited availability. These figures speak for themselves.

The volume under review contains abstracts of 1468 publications which comprise the literature from the effective birth of the subject in 1952 up to the end of 1958. Since they were never intended to serve as effective substitutes for the original papers, they are, in most cases, very brief, and do little more than indicate the contents of the work discussed. Allied with the abstracts, however, is an extremely comprehensive index in which the reference numbers of the abstracts have been grouped under such headings as, for example, "Applications and Specialized Separations," "Sample Type" or "Related Methods and Techniques." Each of these general classifications is further broken down into more specific groupings. Thus, the location of those abstracts relevent to a particular problem is quick and simple. While the volume is of value to all it is evidently particularly useful to those not constantly active in the field and whose interest is in knowing what can be done rather than how it is done, since by judicious use of the index and abstracts the amount of reading of original papers can be reduced to a minimum.

There is no doubt that Dr. Knapman and his associates have eminently succeeded in their aim, and this is the more estimable since the time lapse from the inception of the abstracting service to the appearance of the volume was little over twelve months. In fact the group has been so effective that very shortly after the appearance of the volume under review that for 1959 became available. The standard of production of the volume is high and very few errors are detectable. The compilers and publishers are to be congratulated on the appearance of this most useful book, and it is to be hoped that future volumes in the series will maintain the standards set here.

J. H. PURNELL

Chemical Engineering Science, 1961, Vol. 13, p. 269. Pergamon Press Ltd., London. Printed in Great Britain

Letters to the Editors

Corrections to the paper, "Perforated-plate performance" [1]

TABLE 3, shown below, gives corrected values for the weep points discussed in the reference paper. Table 3 (p. 32), as published (Reference 1, p. 32) gives the co-ordinates of Point A for plate inserts 1 through 5, and gives the co-ordinates of Point B for plate inserts 6 and 7. Weepage between Points A and B is generally not severe, but Point B is the generally accepted weep point. The new data points when compared to the line of HUGHMARK and O'CONNELL [2] give about as good agreement as the previously shown Figure 15 in the original article. Therefore, the remarks about the weepage correlation need not be changed in the original article.

There is one other correction that should be noted in Figure 16, the Oscillation-point correlation, the last value of D_h should be 3/32 in. instead of 9/32 in.

Table 3. Weep points

Plate insert number	L (lb H_2O/ hr ft^2)	ΔP (in. H_2O)	G (lb air/ hr ft^2)	F_h
I	350	2·29	1275	14·8
	1600	2·50	1220	14·1
	3000	2·69	1240	14·4
II	350	2·33	1330	15·4
	1600	2·56	1260	19·6
	3000	2·65	1100	12·7
III	350	2·18	1470	17·0
	1600	2·43	1280	14·8
	3000	2·61	1220	14·1
IV	350	—	—	—
	1600	2·40	1375	16·0
	3000	2·53	1240	14·4
V	350	2·50	1200	13·9
	1600	2·76	1050	12·1
	3000	2·95	1030	11·9
VI	350	2·75	640	14·4
	1600	3·20	665	15·0
	3000	3·55	695	15·6
VII	450	3·74	645	16·4
	720	3·68	630	16·1
	960	4·06	691	17·7
	1380	3·46	586	15·0
	1660	3·86	645	16·4
	2020	4·14	688	17·5
	2450	3·46	574	14·6
	2610	3·90	649	16·5

Department of Chemical Engineering, Lamar State College of Technology
Beaumont, Texas

R. A. MCALLISTER

REFERENCES

[1] MCALLISTER R. A., MCGINNIS P. H. Jr. and PLANK C. A. *Chem. Engng. Sci.* 1954 **9** 25.
[2] HUGHMARK G. A. and O'CONNELL H. E. *Chem. Engng. Progr.* 1957 **53** 127M.

SELECTION OF CURRENT PAPERS OF INTEREST TO CHEMICAL ENGINEERS

G. H. Hudson, J. C. McCoubrey and A. R. Ubbelohde: Vapour diffusion coefficients and collision parameters for cyclic molecules. *Trans. Faraday Soc.* 1960 **56** 1144–1151.

H. Bloom, F. G. Davis and D. W. James: The surface tension and surface heat content of molten salts and their mixtures. *Trans. Faraday Soc.* 1960 **56** 1179–1186.

A. E. Lagos and J. A. Kitchener: Diffusion in polystyrene–sulphonic acid ion exchange resins. *Trans. Faraday Soc.* 1960 **56** 1245–1251.

J. A. Currie: Gaseous diffusion in porous media. Part 1. A non-steady-state method. *Brit. J. Appl. Phys.* 1960 **11** 314–317. Part 2. Dry granular materials *ibid* 1960 **11** 318–324.

G. W. Scott Blair and J. C. Oosthuizen: Rolling sphere viscometer for structural liquids. *Brit. J. Appl. Phys.* 1960 **11** 332–334.

J. V. Cathcart, R. Bakish and D. R. Norton: Oxidation properties of Tantalum between 400 and 530 °C. *J. Electrochem. Soc.* 1960 **8** 668–670.

K. A. Allen and W. J. McDowell: Anomalous solvent extraction equilibria due to violence of agitation. *J. Phys. Chem.* 1960 **64** 877–880.

J. Kobak and D. J. Loveridge: Single tube sedimentation apparatus for the measurement of particle size distribution. *J. Sci. Instrum.* 1960 **37** 266–269.

R. J. French: Foam viscometer. *J. Sci. Instrum.* 1960 **37** 307–308.

J. R. O'Callaghan: Internal flow in moving beds of granular material. *J. Agric. Engng. Res.* 1960 **5** No. 2.

R. H. Spikes and G. A. Pennington: Discharge coefficient of small submerged orifices. *Proc. Inst. Mech. Engng.* 1959 **173** 661–674.

S. Prager: Diffusion in inhomogeneous media. *J. Chem. Phys.* 1960 **33** 122–127.

E. M. Sparrow and R. Siegel: Unsteady turbulent heat transfer in tubes. *J. Heat Transfer* 1960 **82** 170–180.

M. Altman, R. H. Norris and F. W. Staub: Local and average heat transfer and pressure drop for refrigerants evaporating in horizontal tubes. *J. Heat Transfer* 1960 **82** 189–198.

A. L. London, J. W. Mitchell and W. A. Sutherland: Heat transfer and flow friction characteristics of crossed-rod matrices. *J. Heat Transfer* 1960 **82** 199–213.

T. Yuge: Experiments on heat transfer from spheres including combined natural and forced convection. *J. Heat Transfer* 1960 **82** 214–220.

J. P. Holman and J. H. Boggs: Heat transfer to Freon 12 near the critical state in a natural circulation loop. *J. Heat Transfer* 1960 **82** 221–226.

Pau-Chang Lu: Combined free and forced convection heat generating laminar flow inside vertical pipes with circular sector cross sections. *J. Heat Transfer* 1960 **82** 227–232.

L. N. Tao: On combined free and forced convection in channels. *J. Heat Transfer* 1960 **82** 233–238.

R. Eichhorn: The effect of mass transfer on free convection. *J. Heat Transfer* 1960 **82** 260–263.

R. Schnurmann and I. S. Stringer: Initiation of chemical reactions by mechanical forces. *Nature, Lond.* 1960 **187** 587–588.

F. Molyneux: Design of a Venturi liquid mixer. *Fluid Handling* 1960 **126** 184–186.

SELECTION OF CURRENT SOVIET PAPERS OF INTEREST TO CHEMICAL ENGINEERS*

S. N. Ganz: Continuous method of production of ammonium carbonate salts. *Zh. prikl. Khim.* 1960 **33** 1251–1257.

L. P. Ryadneva and A. S. Lenski: Saturated vapour pressure of $S_2O_5Cl_2$. *Zh. prikl. Khim.* 1960 **33** 1272–1280.

Ya. I. Kilman: Determination of boiling points of mixtures of aqueous solutions of nitric acid with ammonium nitrate and urea. *Zh. prikl. Khim.* 1960 **33** 1415–1418.

G. K. Boreskov and M. G. Slinko: Calculation of catalytic processes in industrial reactors. *Khim. Prom.* 1960 (3) 193–201.

A. V. Gordyevski and V. I. Savelyeva: Sorption of uranium, vanadium and phosphorus by anionite AV–17. *Khim. Prom.* 1960 (3) 204–208.

V. A. Chertkov: On effect of composition of the absorbent on the rate of absorption of SO_2 from gases. *Khim. Prom.* 1960 (3) 223–227.

I. I. Zaslavski, L. I. Blyakhman and L. A. Alatyrtsov: Self-regulating method for automatic location of the optimum operating régime in a rectification column. *Khim. Prom.* 1960 (3) 227–233.

N. P. Dolonin: Heat transfer in equipment with various coiled heaters and determination of their heating surface. *Khim. Prom.* 1960 (3) 234–241.

M. E. Aerov, N. I. Nikitina and S. S. Trainina: Investigation of the effect of throughput in chemical engineering equipment by electro-hydrodynamic analogy. *Khim. Prom.* 1960 (3) 242–246.

I. E. Idelchik: Calculation of pressure drop of dry grid trays and partitions. *Khim. Prom.* 1960 (3) 247–251.

V. V. Udovenko and L. P. Aleksandrova: Vapour pressure of ternary systems. III. The system formic acid–water–1, 2-dichloroethane. *Zh. fiz. Khim.* 1960 **33** 1366–1372.

V. S. Merkulov and A. V. Klimushev: Component analysis of binary systems by the absorption of γ-radiation. *Zh. fiz. Khim.* 1960 **34** 1373–1376.

Ya. D. Zelvenski and V. A. Shaligin: Effect of rate of distillate withdrawal on the degree of separation in a distillation column. *Khim. Tekh. Topl. Masel* 1960 **5** (7) 19–23.

A. Yu. Mamiot and S. Ya. Beider: Solubility of *n*-pentant and *n*-hexane in water. *Khim. Tekh. Topl. Masel.* 1960 **5** (7) 52–54.

S. A. Bagaturov: Minimum liquid flow rate for rectification of multicomponent mixtures. *Khim. Tekh. Topl. Masel* 1960 **5** (7).

E. A. Kazakova: Heat transfer to water and ethyl alcohol by natural convection near the critical point. *Inzh.-Fiz. Zh.* 1960 **3** (6) 3–8.

V. V. Konsetov: Heat transfer in condensation of steam inside horizontal .pipes *Inz.-Fiz. Zh.* 1960 **3** (6) 9–16.

V. B. Chernogorenko: Determination of forms of moisture bonds in certain capillary-porous bodies by the electrical conductivity method. *Inzh.-Fiz. Zh.* 1960 **3** (6) 17–22.

E. P. Kovalenko: Two types of systems of differential equations of non-established flow of water in open channels. *Inzh.-Fiz. Zh.* 1960 **3** (5) 42–51.

A. S. Asaturyan and B. A. Tonkoshkurov: Free heat convection near a horizontal cylinder in highly viscous media. *Inzh.-Fiz. Zh.* 1960 **3** (6) 55–61.

M. A. Grishin: Hydrodynamics of large-grained material in a vortex air flow. *Inzh.-Fiz. Zh.* 1960 **3** (6) 82–86.

P. V. Tsoy: Problem of heat and moisture transfer for a semi-infinite three-dimensional medium with boundary conditions of the second type. *Inzh.-Fiz. Zh.* 1960 **3** (6) 112-119.

---

*To assist readers, translations of any article appearing in the above list can be obtained at a reasonable charge. All orders should be addressed to the Administrative Secretary of the Pergamon Institute at either Headington Hill Hall, Oxford or 122 East 55th Street, New York 22, whichever is more convenient.